JPL Publication 02-011, Version 1, Rev. A

Summary Report on Architecture Studies for the Terrestrial Planet Finder

Edited by:

C.A. Beichman, D.R. Coulter, C.A. Lindensmith, and P.R. Lawson

Jet Propulsion Laboratory
California Institute of Technology
Pasadena, California

National Aeronautics and
Space Administration

Jet Propulsion Laboratory
California Institute of Technology
Pasadena, California

June 2002

Abstract

Four teams comprising scientists and engineers from more than 50 universities and 20 engineering firms have assessed techniques for detecting and characterizing terrestrial planets orbiting nearby stars. *The primary conclusion from the effort of the past two years is that with suitable technology investment starting now, a mission to detect terrestrial planets around nearby stars could be launched within a decade.*

Based on the work of the study teams, the Project is recommending that NASA support two paths to the Terrestrial Planet Finder's (TPF) goal of finding and characterizing planets around ~150 stars out to distances of about 15 parsecs (pc):

- At visible wavelengths, a large telescope (4×10-m elliptical aperture in one design and an 8×8-m square aperture in another), equipped with a selection of advanced optics to reject scattered and diffracted starlight, offers the prospect of making direct images of reflected light from Earths.
- At mid-IR wavelengths, nulling interferometer designs using from three to five 3–4-m telescopes—located on either separated spacecraft or on a large 40-m structure—can directly detect the thermal radiation emitted by Earth-like planets.

The TPF Science Working Group (TPF-SWG) established that observations in either the optical/near-infrared or thermal-infrared wavelength region would provide important information on the physical characteristics of any detected planets, including credible signposts of life. The choice of wavelength regime for TPF will, in the estimation of the TPF-SWG and the independent technology board, be driven by the technological readiness of a particular technique.

The TPF-SWG also felt strongly that there were important scientific questions that could be addressed by missions of a smaller scale than the fully capable TPF. For example, a mission of lesser capability would be able to detect Earths around a few tens of stars within ~8 pc (should any exist) and study the composition and physical properties of gas-giant planets around stars as far away as 50 pc.

The challenge of developing the technologies required to enable either of the candidate architectures will require substantial funding over the next four years to bring them to the appropriate level of readiness. TPF is planned to start its formulation phase in 2007.

Finally, it should be noted that scientists from the European (ESA) and Japanese (ISAS) space agencies participated in these discussions as members of the TPF-SWG. The scientific exchanges suggested considerable interest in an international collaboration on a mission to address one of humanity's oldest questions, "*Does life exist beyond our Earth?*"

This document is available in PDF format at JPL's Planet Quest website.
http://planetquest.jpl.nasa.gov/TPF/tpf_review.html

Paper copies of this document as well as CD-ROMs with this document plus supporting material are available upon e-mail request. Address your request with your mailing address in the text of the message and with the subject "TPF 2002" to Peter.R.Lawson@jpl.nasa.gov

Table Of Contents

List of Figures

List of Tables

1 Executive Summary

In March, 2000, the Terrestrial Planet Finder (TPF) Project at JPL selected four university-industry teams to examine a broad range of instrument architectures capable of directly detecting radiation from terrestrial planets orbiting nearby stars, characterizing their surfaces and atmospheres, and searching for signs of life. Over the course of two years, the four teams incorporating more than 115 scientists from 50 institutions worked with more than 20 aerospace and engineering firms (Appendix A). In the first year of study, the teams and the TPF Science Working Group (TPF-SWG) examined approximately 60 wide-ranging ideas for planet detection. In January 2001, four major architectural concepts with a number of variants were selected for more detailed study. These included the previously studied formation-flying infrared interferometer (the "Book Design," Beichman et al., 1999). Of these concepts, two broad architectural classes appear sufficiently realistic to the TPF Science Working Group, to an independent Technology Review Board, and to the TPF Project that further technological development is warranted in support of a new implementation phase start around 2010. *The primary conclusion from the effort of the past two years is that with suitable technology investment starting now, a mission to detect terrestrial planets around nearby stars could be launched by the middle of the next decade (2010–2020).*

The detection of Earth-like planets will not be easy. The targets are faint and located close to parent stars that are > 1 million times (in the infrared) to > 1 billion times (in the visible) brighter than the planets. However, the detection problem is well defined and can be solved using technologies that can be developed within the next decade. We have identified two paths to the TPF goal of finding and characterizing planets around ~150 stars out to distances of about 15 pc:

- At visible wavelengths a large telescope (4×10-m elliptical aperture in one design and an 8×8-m square aperture in another) equipped with a selection of advanced optics to reject scattered and diffracted starlight (apodizing pupil masks, coronagraphic stops, and deformable mirrors) can make direct images of reflected light from Earths. While conceptually simple to operate, this instrument offers significant technical challenges at the component level, including construction of a very high surface quality (~1–5 nm rms), large aperture telescope and precise (< $\lambda/3{,}000$) and stable (< $\lambda/10{,}000$) wavefront control. The time to survey 150 stars three times each to ensure high reliability detections of planets is estimated to range from 45 days for one coronagraph design to 2 years for one of the shaped-pupil designs using a lower-precision primary mirror.

– At mid-IR wavelengths nulling interferometer designs using from three to five 3–4-m telescopes—located on either *separated spacecraft* or on a *large 40-m structure*—can directly detect the thermal radiation emitted by Earth-like planets. While no single component appears to be unusually challenging, this architectural class presents significant technical challenges at the system level, including passive cooling, nulling, beam transport, and formation flying or large precision deployable structures. The time to survey 150 stars three times each is estimated to be approximately 120 days for both of the interferometer concepts.

The TPF-SWG established that observations in either the optical/near-infrared or thermal infrared wavelength region would provide important information on the physical characteristics of any detected planets, including credible signposts of life. In fact, the two wavelengths provide complementary information so that in the long run, both would be desirable. The choice of wavelength regime for TPF will—in the estimation of the TPF-SWG and the independent Technology Review Board—be driven by the technological readiness of a particular technique.

The TPF-SWG also felt strongly that there were important scientific questions that could be addressed by missions of smaller scale than the fully capable TPF. For example, a mission of lesser capability would be able to detect Earths around a few tens of stars within ~8 pc, should any exist, and study the composition and physical properties of gas-giant planets around stars as far away as 50 pc. Such a mission—perhaps consistent with the scale of NASA's Discovery or New Frontiers programs—might be carried out either in the visible (an active coronagraph on an apodized 2–3-m aperture) or in the infrared (a nulling interferometer with ~1–2-m telescopes on 10–20-m structure).

Each team investigated the prospects of its designs for general astrophysical observations, assuming it were possible with a low additional cost to the overall mission. A large, conventional telescope equipped with a visible coronagraph readily lends itself to a traditional suite of astronomical instrumentation. An infrared interferometer offers dramatic gains in sensitivity and angular resolution, but would probably be used for more specialized classes of targets such as star-forming disks or the cores of active galaxies.

The challenge of developing the technologies required to enable either of the candidate architectures will require substantial funding over the next four years to bring them to the appropriate level of readiness. Based on results from the industrial/academic studies and the advice of the independent Technology Review Board, the TPF Project has developed a plan incorporating mission studies, technology development, and scientific research. Much of the content of this program will be selected through competitive opportunities for universities and industry using either NASA Research Announcements or JPL procurements. The status of these developments, as well as mission-design concept studies of each of the architectures, will be reviewed annually to support a final architectural selection at the earliest opportunity, but no later than 2006. TPF is planned to begin the formulation phase in 2007.

Finally, it should be noted that scientists from the European (ESA) and Japanese (ISAS) space agencies participated in these discussions as members of the TPF-SWG. The scientific exchanges suggested considerable interest in an international collaboration on a mission to address one of humanity's oldest questions, "*Does life exist beyond our Earth?*"

2 Science Goals for TPF

2.1 Statement of Science Requirements

The scientific motivation and goals for the Terrestrial Planet Finder (TPF) have been described in a series of reports over the past decade (*The TOPS Report*, 1992; *The ExNPS Report,* 1996; the *HST and Beyond Report,* 1996; and the *Terrestrial Planet Finder Book*, 1999). The interested reader is referred to these documents for more detailed information and numerous references to the scientific and technical literature. Building on these earlier statements of the goals for the mission, the TPF-Science Working Group (TPF-SWG) adopted three baseline requirements for TPF, as outlined in the Design Reference Program (see inset next page).

1) TPF should search for habitable planets around a sufficient number (~150) of nearby solar-type stars so that the mission would have a reasonable likelihood of success in finding planets or, at least, would set a statistically meaningful upper limit in the event that no such planets were found. TPF should also be able to characterize the physical properties of the brightest Earth-like planets, including a search for potential biomarkers.

2) TPF should provide information on all the constituents (large planets, dust clouds, etc.) of the planetary systems it observes.

3) TPF should carry out a significant program of general astrophysics observations, if these are possible at little or modest incremental cost to the mission.

Each study team was free to interpret these goals in light of the capabilities of its particular concept(s). As described in Section 3.3, a primary scientific metric derived from these criteria was the total time required for a particular instrument to carry out an initial survey of stars and the spectroscopic follow-up needed to look for atmospheric and biological signatures.

TPF Design Reference Program
TPF Science Working Group

From a humanistic perspective, one of the most profound questions that modern science can address is whether or not Earth-like planets—habitable or already life-bearing—exist elsewhere in the Universe. Thus, a defining goal of NASA's Origins program is to understand the formation and evolution of planets and, ultimately, of life beyond our Solar System. This goal requires a complete census of planets orbiting nearby stars down to the mass of the Earth; an understanding of the physical and biological processes that make a planet habitable and that might lead to the evolution of a "living" planet and the direct examination of nearby planets for signs of life. With these objectives in mind, we define the primary goal for Terrestrial Planet Finder (TPF) as follows:

I. Primary Goal for the Terrestrial Planet Finder (TPF)

The Terrestrial Planet Finder (TPF) must detect radiation from any Earth-like planets located in the habitable zones surrounding ~150 solar-type stars (spectral types F, G, and K). TPF must: 1) characterize the orbital and physical properties of all detected planets to assess their habitability; and 2) characterize the atmospheres and search for potential biomarkers among the brightest Earth-like candidates.

II. The Broader Scientific Context

Our understanding of the properties of terrestrial planets will be scientifically most valuable within a broader framework that includes the properties of all planetary system constituents, e.g., both gas giant and terrestrial planets, and debris disks. Some of this information, such as the properties of debris disks and the masses and orbital properties of gas-giant planets, will become available with currently planned space or ground-based facilities. However, the spectral characterization of most giant planets will require observations with TPF. TPF's ability to carry out a program of comparative planetology across a range of planetary masses and orbital locations in a large number of new solar systems is by itself an important scientific motivation for the mission. The architecture studies should address how particular designs will be able to contribute to our physical understanding of gas-giant planets around nearby stars.

III. Astrophysics with TPF

An observatory with the power to detect an Earth orbiting a nearby star will be able to collect important new data on many targets of general astrophysical interest. Architectural studies should address both the range of problems and the fundamental new insights that would be enabled with a particular design.

2.2. Biomarkers Suitable for TPF

Early TPF-SWG discussions made it apparent that observations in either the visible or mid-infrared portions of the spectrum were technically feasible and scientifically important. A sub-committee of the TPF-SWG was established under the leadership of Dr. Dave Des Marais, an astrobiologist from the NASA Ames Research Center, to assess the wavelength regimes for biomarkers suitable for addressing TPF science requirements. Their report (Des Marais et al. 2001; Des Marais et al. 2002) can be summarized briefly as follows (Figures 2-1 and 2-2):

- Photometry and spectroscopy in either the visible or mid-IR region would give compelling information on the physical properties of planets as well as on the presence and composition of an atmosphere.
- The presence of molecular oxygen (O_2) or its photolytic by-product ozone (O_3) are the most robust indicators of photosynthetic life on a planet.
- Even though H_2O is not a bio-indicator, its presence in liquid form on a planet's surface is considered essential to life and is thus a good signpost of habitability.
- Species such as H_2O, CO, CH_4, and O_2 may be present in visible-light spectra (0.7 to 1.0 μm minimum and 0.5 to 1.1 μm preferred) of Earth-like planets.
- Species such as H_2O, CO_2, CH_4, and O_3 may be present in mid-infrared spectra of Earth-like planets (8.5 to 20 μm minimum and 7 to 25 μm preferred).
- The influence of clouds, surface properties, rotation, etc. can have profound effects on the photometric and spectroscopic appearance of planets and must be carefully addressed with theoretical studies in the coming years.

The TPF-SWG agreed that either wavelength region would provide important information on the nature of detected planets and that the choice between wavelengths should be driven by technical considerations.

From the Executive Summary of the
Report of the TPF Biomarkers Group (Des Marais et al., 2001)

The minimum required mid-infrared wavelength coverage from 8.5 to 20 µm includes CO_2, O_3, and H_2O. The preferred mid-IR coverage from 7 to 25 µm adds CH_4 and H_2O rotation bands. The minimum required VIS-NIR wavelength coverage from 0.7–1.0 µm includes O_2, H_2O, CH_4, and O_3. The preferred VIS-NIR coverage from 0.5 to ~1.1 µm adds CO_2 and the broadband absorption by O_3. O_3 might be detected in a UV range (at 0.34 to 0.31 µm), however more studies are required to evaluate potential interferences.

Detection of O_2 or its photolytic product O_3 is the highest priority because it is the most reliable biomarker gas. However, we must be cautious of "false positives" due to abiotic O_2 sources. Three additional features share equivalent priorities. First, water vapor bands can indicate the presence of liquid water, which is essential for life, but they can also indicate H_20 situated high in a Venus-like atmosphere or else an ice-covered planet. Second, the carbon gases CO_2 and CH_4 offer multiple benefits. CO_2 is required for photosynthesis and for other important metabolic pathways. The combination of CO_2 and CH_4 provide useful information about the planet's oxidation state; CO_2 can indicate a solar system-like terrestrial planet, and CH_4 might be a biomarker in cases where hydrothermal emission of CH_4 is relatively minor. Third, albedo and temperature of the observable emitting region of a planet can give its size, which is important for confirming the presence of a terrestrial planet and also indicating whether it is geologically active, an essential requirement for habitability. Planet size can be estimated in the mid-infrared, but not in the visible to near- infrared range.

Both the mid-infrared and the visible to near-infrared spectral ranges offer valuable information regarding biomarkers and planetary properties, therefore both ranges merit serious scientific consideration for TPF. The best overall strategy for the Origins program includes a diversity of approaches, therefore both wavelength ranges ultimately should be examined prior to launching the "Life-Finder" mission.

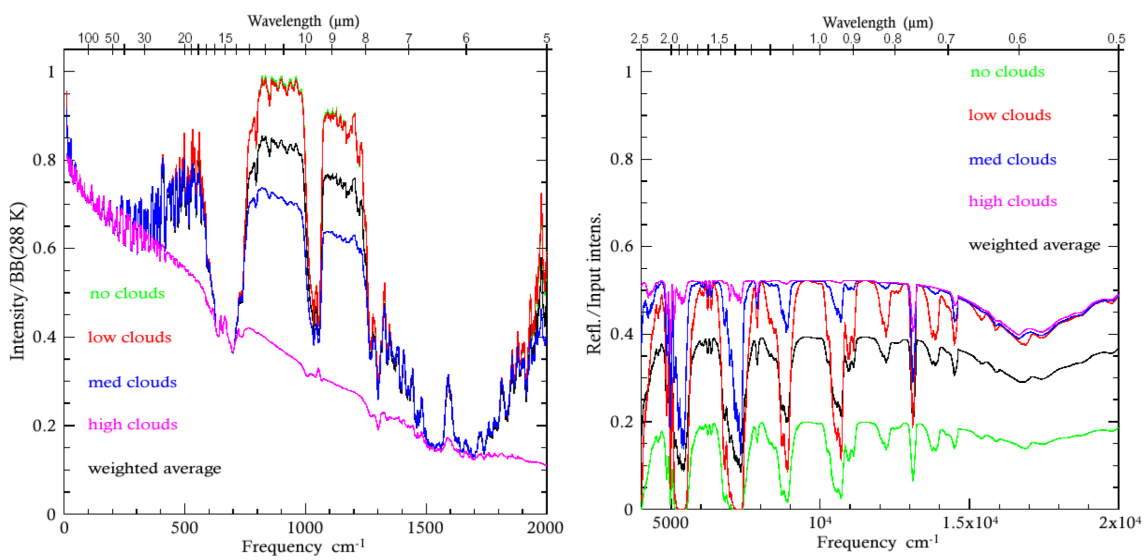

Figure 2-1. Models of the mid-IR and visible light spectra of the Earth showing key spectral features as well as the influence of clouds on the emergent spectra.

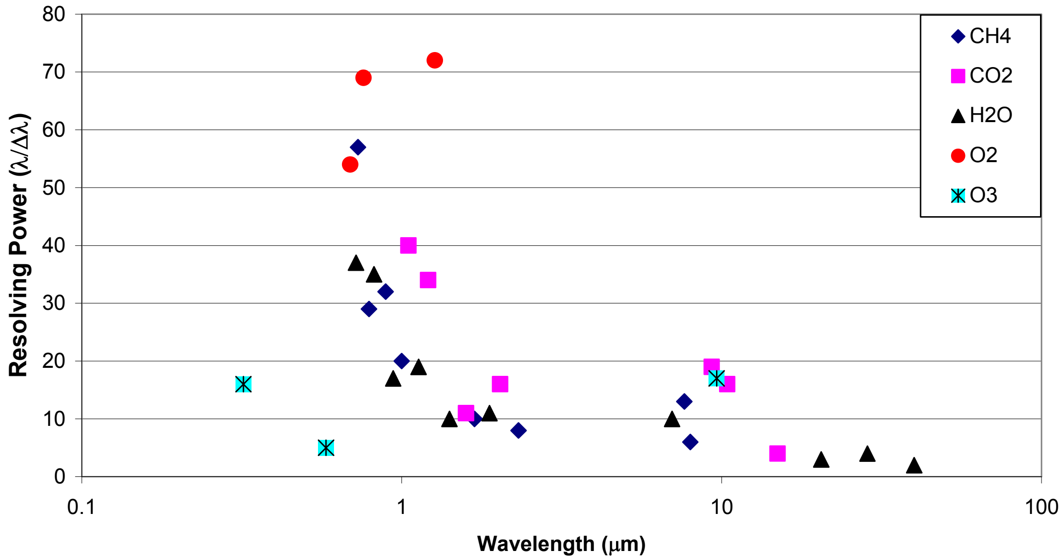

Figure 2-2. The wavelengths of key species and the spectral resolving power needed to resolve those lines as they appear in the Earth's atmosphere (Appendix C). The visible lines typically require greater spectral resolution for detection than those in the mid-IR (Des Marais et al. 2002).

2.3. TPF Precursor Science

The TPF-SWG addressed the issue of what astronomical information might be pertinent to the definition of TPF. Two key topics were identified as desirable for further investigation.

2.3.1 Distance to Nearest Habitable Planets

Probably the largest unknown affecting the design of TPF is the distance to the closest habitable planets. From the most naïve signal-to-noise (SNR) considerations in either the visible or the infrared, the diameter of the collecting aperture needed to detect a planet scales directly with distance. In addition, the telescope size (or interferometric baseline) needed to resolve the "habitable zone" scales with distance for a star of a given spectral type. Both of these effects make it much harder to find Earths at 15 pc than at 5 pc. There was considerable discussion within the TPF-SWG as to whether TPF should conduct a survey of 150 stars or whether a simpler, less expensive mission might target only the nearest stars. The successful flights of the recently selected Kepler (NASA) and Eddington (ESA) missions will, before the end of this decade, give us statistical information on the incidence of Earths using the planetary transit technique. This information will be useful in setting the distance out to which TPF must look to have a high probability of finding planets. For the present study the TPF-SWG took the conservative approach of requiring TPF to make a complete survey of ~150 nearby stars. As discussed further in Section 6.5, a smaller-scale version of TPF could study Earths around the closest stars (< 8 pc).

2.3.2 The Environment of Habitable Earths

2.3.2.1 The Existence of a Stable Habitable Zone

The presence of giant planets can have an enormous effect on the existence of stable orbits suitable for habitable planets. Much of the information needed to assess the suitability of individual nearby stars as TPF targets will come from astrometric and radial velocity measurements. Of particular importance to this investigation is continuing support for ground-based radial velocity measurements, and the astrometric capabilities of the Keck Interferometer, the VLT Interferometer, and the Space Interferometer Mission (SIM). A dynamical census of nearby planetary systems is important for selecting TPF targets as well as for determining the masses of any planets detected by TPF.

2.3.2.1 Exozodiacal Clouds

Searches for planets are susceptible to interference from zodiacal dust emission in the target system. This emission adds both photon noise and the possibility of confusion between planets and structures in the zodiacal clouds. These effects become serious when the level of zodiacal dust exceeds about 10 times that in our own solar system (*TPF: Terrestrial Planet Finder*, Beichman et al.1999). This is important for future missions because, as discussed in Section 3.3.5, both the interferometers and the coronagraphs show a two- to four-fold increase in integration time per star as the amount of extra-zodical light increases from the level within our solar system to 10 times that amount. The visible instruments are somewhat more robust against zodiacal emission. The SIRTF mission will provide extensive information on the Kuiper Belts (10–500 AU) of potential TPF targets while the Keck, Large Binocular Telecscope (LBT), and VLT interferometers will provide information on zodiacal clouds inside 1 to 10 AU.

3 Summary of Concepts Studied

3.1. Phase I Concepts

In May 2000, the four study teams began their investigations into architectures capable of performing the TPF mission. The teams, composed of scientists, engineers, and technologists, were asked to analyze the ability of different architectures to perform the basic TPF mission and to assess the technical feasibility of the various concepts. In the first phase of the studies the teams were encouraged to explore the broadest possible range of ideas. In the second phase the teams carried out detailed analyses and trade studies on the most promising approaches for a TPF mission planned to start development around 2010.

Each of the study teams defined their own approach for identifying and evaluating mission concepts. The Phase I concepts are shown in Table 3-1. They generally fall into three categories—the two largest categories are interferometers and coronagraphs, with most of the interferometers designed to detect the thermal infrared signal from planets, and most of the coronagraphs designed to detect the visible light reflected from the parent star. Within each of these two categories is a broad range of architectural concepts. The third category consists of architectures that are neither interferometers nor coronagraphs. In general, the mission concepts in the third category either cannot perform the full TPF mission of detection and characterization or are based on new technologies that are judged well beyond what is achievable in the next decade. Examples of these are a separated-spacecraft Fresnel-lens coronagraph, and a separated-spacecraft occulter. A number of concepts that do not satisfy the full mission requirements do, however, provide complementary science about the formation of planetary systems.

After about seven months of work, each team provided a ranked list of their five preferred designs at the preliminary architecture review in December 2000. The original plan for the architecture studies was to select the two most viable concepts from each team for more thorough investigation. Budgetary constraints, however, resulted in the Project funding only one in-depth study per contractor. With additional input from the study teams and the aid of the TPF-SWG, JPL selected from among the top-ranked concepts to provide a diverse set of concepts for more detailed study. Some of the contractors elected to investigate an additional concept at a lower level of effort. The results of these detailed studies, including a re-examination of the JPL separated spacecraft interferometer concept, are summarized in Table 3-1.

Table 3-1. Phase I Architectural Concepts

Architecture Families	Variants
Ball Aerospace	
Interferometers: Including nulling with connected structures; tethered in 1-D and 2-D; Separated Spacecraft: Laurance hexagon, dual-Bracewell, Mariotti array Fizeau imager	10
Coronagraphs: Including Spergel-Kasdin pupil; image-plane masking; "microtube" block, focal-plane phase mask	7
Occulting screens	2
Hypertelescope	2
Boeing-SVS	
Interferometers: Including nulling with separated spacecraft or connected structure	3
Coronagraphs: Including apodized square apertures in 3, 10, 30 m size; Lyot coronagraph; phase-mask coronagraph; four-quadrant coronagraph	7
Hypertelescope: Including snapshot imaging array, redundant linear array	3
Laser-trapped ion mirror	1
Lockheed-Martin (LMSS)	
Free-flying interferometers	4
Fizeau interferometer	1
Structurally connected interferometers	3
Tethered interferometers	1
Coronagraphs	1
TRW	
Large-aperture coronagraph	3
Structurally connected interferometer	1
Separated spacecraft interferometer	7
Separated sunshield and spacecraft	1
Fresnel coronagraph w/free flying elements	1
100-m sparse aperture	1
Free-flying occulter	1

3.2. Phase II Concepts

The four study teams plus JPL investigated four major concepts with a number of variants: a nulling IR interferometer, a visible coronagraph, an IR coronagraph, and a hypertelescope (sparse-aperture IR coronagraph), as listed in Table 3-2. High-level descriptions of these architectures are given below; more detailed information is available in the final reports from the teams and, for the separated spacecraft interferometer, in the TPF Book (Beichman et al. 1999). The descriptions given below were assembled using inputs from the individual teams, the TPF-SWG, the independent TPF Technology Review Board, and the TPF Project team at JPL.

Table 3-2. Phase II Architecture Studies

Study Team	Architecture Class
Ball Aerospace	Shaped-pupil, Visible-Light Coronagraph, Classical Coronagraph
Boeing-SVS	Non-Redundant Linear Array (hypertelescope), Apodized Square Aperture (partial study)
Lockheed-Martin (LMSS)	IR Interferometer (structurally connected and separated spacecraft)
TRW	Large IR Coronagraph
JPL	Re-examination of Separated Spacecraft IR Interferometer (TPF Book design)

3.2.1 Visible Coronagraph (Ball Aerospace)

3.2.1.1 Basic Description

The Ball Aerospace team evaluated the performance of a visible-light coronagraph and determined that a single large telescope with a light-collecting area of about 30 m^2 is needed to complete both the planet search and astrophysics observations in the allotted five-year mission time.

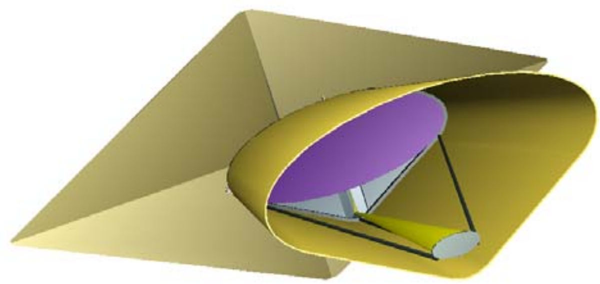

Figure 3-1. The Ball system uses an off-axis, elliptical 4 × 10-m telescope.

The design uses a large, thermally-shielded coronagraph, an elliptical primary mirror, 4 × 10 meters in size with shape control actuators, and a deformable mirror located at an interior pupil plane. This system maintains extremely high wavefront quality and minimizes the scatter of light from the planet's host star. With the spacecraft in an environmentally benign part of our solar system, either in an L2-halo or a heliocentric-drift-away orbit, the optical surface figures are *actively* maintained during an observation with a stability better than $\lambda/10{,}000$. The design team studied the ability of 1) a *classical coronagraph* using image-plane masks and 2) specially *shaped pupil* masks (such as the Spergel-Kasdin pupil) to provide a large region around the image of a star, free of scattered light, in which to search for planets. Nearly all the diffracted and scattered starlight is diverted from that region, permitting planet detection in modest integration times.

In the Ball coronagraph designs, the search area extends from approximately four Airy rings in the image plane ($5\lambda/D$) out to $N\lambda/D$ where N is the number of actuators across the aperture on the deformable mirror. For D = 10 m (the long axis of the Ball elliptical mirror) and a 10^4 element deformable mirror, N = 100, the search area extends from ~50 mas to ~1500 mas at 0.5 μm. Because of the high optical quality and angular resolution of the system, the ratio, *Q,* of the planet's brightness to the background light (from diffracted and scattered starlight, and exozodiacal emission) is approximately unity.

3.2.1.2 Strong Points

1) With the performance assumptions made in this study, the Ball coronagraph has an observing efficiency that is 2 to 3 times better than a mid-infrared interferometer. The time to search the 150 most favorable stars (once each) is 50 days with the shaped-pupil and 15 days with the classical coronagraph. H_2O (at terrestrial levels) can be detected with integration times of under 15 hours, even for the case of a target with exozodiacal emission 10 times greater that in our solar system. O_2 can be seen in less than two days for most cases.

2) The coronagraph or shaped-pupil designs are more robust than interferometers for detecting planets in systems with large amounts of zodiacal dust. In the coronagraph, the

exozodiacal light is resolved into many ~0.1-AU-sized pixels with a relatively low influence on the instrumental noise. By contrast, for the interferometer, the planet light as well as all the exozodiacal light within the diffraction beam of the primary mirror (typically a few AU at the star) falls on one detector, adding noise and possible confusion. It should be noted that, as described in Section 3.3.5, both systems, coronagraphs and interferometers are significantly affected at zodiacal levels exceeding 10 times that of our solar system.

3) A wide range of critical astrophysical observations can be made with modest investments in additional instrumentation. Diffraction-limited performance at ultraviolet wavelengths is an exciting possibility if adequate steps are made to maintain a contamination-free environment.

3.2.1.3 Weak Points

The main challenges for the visible-light coronagraph are maintaining extremely accurate wavefront control (for suppression of scattered starlight), and the manufacture and deployment of a very large aperture *monolithic* telescope in space. Thermal and vibrational disturbances to the wavefront must be kept very small, as must reflectivity irregularities on the mirror surfaces. For the classical-coronagraph design, the transmission of the pupil masks must be controlled very accurately. For the shaped-pupil design, the small size of azimuth-angle sector with good starlight suppression close to the star necessitates a large number of instrument rotations (up to 9) to search for planets throughout the inner regions of the habitable zone.

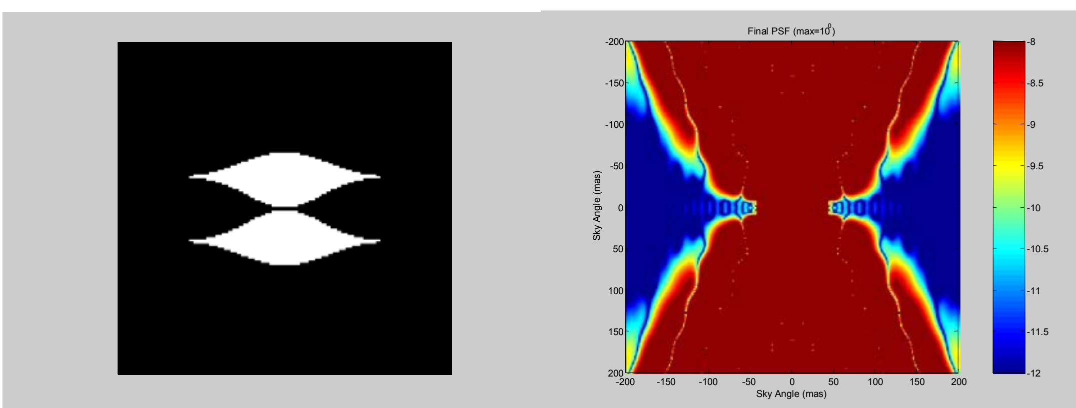

Figure 3-2. The shaped-pupil mask (left) operating with an elliptical telescope produces two dark areas for planet searches (right).

3.2.1.4 Areas Of Chief Concern

- TPF would have to develop wholly new techniques for manufacturing a large (> 10 m), lightweight, highly polished (1–5 nm rms surface error, depending on spatial scale), monolithic mirror for space.
- The effects of any print-through patterns present on the monolithic mirror surface due to the structure of the back surface must be thoroughly understood and carefully controlled.

- The modeling and laboratory tests must be carried out to demonstrate that wavefront errors can be both measured and corrected at the required levels of precision (λ/3,000) and stability (λ/10,000).

3.2.1.5 Precursor Possibilities/Requirements

Obvious technological and scientific precursor opportunities would involve smaller coronagraphs, with apertures ranging from 1.5 to 4 meters, in low-Earth or heliocentric orbits. Small versions would detect Jupiter-sized planets out to large distances, while a 4-m coronagraph might even observe a few Earth-sized planets around the nearest 10–20 stars. Such precursors could demonstrate the potential of a coronagraph to maintain the wavefront accuracy and stability for the integration times needed to observe Earth-like planets with a larger system.

3.2.1.6 Other Astrophysics

The particular advantages for astrophysics of the single large-aperture telescope include its wide field-of-view and suitability for use with large detector arrays, its very highly-corrected optical wavefront (enabling diffraction limited imaging at ultra-violet wavelengths), and its ability to incorporate a variety of instruments sharing the field-of-view either spatially or temporally. The instruments would help greatly to add to our knowledge about most objects and phenomena which represent objectives for NASA's Origins and Structure and Evolution of the Universe themes. Likely instruments would include the following:

- A planet-finding coronagraph, a narrow-field, high-contrast, imaging instrument with a variety of pupil stops and image stops to operate at desired contrast levels in specified spectral bands at selected angular separations from bright sources; it could also house an embedded medium-resolution spectrograph.

- A wide-field UV/visible imager to gather very high-resolution images of faint objects such as distant galaxies.

- A powerful UV/visible high-resolution spectrograph to take advantage of the telescope's large aperture and wide spectral coverage. With a collecting area 8 times that of the Hubble Space Telescope (HST), the spectroscopic sensitivity would be up to 64 times better than that of the HST.

3.2.1.7 Project Assessment

A visible-light coronagraph or shaped-pupil system working in conjunction with an advanced deformable mirror would be a powerful instrument for planet searches and general astrophysics. However, the angular resolution needed to put the habitable zones of a reasonable sample of stars at a minimum angular separation of ~5λ/D forces a minimum dimension for at least one axis of the telescope to be ~10 m. The requirement for low scattering forces the telescope to be a monolith of unprecedented size and smoothness (1–5 nm rms depending on spatial scale); this despite the use of an active deformable mirror yielding the required precision of λ/3,000. Together these attributes would make the ratio, Q, of planet's brightness to that of residual and scattered light equal to unity. Under these assumptions, the Ball design can detect and characterize Earths out to ~15 pc.

However, the resultant performance comes at a steep cost. The technology panel emphasized that the manufacture of such a telescope is well beyond the state of the art for ground-based, not to mention space-based, optical systems. The fabrication of this telescope represents a major challenge for TPF that will require a very substantial investment in technology and facilities. A segmented mirror with its gaps oriented parallel to the minor axis of the telescope might ease the fabrication problem with, perhaps, only a modest impact on performance. A particular strength of this design is that a mission of smaller scale (2–4-m diameter telescope) is potentially within the realm of present day technology. Such a mission would be able to detect and characterize Jupiters around other planets and even detect Earths around the nearest few stars, if such planets exist. In summary, the Project recommends that NASA investigate actively-controlled coronagraphs for TPF and potential precursor missions.

3.2.2 Apodized Square Aperture (Boeing-SVS)

3.2.2.1 Basic Description

The Boeing-SVS team examined a design called the Apodized Square Aperture (ASA) which would accomplish the TPF mission with a segmented, 8-m square primary operating in the 0.5–1-μm wavelength range, using a specialized apodizing mask and a prism spectrometer for atmospheric characterization. The mirror quality is λ/1,800 over the critical range of spatial frequencies (3 to 30 cycles over the aperture). The system uses an off-axis primary mirror to minimize diffraction from the edges of the telescope and from the support structure of the secondary mirror.

A pupil mask with radially-variable transmission (several radial functions provide adequate performance) provides an apodization that suppresses the sidelobes of the diffraction pattern of the square aperture. It also suppresses stellar light in the four quadrants of the image plane while leaving the planetary light intact (Figure 3-3). The entire search space around a star can be imaged with two rotations of the telescope.

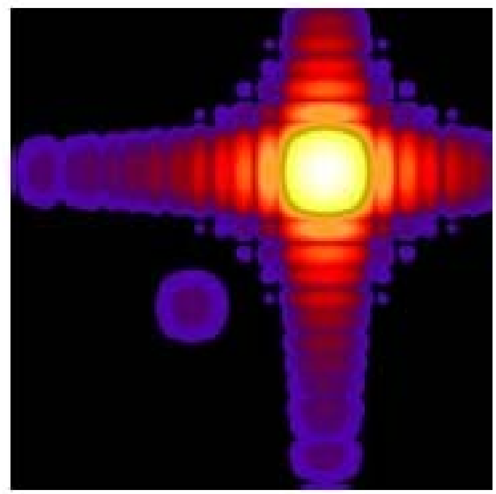

Figure 3-3. The combination of a square aperture and a Sonine-function apodization mask reduces the diffracted starlight so that a planet 10^8 fainter than its star can be seen in this simulation.

3.2.2.2 Strong Points

The ASA would be able to survey 150 stars in approximately 290 days (one visit per star). As an imaging system, it would provide data that would allow a straight-forward interpretation of multi-planet systems and would be readily adaptable to other astrophysical investigations. The design could leverage the Next Generation Space Telescope (NGST) design in terms of primary mirror and sun-shade deployment as well as L2 operations. The ASA is tolerant of low and very high-frequency wavefront errors that scatter light into the image core or to the far wings. Like NGST, the ASA can be put into orbit with a single launch. The ASA performance has multiple cost and risk mitigation options, including changes to the primary size, the wavelength range, the surface accuracy, the wavefront error correction, and the integration time. The design is easy to scale up or down as our knowledge of the distance to the closest planets improves in the coming years.

3.2.2.3 Weak Points

Improved performance would require improved wavefront quality for operation at higher Q, e.g., $Q \approx 1$ as in the Ball design, which could be obtained through either fabrication of a primary mirror of extreme quality (Section 3.2.1) or the addition of a static or active correction element. As proposed, the ASA operates at a low planet-to-scattered-light ratio, $Q \approx 0.01$, which lowers the achievable SNR for planet detection. The higher residual stellar background places stringent requirements on the stability of the system for accurate background subtraction. The (probable) need to assemble the 8-m square aperture system on orbit raises a variety of concerns.

3.2.2.4 Areas of Chief Concern

The areas of chief concern for the ASA include the optical surface quality and stability, the levels of amplitude error in the apodization masks, the effects of segmentation of the telescope primary mirror, spacecraft body pointing, and image stabilization. The ASA concept relies on a high quality wavefront to provide high dynamic range.

3.2.2.5 Precursor Possibilities/Requirements

Several ASA concepts of different sizes have been studied, resulting in a range of performance and budget options. This progressive approach incrementally advances the TPF science, while reducing implementation risks. A TPF precursor using a 3-m Apodized Square Aperture could perform an important science mission, that of surveying and characterizing gas giants around stars in the solar neighborhood.

3.2.2.6 Other Astrophysics

In satisfying the TPF mission with a high-dynamic-range imager, the ASA concept offers exciting astrophysics capability, comparable to those described above for the Ball design. No augmentation or optimization apart from the addition of suitable focal plane instrumentation is required to implement the astrophysical capabilities of the TPF mission.

3.2.2.7 Project Assessment

The strengths and weaknesses of the ASA design are similar to those described above for the Ball coronagraph. In particular, the development of large, lightweight, high-quality optics (0.35 to 4 nm rms on various spatial scales) represents a difficult technological challenge. The segmented nature of the 8 × 8-m primary will require careful manufacture and on-orbit alignment to enable diffraction-limited matching of four telescopes into the equivalent of a single large telescope. The nominal ASA design operates without a deformable mirror and thus operates at a lower Q than the Ball system, 0.01 versus 1. The addition of a deformable mirror to the ASA concept represents a mitigation against residual scattered light that would bring the performance of ASA closer to that of the Ball design. The two systems would then be distinguished primarily by the angular resolution of an 8 × 8-m versus a 4 × 10-m telescope and the scattered light from a segmented mirror versus a monolith. The technology panel noted that fabricating the apodizing masks with the required precision and uniformity also represents a significant technological challenge.

3.2.3 Structurally Connected IR Interferometer (Lockheed Martin)

3.2.3.1 Basic Description

The Lockheed Martin (LMSS) team studied a structurally connected infrared interferometer with four 3.5-m diameter telescopes on a fixed 40-m baseline (Figure 3-4). The system uses four collinear telescopes, arranged as two interleaved Bracewell nulling interferometers with telescope spacings chosen so that stellar leakage does not compromise the overall system noise.

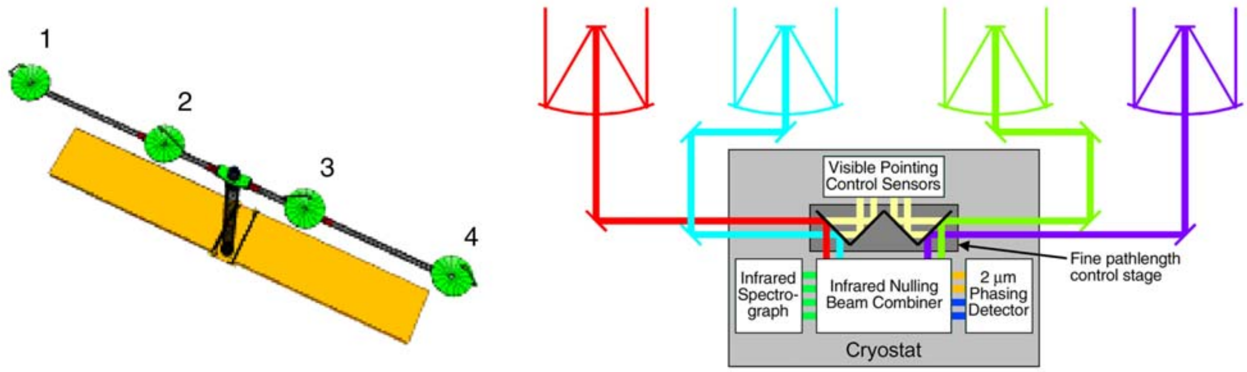

Figure 3-4. The Lockheed nulling interferometer uses four 3.5-m telescopes on a 40-m truss. Light can be combined in a number of nulling configurations.

The array is rotated, over a 6–8 hour period, around the line-of-sight to the star. The telescopes can be combined in pairs 1-2 and 3-4, or in pairs 1-3 and 2-4, to achieve the short or long baselines (28.6 and 11.4 m) used to observe distant or nearby stars. The nulled outputs of the combined pairs are then combined again and both outputs of the final combination are observed with an θ^4 null, or an effective θ^3 null with phase chopping. The system would be able to resolve the habitable zones of approximately 167 stars (including 1 M, 37 F, 88 G, and 41 K stars) with initial observations lasting 1 day or less per star. Key spectral lines (CO_2, H_2O, O_3, or CH_4) would be detectable with an SNR = 5 in integrations of a few days.

3.2.3.2 Strong Points

For system sizes of ~40 m or less, a structurally connected interferometer may be simpler to build and operate than a separated spacecraft interferometer. The truss enables the required rotation of the telescopes around the line-of-sight without the expenditure of large amounts of propellant. The structurally connected system would also have a simple beam transport scheme from the collectors to the combiner, and the entire structure could be passively cooled behind a single sunshade.

Table 3-3. Comparison of Different Nulling Architectures (Overall Length = 40 m; 10 μm)

Design	Resolution (mas)*	Null Depth (with chopping)	12 μm Null OPD Error (nm)	OPD Stability** (nm)	Planet/Stellar Leak @ 12 μm
OASES	68	θ^6	1×10^{-5}	0.3 nm	0.02
		(θ^4)	< 20		(Table A.4 in TPF Book)
Double Bracewell	36	θ^4	4×10^{-5}	0.1 nm	0.004
(LMSS)		(θ^3)	< 40		(Appendix F)

**Location of first maximum in null pattern.*
***Per chop (> 1 Hz)*

3.2.3.3 Weak Points

Large, ~40-m, precision structures represent a stowage and deployment challenge. A fixed interferometer configuration limits the angular resolution of the system and precludes tuning the null for each star, thereby limiting the range over which this version of TPF could look for and characterize planets (particularly at $\lambda > 15$ μm where CO_2 and the long wavelength lines of H_20 can be detected). This limitation places more stringent requirements on a nuller that must work at all angular scales. The LMSS design partially mitigates this problem by using different double Bracewell configurations for nearby and distant stars. The OASES interferometer design (Angel and Woolf 1997) discussed in Appendix A of the *TPF Book* (Beichman et al., 1999) provides a θ^6 null, or θ^4 with interferometric chopping, but requires a factor of ~2 greater physical separation to achieve comparable resolution (Table 3-3).

A comparison of the null patterns for the two designs, illustrated in Figure 3-5, shows both the improved efficiency of the new design, but also its shallower null, resulting in a lower ratio of planet signal to stellar leakage than in the separated spacecraft OASES design. While the overall *Q* of both interferometers (and thus the total photon shot noise) is dominated by the local zodiacal emission, the ratio of planet to stellar leak is five times worse for the new structurally-connected system, which has a correspondingly greater stability requirement (Table 3-3).

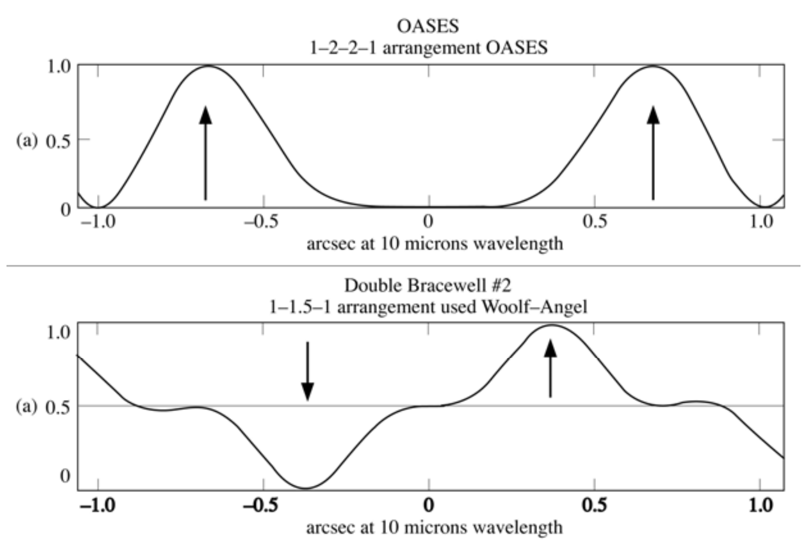

Figure 3-5. The nulling interferometer response function for the OASES (top) and dual-Bracewell (bottom) configurations. For the same overall baseline length, the dual-Bracewell design has better (a factor of 2) angular resolution.

Chopping of some sort will be essential for any interferometer since the overall Q is ~10^{-3}–10^{-4}. However, unlike the case of the large, single-aperture telescope, the majority of this background light is the very stable local zodiacal emission which can be effectively subtracted away in the interferometer by chopping at > 1 Hz.

Additional concerns with the structurally connected system include system mass, integration and test procedures for a large, cold truss structure and lack of scalability to missions requiring still longer baselines.

3.2.3.4 Areas Of Chief Concern

- The development of a cryogenic nulling system capable of the requisite 10^{-5} rejection ratio including optics design, mechanical implementation, beam splitters, dichroics, amplitude matching capabilities, phase plates and coatings, etc., will be a considerable technological challenge. Large scale, high-fidelity, ground-based testbeds will be necessary.

- The development and packaging of a large, 40-m, low-mass, deployable truss with suitable vibration characteristics represents a major challenge.

- Integration and test facilities and procedures represent formidable challenges and should be addressed early in the study phase.

3.2.3.5 Precursor Possibilities/Requirements

A structurally connected interferometer with two collectors on a modest-sized truss would demonstrate key technologies and could yield important science data on any existing nearby planetary systems. A system with two 60-cm diameter mirrors separated by 9 m could observe young, self-luminous Jupiter-like planets at 4 to 10 μm out to 50 pc. A larger system using two 1.4-m telescopes, separated by 18 m could search 26 nearby solar type stars at 8 to 12 μm for the presence of Earth-like planets.

3.2.3.6 Other Astrophysics

A structurally connected interferometer would be useful for exploring the angular structure of objects such as quasars/Seyfert galaxies and the disks around forming stars. The simplest interferometer would require that these objects have a central bright point source visible at ~2 μm (K ≈ 17 mag) to use as a phase reference. Even though the angular resolution of the 40-m truss system would not be as good as that of existing ground-based interferometers, the sensitivity of a space-based system would be orders of magnitude greater. The angular resolution of the 40-m interferometer would be much better than that of a 6-m NGST (60 mas vs. 420 mas at 10 μm).

3.2.3.7 Project Assessment

The structurally connected interferometer offers significant simplifications compared with the separated spacecraft version of TPF, including a single spacecraft with an uncomplicated operations concept, a constant geometry for beam transport, and straightforward cooling for the entire optical system. Compared with the separated spacecraft interferometer (*TPF Book* design), this system makes more effective use of baseline length at the expense of shallower, less flexible nulling. The biggest drawbacks of the structurally connected system include: 1) limited resolving power for a < 40-m system; 2) greater stability requirements implied by the shallower stellar null; and 3) the challenges of extending the design to a baseline greater than about 25 m. The connected interferometer would be a credible, low-risk system for a near-term implementation of TPF. A 40-m or larger system would come close to fulfilling the goals of the full TPF mission to survey 150 stars, but would, in the opinion of the technology panel, present a significant development risk. The Project recommends that a structurally connected interferometer be included as one of the designs in the next phase of the TPF program.

3.2.4 Separated Spacecraft Interferometer (Lockheed Martin and JPL)

3.2.4.1 Basic Description

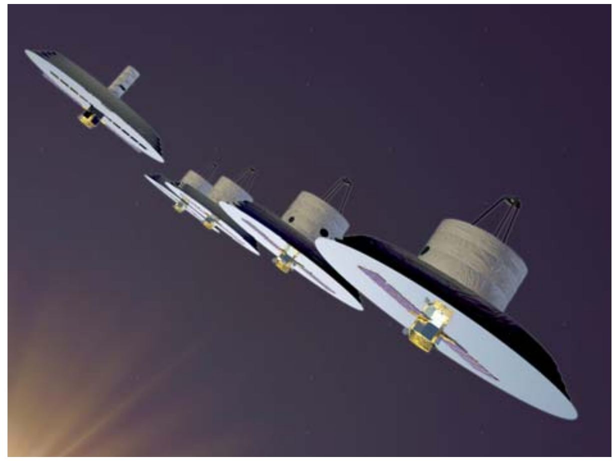

Figure 3-6. An artist's concept of the free-flying TPF constellation

The *TPF Book* (Beichman et al., 1999) describes a formation-flying, nulling infrared interferometer consisting of four spacecraft each supporting a 3.5-m telescope, and a separate spacecraft for the beam combiner (see also Woolf and Angel 1998). The optics on each spacecraft have a multi-layer thermal shield to provide passive cooling to 35 K. In the *TPF Book* design, the spacecraft are positioned along a line oriented normal to the direction of observation. In this position, they relay the starlight to a beam combiner to maintain the optical paths through the system equal to within a few centimeters. The array is rotated around the line-of-sight over a 6-hour period while observing the source. The starlight is rejected in a nulling beam-combiner and the planet light is sent through a spectrometer. Two or more beam combining modules allow the flexibility of changing the observing mode (θ^6 null or θ^4 null with chopping). The free-flying interferometer described in the *TPF Book* is capable of observing planets and their atmospheres in a few hours (basic detection) to a few days (detection of O_3 at SNR = 5), which is comparable to the connected-interferometer design. Other similar designs are possible, such as ESA's Darwin mission which uses a two-dimensional formation-flying array that has some advantages for the rejection of exozodiacal light.

3.2.4.2 Strong Points

The ability to vary the interferometer baseline over a wide range greatly improves TPF's planet-searching capabilities since the width of the null can be tailored for observations of stars that have distances from a few parsec to beyond 20 pc. The outer limit of TPF's search space would be limited by sensitivity considerations (telescope diameter), not angular resolution (baseline). With the longer baselines possible with this system, it is feasible to arrange the interferometer configuration to have a sharper, deeper, null than is possible for the fixed-baseline system. The long baselines required for high-angular resolution at infrared wavelengths are easily achieved.

In the event of the loss of a spacecraft, appropriate subsystem design could conceivably allow the remaining spacecraft to be repositioned into an optimum configuration, although with less capability. The possibility for this system to have a "graceful degradation and reconfiguration" might safeguard its science throughput (compared to a structurally-connected system) should failures occur.

The ancillary astrophysics program would benefit from much longer baselines than are possible with present ground-based systems. The ability to perform milliarcsecond imaging using baselines as long as 1 km would represent a breakthrough capability in many fields of astronomy.

The successful implementation of a formation flying architecture for TPF would pioneer techniques for later, yet more ambitious missions. A separated spacecraft interferometer dramatically breaks the linkage between telescope aperture and maximum baseline, revolutionizing high-resolution imaging in a way that can be used for astronomy missions from the submillimeter to x-ray wavelengths.

The integration and testing of a formation flying interferometer might be simpler than that of an interferometer on a structure; the full interferometer may be tested in its closest configuration, requiring only a fraction of the volume necessary to test a structure-based system.

3.2.4.3 Weak Points

- The free-flying interferometer will require multiple spacecraft buses and a complex system for command and control. Extensive technology development, possibly including a flight demonstration, will be required to develop the hardware and software for formation flying.

- Contamination of optical surfaces by exhaust propellant from neighboring spacecraft may degrade the optics and the performance of the thermal shields. Electromagnetic formation flight for array position maintenance, re-targeting, and momentum management provides an interesting alternative. Initial studies indicate that such an alternative to propellant-based formation flight may be realized for modest penalty in mass (~5% to 10%) when compared to propulsion systems with I_{sp} = 1000 s.

- As with the structurally-connected interferometer, the development of a cryogenic nulling system capable of the requisite 10^{-5} rejection ratio will be a considerable technological challenge. Technology to be developed includes the optics design, mechanical implementation, beam splitters, dichroics, amplitude matching capabilities, phase plates and coatings, etc. Large scale, high-fidelity, ground-based testbeds will be necessary.

- Coordinating coarse formation flight with fine optical pointing and phasing control, poses a challenge, especially if drift-through fringe tracking is required for adequate science throughput. Structurally-connected systems provide this coarse alignment through passive means. This extra layer of staged control needs to be refined.

- Stray light suppression and beam transport present difficult challenges when large and variable baselines are used, since there would be no continuous sunshield across all the interferometer elements.

3.2.4.4 Areas Of Chief Concern

This architecture will require the development of technologies for cryogenic nulling and formation flying. In addition, a formation-flying precursor may be necessary to validate this technology before embarking on the full TPF mission. The integration and testing of the interferometer will be challenging.

3.2.4.5 Precursor Possibilities/Requirements

A technology precursor such as StarLight (NASA) and SMART-2/3 (ESA) can test formation flying maneuvers and demonstrate closed-loop operation of the spacecraft-telescope-interferometer combination. A science and technology precursor consisting of a cold IR nulling interferometer using modest apertures on a truss would reduce the risk of developing and operating the full TPF system.

Missions like StarLight and SMART-2/3 could provide end-to-end systems-level demonstrations of combined formation flight and interferometer operation. However, lower cost and more near-term (FY 2003 to FY 2005) flight facilities, such as SPHERES (http://ssl.mit.edu/spheres), can provide a cost-effective means for maturing the formation metrology, autonomy, path planning and control algorithms.

3.2.4.6 Other Astrophysics

As mentioned above, the separated-spacecraft version of the infrared interferometer would provide a dramatic new capability for astronomy. With baselines as long as 1 km and operation at wavelengths as short as 3 μm in the non-nulling mode, TPF would offer sub-milliarcsecond resolution with NGST-like sensitivity. With *uv*-points collected as telescopes drifted radially between rotational steps, TPF would be able to produce complex images of the central regions of many interesting astronomical objects, from planetary nebulae and star-forming disks to distant quasars.

3.2.4.7 Project Assessment

The separated-spacecraft system represents the most general and powerful of the nulling interferometer concepts. The longer baselines and the prospect of two-dimensional array configurations make it possible to consider deeper and more complex nulling patterns tuned to each star and extending to larger distances and longer wavelengths. These are fundamental advantages to this architecture. However, formation flying and the associated beam transport represent substantial technology challenges that must be overcome before implementing this architecture for TPF. The Project recommends that the structurally connected and separated spacecraft versions of this architecture be carefully investigated by NASA for optimum cost, risk, performance, and schedule.

3.2.5 Hypertelescope (Boeing-SVS)

3.2.5.1 Basic Description of The Non-Redundant Linear Array (NRLA)

The Non-Redundant Linear Array (NRLA), studied by the Boeing-SVS team is a hybrid interferometer/coronagraph and exploits the concept of pupil densification at mid-infrared wavelengths. An array of seven 3-m telescopes is distributed along a 100-m long structure in a way that optimizes image formation and provides the angular resolution necessary to find planets. The telescopes and beam combiner would be cooled to < 40 K. Densification consists of rearranging the pupils so that the spacing between beams is reduced before forming an image. In contrast to other types of dilute aperture telescopes, the NRLA produces a compact, clean point-spread function. A phase mask in the image plane produces a highly-efficient coronagraphic nulling of the stellar light. The observatory, located at L2, rotates to collect data suitable for planet detection and characterization.

3.2.5.2 Strong Points

The NRLA exploits Fourier image synthesis, a mature technique in radio astronomy (with telescope arrays) and infrared wavelengths (with aperture masking). Optical interferometric beam combination, with path control and phasing, has also been developed for optical/IR long-baseline arrays. Hypertelescope design studies have been carried out by groups at the Observatoire de la Cote d'Azur, Observatoire de Haute Provence, and the University of Hawaii, with both lab and telescope demonstrations. The Goddard Space Flight Center Fizeau Testbed will include a pupil densification experiment. Detection of exoplanets in the mid-infrared directly yields an estimate of exoplanet temperature from the color temperature of the spectrum. The mid-infrared is also well suited for general astrophysics in the TPF-related areas of star formation and early evolution of planetary systems. The NRLA is scalable to future, much larger and more powerful architectures to conduct more ambitious scientific programs.

3.2.5.3 Weak Points

The NRLA is a very large observatory requiring multiple launches and in-space construction. In addition, the NRLA optical configuration is relatively complex.

3.2.5.4 Areas of Chief Concern

The chief areas of concern for the NRLA are the development of system modeling tools that deal with the combination of an interferometer and a coronagraph, verification of the capability to integrate a spectrometer with a hypertelescope , and the ability to manufacture phase masks with a performance consistent with the NRLA's requirements. A further major challenge with the NRLA is the implementation of a 100-m precision structure in space.

3.2.5.5 Precursor Possibilities/Requirements

Some of the required technology will be inherited from related programs. For example, SIM will provide mature technologies for nanometer/picometer metrology and modeling technology for a large dilute aperture system. NGST will provide experience with the design and operation of a large thermal shade at L2.

Smaller telescopes on a smaller structure can demonstrate the technologies needed for the NRLA while doing unique and relevant science. A 1/3 scale version of the NRLA could survey the immediate solar neighborhood for large planets outside the habitable zones that TPF will search. The results would lead to refinements in the design of a full-sized NRLA while also demonstrating technology and reducing risk for the larger, more ambitious system.

3.2.5.6 Other Astrophysics

A true imaging TPF would have outstanding capability for general astrophysics. No enhancement of the mission is required to make it suitable for other astrophysics programs. This is true for NRLA in both its precursor and full TPF implementations.

The sensitivity, imaging capability, and field-of-view of the NRLA are well suited for the suite of astrophysics described in the Phase I report. The mid-infrared spectral region is well-suited to detection of both hot structures (stars and stellar systems) and cool material (dust, cool companions), and to measurements of molecular bands in stellar, circumstellar, and interstellar gas.

3.2.5.7 Project Assessment

The challenge of properly modeling the imaging performance of the NRLA, and especially its coronagraphic performance, makes it difficult to assess the NRLA's ultimate potential for satisfying TPF's needs. Futhermore, the realization of 100-m precision structures in space seem well beyond current capabilities. From the standpoint of cost and risk alone, the multiple launches and on-orbit assembly needed for this system make this design less desirable than the interferometer or the coronagraphic options. Thus, the Project does not recommend that NASA pursue this architecture for the purposes of planet detection.

3.2.6 Large IR Telescope with a Coronagraph (TRW)

3.2.6.1 Basic Description

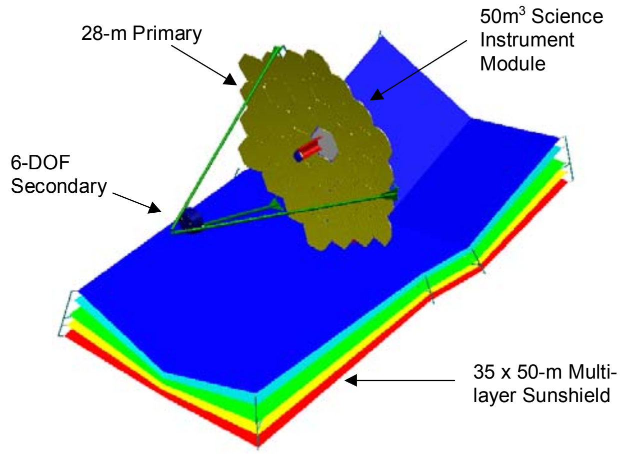

Figure 3-7. The TRW system consists of a passively cooled 28-m telescope equipped with a coronagraph for operation at 10 μm.

The TRW team examined the performance of a large aperture IR telescope equipped with a coronagraph (Figure 3-7). The design greatly resembles a scaled version of the NGST, including a large multi-layer sunshield that allows both the segmented deployable telescope and the science instrument module to be passively cooled to less than 30 K. The primary mirror consists of 36 hexagonal panels measuring ~4-m flat-to-flat, arranged in 3 rings around a central opening. Each panel has a thin, gold-coated composite membrane mirror attached to a composite backing structure by six rigid-body actuators for tip-tilt-piston control, and seven figure-control actuators for control of low-order figure errors. The mirrors are produced with a low-cost replica optics process. The panels' areal density is ~5 kg/m^2. A science instrument module behind the primary houses a coronagraph with an IR imager for planet detection and an IR spectrometer for planet characterization. The coronagraph occupies ~1/3 of the instrument module's 50 m^3 volume, leaving room for other instruments for general astrophysics observations. This science payload is attached to the sunshade and the spacecraft bus by a deployable mast that also provides thermal and vibration isolation from the ~300 K spacecraft. The entire observatory can be packaged to fit in the fairing of the Delta IV Heavy launch vehicle that has the capability required to place the system in a transfer orbit to the L2 point.

3.2.6.2 Strong Points

The telescope is particularly well suited for comparative planetology studies with emphasis on giant planets and debris disks located beyond the habitable zone. From a pure photon statistic point of view, an Earth at 10 parsecs could be detected with a SNR = 5 in ~2 hours, and its 6 to 12 μm spectrum could be obtained at SNR = 7 and R = 20 in ~25 hours.

Its 28-m aperture, 21 K average optics temperature, ~490 m^2 collecting area and 2.4×7.2 arc-minute field-of-view (FOV) make this facility a powerful tool for general astrophysics.

3.2.6.3 Weak Points

While the facility has excellent sensitivity, its angular resolution is a factor of ~3 less than that required to detect and characterize Earth-like planets for the 150 stars envisioned for TPF. As discussed in Section 3.3.3 (Figure 3-4), there are fewer than 25 stars for which the center of the habitable zone subtends an angle larger than 100 mas which corresponds to the *first* dark ring in the Airy pattern of a 28-m telescope (~90 mas at 10 μm). Detection of Earth-like planets at separations as small as λ/D is possible only with an extremely stable point spread function whose intensity does not vary by more than a few parts in ~10^5 at the location of the planet, during the time it takes to obtain observations at multiple roll angles.

3.2.6.4 Areas of Chief Concern

The primary concern is the stability of the point spread function which is sensitive to mechanical vibrations and thermal variations. The predicted vibration levels can be controlled with current technology, but the thermal control needed to minimize low spatial frequency primary mirror deformations will require technology development. If necessary, a low-bandwidth active figure control system might be implemented to achieve the necessary PSF stability. Lesser concerns include the development of lightweight cryo-optics, large format Si:As detectors, large IR filters, broadband transmissive substrates and high-contrast imaging technologies.

3.2.6.5 Precursor Possibilities/Requirements

Many of enabling technologies for this system are currently being developed and will be demonstrated by SIM and NGST. A visible coronagraphic mission would validate some of the critical hardware and software required for high-contrast imaging in space. Such a mission could survey potential TPF targets to determine their exozodiacal dust/debris structures and to detect giant planets on distant orbits that might be the "signposts" for stable planets in the habitable zone.

3.2.6.6 General Astrophysics

With a point source-sensitivity ~10^4 times greater than SIRTF and ~10^2 times greater than NGST, this telescope would be well suited to follow up their discoveries in the 3 to 50 μm spectral region. The science of this version of TPF is very close to that of the SAFIR telescope called out by the NAS/NRC Decadal Committee. With angular resolution at 7 μm (63 mas) equal to HST's resolution at 0.6 μm, this telescope's sensitivity is such that a 3-color HST Deep Field image that required a ~4 day integration with HST could be obtained in ~45 minutes. Since the image quality in the coronagraph's 15 arcsecond FOV is < $\lambda/15$ at 0.6 μm, an InSb detector module could obtain images in the 0.6 to 3 μm region with ~10 times the resolution of HST. This would provide a resolution of ~2.5 km for Mars, ~27 km for Jupiter, and ~190 km for Neptune and its satellites. Other possible projects include:

- Obtain images of the disk around a proto star at 100 parsecs with a resolution of ~0.9 AU
- Extend the Cepheid distance scale to > 200 Mpc
- Obtain spectra and follow the light curve of median Type Ia Supernova at $z = 3$ for several months
- Obtain images of the first luminous objects at $z > 20$
- Measure IR surface brightness fluctuations out to Gpc
- Obtain images of the host galaxy of active galactic nuclei with a resolution of ~45 pc at 1000 Mpc

3.2.6.7 Project Assessment

In the estimation of the Project, the angular resolution of a 28-m telescope is simply not adequate to detect Earths at any reasonable distance. Visible coronagraphs typically cannot operate within the first three or four Airy rings (3.6–5 λ/D) to ensure a favorable ratio of planet light to residual starlight. The fact that the habitable zone (1 AU for a G star) lies at or within the first Airy ring (90 mas at 10 μm) of this telescope for stars beyond 9 pc raises issues of PSF stability that the Project and the technology panel agree are close to insurmountable. In the TRW design an Earth at 10 pc would be ~10^4 fainter than the residual starlight at 1 Airy radius (Figure 3-8). To find this planet at a signal-to-noise of SNR = 5, one would have to subtract away the residual starlight with an accuracy of a few times 10^4 using images obtained at multiple rotation angles over a few hours.

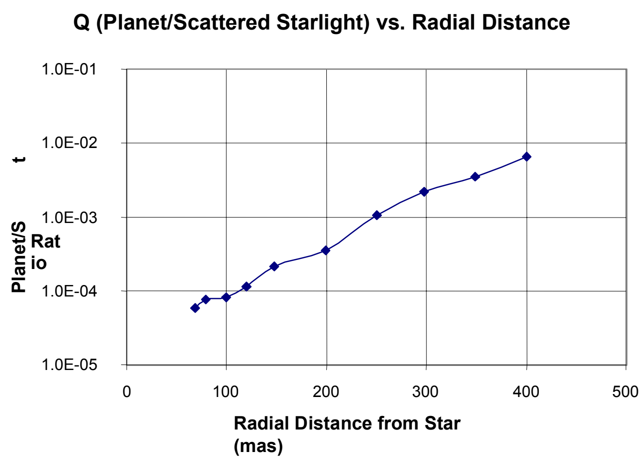

Figure 3-8. In the TRW concept the ratio of planet light to residual starlight is very low within 0.1 arcsec. (TRW Report).

The implications of this stability requirement can be understood simply as follows: in the limit of infinite observing time, the limiting noise source will be fluctuations in the residual scattered starlight. The scattering is roughly given by $I_{scatt} \propto \sigma^2$ where wavefront errors are denoted by σ. The fluctuations in the scattered light, dI_{scatt}, are proportional to $\sigma\, d\sigma$. If the ratio of planet to scattered light is denoted by $Q = I_{planet}/I_{scatt} = 10^{-4}$, then the wavefront stability required over ~1 hour (two integration periods plus an intermediate rotation) is given by $d\sigma/\sigma \approx (I_{planet}/I_{scatt})/\mathrm{SNR} \approx Q/\mathrm{SNR}$. Although the wavefront for this telescope is nominally corrected to λ/3,000 at 10 μm, or roughly 3 nm, the resultant, average, wavefront must be held stable to at least $d\sigma/\sigma \approx 10^{-4}/\mathrm{SNR} = 2 \times 10^{-5}$ better than this, or << 1 pm, lest the structure in the PSF at the position of the planet change by an amount that equals or exceeds the planetary signal. Furthermore, because the coronagraph is operating at maximum angular resolution (λ/D), the modes that must be controlled to picometer levels are the lowest modes of the entire structure. These problems would be much less severe beyond 3.6λ/D, but at 10 μm such a system would require a telescope diameter of 100 m. Thus, the Project does not recommend that NASA carry forward the IR coronagraph architecture for the purposes of planet detection. However, we note with enthusiasm the applicability of the technology outlined in the TRW report for SAFIR mission for which there is an abundance of exciting astrophysical applications. Such a large IR telescope equipped with a coronagraph would be able to study any planets found to exist around the closest stars, that is, within 3 to 5 pc.

3.3. TPF Design Reference Mission and Comparative Performance of Architectures

3.3.1 Detection of an Earth Twin

In order to provide a consistent benchmark for comparison, each team was asked to determine how long a particular configuration would take to detect an Earth located at 1 AU from a solar type star (G2V), at various distances, in the presence of varying amounts of zodiacal emission (Appendix B). The quoted time includes the integration time to achieve SNR = 5 on the planet *plus* any spacecraft maneuvering time needed to accomplish any motions (rotations) to survey the full area of the habitable zone. These observations would be made at three different epochs to confirm common proper motions and to detect planets at different orbital positions. While complete results can be found in the Appendices giving information from each team, Table 3-4 lists the time it would take each architecture to detect an Earth twin at 10 pc with our level of zodiacal emission. The Ball coronagraph is the fastest system primarily because it requires the fewest number of repointings to cover completely the habitable zone around the star.

Table 3-4. Time to Detect and Characterize Earth Twin at 10 pc

Architecture	Time to Detect Earth Twin (SNR = 5)	Time to Detect Planet's Atmosphere	Time to Detect Oxygen or Ozone
Boeing-SVS Apodized Square Aperture (ASA) Coronagraph	6.3 hr (incl. 2 rotations)	1 d (H_2O) R = 20,SNR = 5	3.8 d (O_3) R = 20, SNR = 5
Boeing-SVS Nonredundant Linear Array (NRLA)	2.5 hr (one half rotation)	2.7 d (CO_2) R = 10, SNR = 5	2.1 d (O_3) R = 20, SNR = 5
Ball Classical Coronagraph	0.86 hr (incl. 2 rotations)	0.14 d (H_2O) R = 24, SNR = 5	0.8 d (O_2) R = 70, SNR = 5
Ball Shaped-pupil Coronagraph	5.3 hr (incl. 9 rotations)	0.09 d (H_2O) R = 24, SNR = 5 ≤ 10 pc	0.7 d (O_2) R = 70, SNR = 5 ≤ 10 pc
LMSS Structurally Connected Interferometer (40-m truss)	6 hr (incl. 1 full rotation)	0.9 d (H_2O, CO_2, O_3) R = 20, SNR = 5	
LMSS/JPL Separated Spacecraft Interferometer (TPF Book)	6 hr (incl. 1 full rotation)	0.7 d (H_2O, CO_2, O_3) R = 20, SNR = 5	

3.3.2 Characterization of an Earth Twin

Each team was asked to assess the time required to make spectroscopic observations of a planet whose existence and position was known via an initial survey as given above. Based on the report of Des Marais et al. (2002), each team determined the observing time (integration time plus spacecraft maneuvering time as required for a source at a *known* position) needed to detect the following:

1) spectral lines characterizing the planet's atmosphere, e.g., CO_2 or H_2O.
2) spectral lines indicative of the presence of photosynthesis life, e.g., O_2 or O_3.

The teams used the spectral information presented in Appendix C (Des Marais et al. 2002) to determine the wavelengths and approximate spectral resolution for their observations. Representative times are given in Table 3-4. Note that for some systems the spectroscopic times can be smaller than the detection time since it is assumed that the position of a planet is known which obviates the need for a large number of repointings.

3.3.3 Detection of Earth Twin Around Real Stars

The final step in assessing the performance of each architecture was to investigate the time needed to survey a real sample of stars. To simplify the problem, each team investigated a search radius at the habitable zone (Kasting, Whitmire and Reynolds, 1993), R_{HZ}, defined by the luminosity of the star, $R_{HZ} = 1\times(L_*/L_{sun})^{0.5}$ AU, and a visible spectrum defined by $B_\nu(T_*)/B_\nu(T_{sun})\times F_\nu(Earth)$ using a terrestrial spectrum prepared by Traub (see refs in Des Marais et al., 2002). These assumptions keep the planet at a constant temperature for the IR instruments, while accounting for the changing reflection spectrum for the visible light instruments.

Potential TPF target stars were drawn from a representative list of more than 250 stars for which the center of the habitable zone subtends an angle greater than 35 mas. F stars have habitable zones that are resolvable at distances as large as 25 pc and thus sensitivity, not angular resolution, will be the key issue for these systems. The converse is true for the habitable zones around K stars; angular resolution will be the issue. Not all stars will be accessible to all architectures based on viewing constraints, the influence of stellar companions, angular resolution, or sensitivity. Figure 3-9 summarizes the limits set by angular resolution on the detectability of these stars.

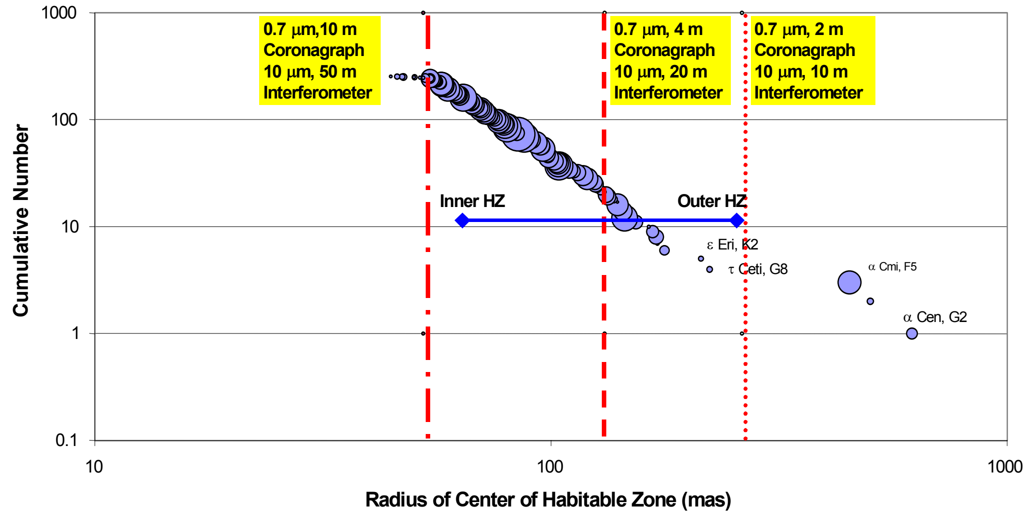

Figure 3-9. The cumulative number of nearby (FGKM) stars for which the center of the habitable zone is smaller than a particular angular extent. The horizontal bar shows the rough width of the habitable zone. The typical Inner Working Distance—the closest angular separation at which a planet can be resolved ($3.6\lambda/D$ for coronagaphs and λ/Baseline for interferometers)—of different observing systems is shown.

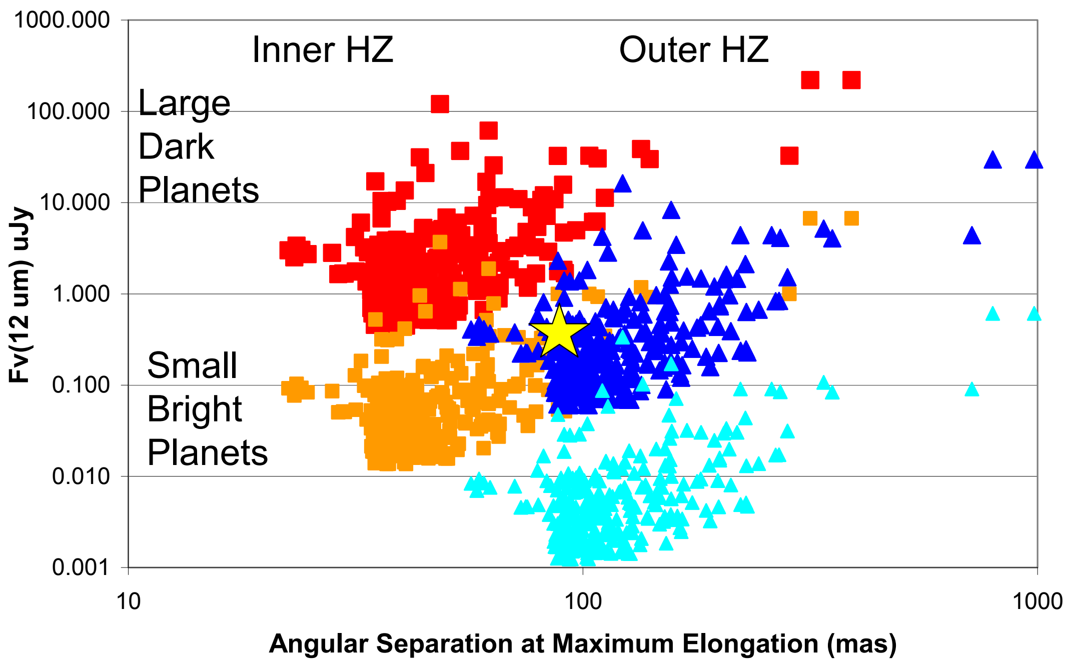

Figure 3-10. Plots showing predicted 12 µm brightness of planets around 250 of the closest stars. (See Figure 3-11 caption for definition of symbols.) Note that low albedo ("dark") planets appear bright in the infrared because they absorb more starlight (and thus are warmer) than high albedo ("bright") planets.

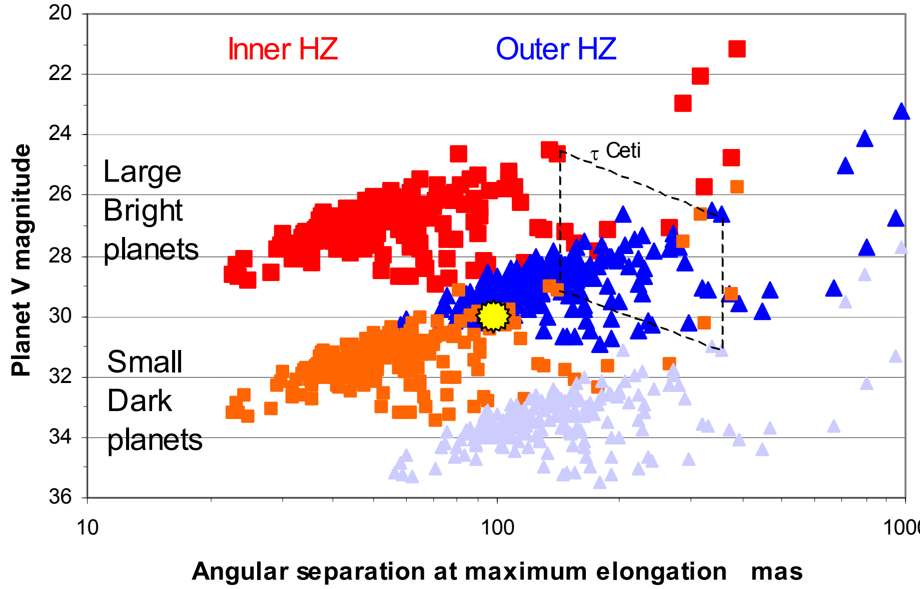

Figure 3-11. Plots showing predicted visible magnitudes (V) of planets around 250 of the closest stars. Each star appears four times with different locations in the habitable zone (inner and outer) and with different radii/albedo combinations. Different symbols denote: planets at the inner and outer edges of the habitable zone; planets with either one-half or twice the radius of the Earth planets; and planets with either one-half or twice the visible albedo of the 0.3 Earth (Ball Final Report).

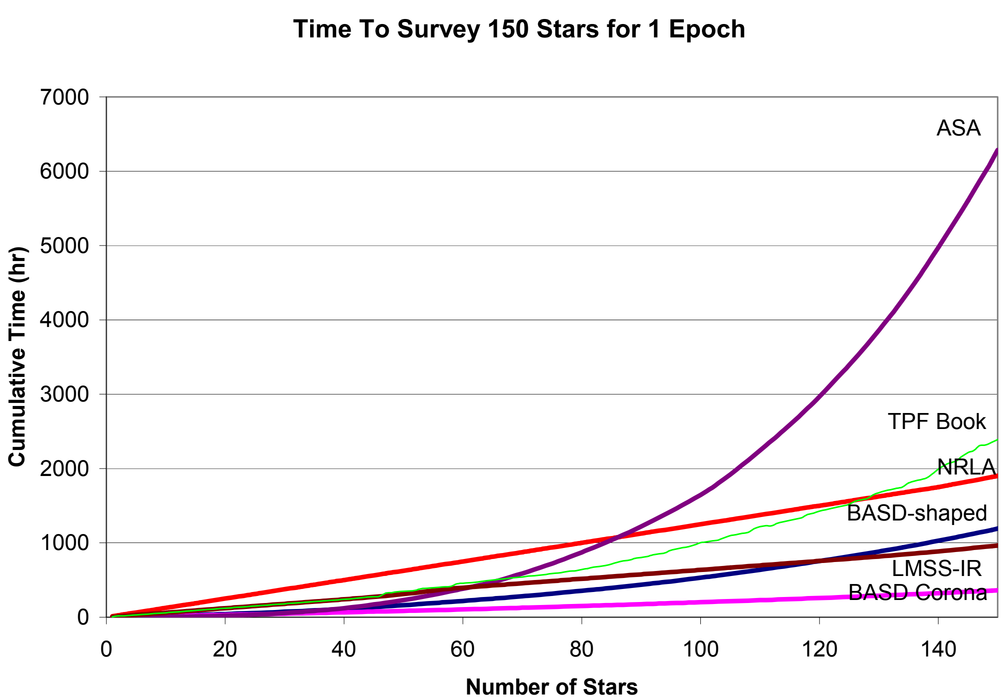

Figure 3-12. The cumulative time to search the habitable zones around a sample of 150 stars (1 epoch) is shown for 6 different architectures. (Note: The ASA performance could be improved with the implementation of a deformable mirror to further reduce scattered light and increase *Q*. Such an augmentation would make the ASA performance similar to that of the other systems.)

3.3.4 Results of Comparison

Figure 3-12 and Table 3-5 summarize the time required to complete a survey of 150 stars. Because of the need to observe these stars at three epochs to confirm the detections and make a preliminary determination of orbital parameters, the full survey would take approximately three times longer. These estimates have not been optimized for observing strategies appropriate to particular designs or sky coverage through the year.

Table 3-5. Time to Survey 150 Stars for 1 Epoch (days)

Architecture	Survey Time (days)
Ball Coronagraph	15
Ball Shaped pupil	50
Boeing-SVS ASA	262
Boeing-SVS NRLA	55
LMSS 40-m truss	40
Separated Spacecraft (Book Design)	106

The Ball coronagraph completes the survey in the shortest time, but in all cases except the ASA, the three-fold redundant survey can be completed in less than one year. The factor of two difference in speed between the two infrared interferometers is probably not significant given the large number of assumptions about instrumental and observational parameters. The performance of the Boeing-SVS ASA coronagraph could be made comparable to that of the Ball systems by the addition of a deformable mirror to improve the ratio of planet light to residual starlight.

Combining the information in Tables 3-4 and 3-5 shows that a program of searching 150 stars along with follow-up observations to characterize ~50 planets in greater spectroscopic detail at a few days apiece could be carried out in half of a five-year mission. The remainder of the five-year mission duration could be spent on general astrophysics investigations or kept as a reserve against decreases in instrument capability or operational efficiency.

3.3.5 Effects of Zodiacal Emission

The effect of increased high levels of exozodiacal emission on the detectability of a planet depends on the total noise budget for a particular architecture. Depending on the wavelength and architecture, this budget will include residual starlight (scattered, diffracted, or interferometric leakage), local zodiacal background, detector noise, telescope emission, and the degree to which the exozodiacal light is resolved (and hence on the distance to the star). Figure 3-13 shows the increase in integration time for the Ball visible coronagraph and the LMSS nulling-IR interferometer at two distances and for a variety of exozodiacal levels. The performance of both systems degrades as the exozodiacal emission and the distance to the star increase. The visible light system is less susceptible than the infrared interferometer to these effects (a factor of 2 increase in integration time compared with a factor of 3.6 increase at 10 times the exozodiacal level of our solar system for a star at 10 pc). Below 10 times solar-system levels, the observing-time penalty due to exozodiacal emission is not severe.

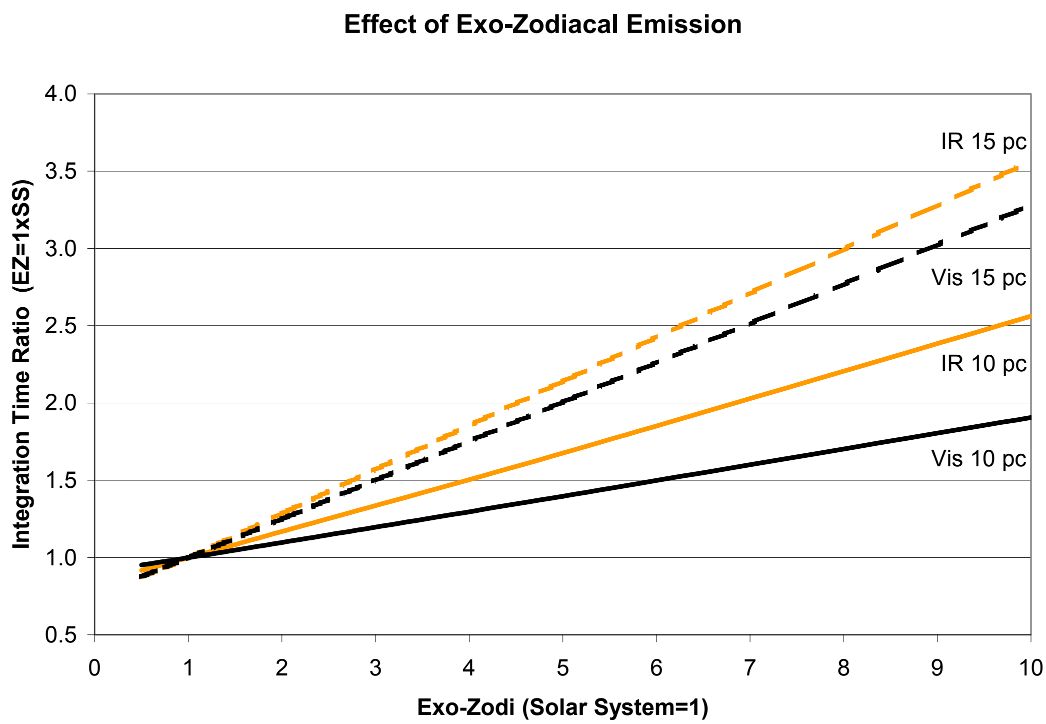

Figure 3-13. The effect of zodiacal emission around target stars at two distances on the integration time to detect an Earth for the LMSS nulling interferometer and the Ball Coronagraph.

3.4. Precursor Missions to Detect Gas-Giant Planets and Nearby Earths

The TPF-SWG considered the potential application of TPF technology to the study of gas-giant planets and was emphatic that detection and characterization of such planets was of great scientific interest in its own right. For example, Figures 3-14 and 3-15 show visible and mid-IR spectra of various gas-giant planets. Gas giants that have appeared in our own solar system have been quite distinct from one another, and the physical properties and evolutionary history leading to those differences represent fundamental questions for our understanding of planets in general.

In many cases, gas giants can be detected more easily than terrestrial planets, depending on the observing wavelength band and orbital location. Advantages of direct detection of giant planets, particularly those on more distant orbits, include immediate and simple identification of multiple planets and planets on long periods that would be difficult to detect with radial velocities or astrometric techniques. In the long run, spectral or color information available from direct detection techniques could yield radius and mass estimates that might be accurate enough to distinguish between gas-giant and terrestrial planets, but verifying such an assertion will require dynamical and photometric data on a larger sample of objects than the nine planets in our own solar system.

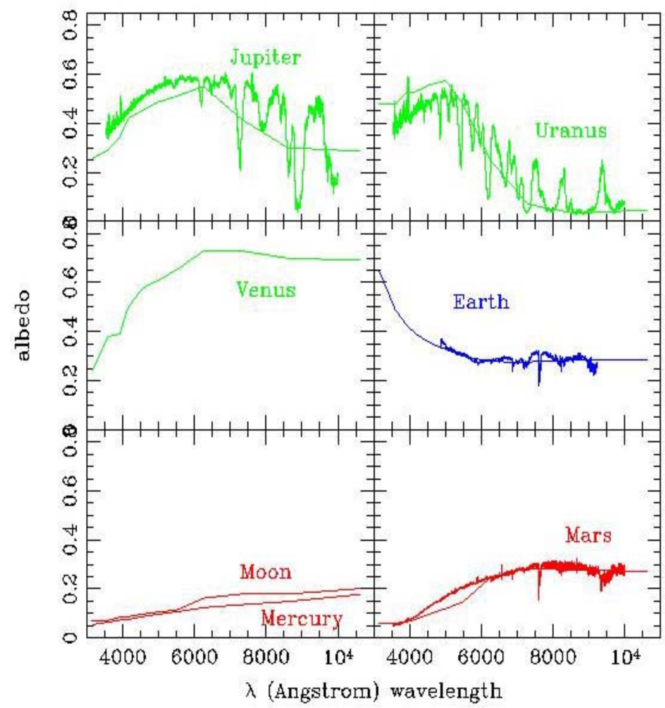

Figure 3-14. The visible spectra of planets in our solar system reveal a great deal of information about the physical properties of these planets.

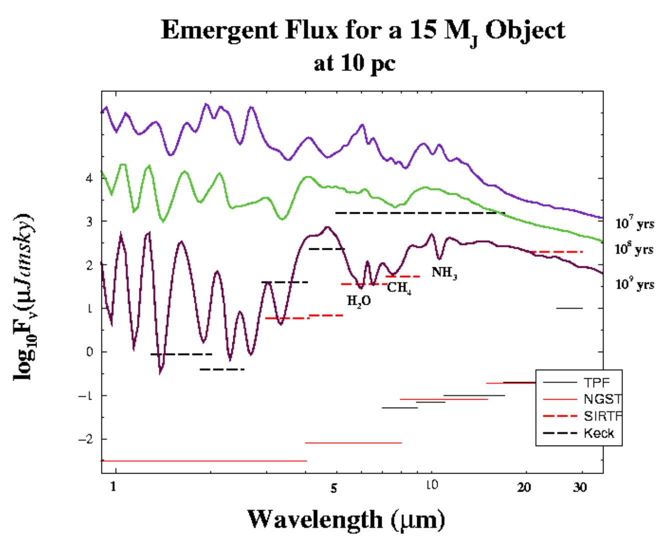

Figure 3-15. The infrared spectrum of giant planets offers a number of important spectral features observable at low resolution. (Burrows et al. 1998).

The TPF-SWG emphasized that a mission capable of studying a large number of giant planets and a small number of terrestrial planets (those within 8 pc) would be a scientifically credible and important mission (Lunine 2001). Such a mission would also serve as a technological first step along the way to missions capable of finding and characterizing in greater detail more Earths around more distant stars. The case for a mission of smaller scope than the full TPF mission described in this report would be greatly bolstered if transit experiments, such as the Kepler mission or by other means, were to determine that terrestrial-sized planets in the habitable zones of solar-type stars were a common occurrence, $\eta_{\oplus} \approx 1$ (Beichman 2000). As described in their final reports, a number of the teams investigated smaller-scale yet scientifically meritorious missions that would potentially be less technologically challenging, lower in cost and risk, and ready to proceed into implementation before the full scale TPF.

4 Technical Assessment

TPF will be a technologically challenging mission regardless of the architecture that is ultimately chosen. The current studies have shown clearly that there are TPF architectures that are feasible for development and launch by the middle of the next decade. However, significant technical challenges exist for all of the candidate architectures studied. These must be overcome for at least one architecture before the mission can be realized. There must be adequate technology development over the next few years, building on a technical base of earlier missions and ground-based activities. The TPF-SWG has suggested that technology readiness, rather than a scientific preference for particular wavelength region, will probably be the determining factor in the selection of the final mission architecture.

The Project and the independent TPF Technology Review Board (Appendix A) carried out comprehensive technical assessments of the various concepts and concluded that the most technologically viable architectures for TPF are visible coronagraphs and infrared nulling interferometers. The latter category would include both formation flying interferometers with selectable baselines and structurally connected interferometers with fixed baselines of 25–40 m. A large infrared coronagraph was excluded on the basis of limited angular resolution and for the technical demands of a 30-m diameter class, segmented, cryogenic, deployable primary mirror. The NRLA hypertelescope concept was excluded principally on the basis of its requirement for a 100-m class, precision structure and the overall complexity of the concept. Very long baseline (≥40 m) structurally connected infrared nulling interferometers were similarly excluded on the basis of their requirement for very large, precision, cryogenic, deployable structures.

4.1. Infrared Nulling Interferometer Technology

The technology for infrared nulling interferometers is being firmly established by missions such as SIM, NGST, and SIRTF, as well as ground-based activities including the Keck Interferometer, the LBT-Interferometer, and ESO's VLT-Interferometer. The formation-flying version of this architecture has been the subject of development by the StarLight Project which recently transitioned from a flight project to a ground demonstration effort. While NASA does not currently plan a flight demonstration of StarLight technology, ESA's SMART-2 or SMART-3 mission may demonstrate the precision formation flying aspects necessary to support their Darwin concept.

4.1.1 Nulling

Taken individually, the technology needs for the infrared nulling interferometers do not represent major, insurmountable challenges. The fundamental measurement requires starlight suppression by interferometric nulling of the light from multiple collectors. Nulls stable to one part in ~10^6 are required over a band between ~7–20 μm. This basic technology was initially developed several years ago by SIM for visible applications where transient nulls of better than 10^6 were achieved with a visible laser source and stable nulls of ~5×10^4 were achieved with "white light" ($\Delta\lambda/\lambda$ = 18% bandwidth). The mid-IR nulling of direct relevance to TPF is being developed at JPL for the Keck-Interferometer and at the University of Arizona for the LBT-Interferometer. Laboratory experiments to date have demonstrated mid-IR nulls of better than 1.5×10^{-4} at 9 μm with ~5% bandwidth (see Figure 4-1). These experiments were performed at room temperature in air and are adequate for ground-based observatories. The technology panel noted that with appropriate additional effort, including operation in a cryogenic vacuum environment, the IR nulling performance required for TPF can be demonstrated in the laboratory within one to two years.

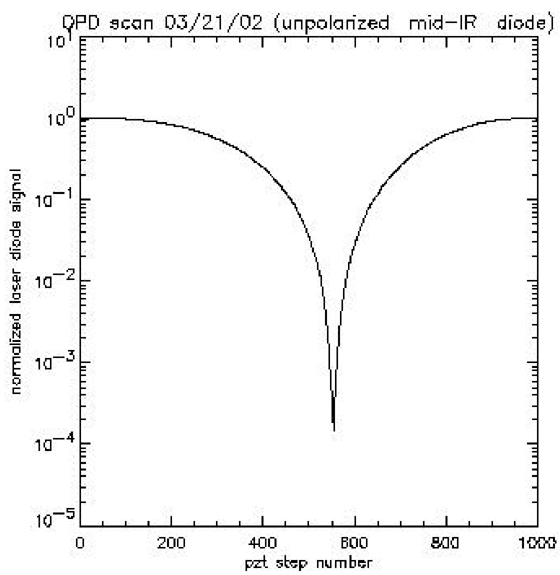

Figure 4-1. A JPL testbed has produced a deep, stable null at 9 μm.

4.1.2 Detectors and Cryocoolers

The 7–20 μm mid-IR detectors for TPF are likely to be derivatives of SIRTF/NGST technology. These low-noise Si:As IBC devices will require reliable, long-life cooling to ~6 K. Carrying stored cryogen to provide the cooling power needed for a 5 to 10-year mission may prove to be difficult, making long-lived mechanical cryocoolers with moderate cooling power (~5 to 15 mW) and low vibration highly desirable. NASA's Advanced Cryocooler Technology

Development Program is currently funding efforts to develop “engineering model” cryocoolers meeting the TPF needs by the end of FY 2005. Current candidate cooler systems include pulse tubes and turbo-Braytons, as well as hybrid systems using Stirling/Joule-Thompson and pulse tube/Joule-Thompson combinations. Two different coolers are expected to be undergoing tests by the end of FY 2005.

4.1.3 Optics

The TPF collector telescopes require 3.5 to 4-m diameter primary mirrors with diffraction-limited performance in the near IR and cooled to ~40 K. The use of spatial filtering in the nulling beam combiner relaxes the requirement of obtaining extraordinary wavefront quality from the collectors. As with the detectors, these optics are likely to be derivatives of the NGST and/or SIRTF optics and are not considered to represent a significant technology development item.

4.1.4 Precision Deployable Structures

From a performance standpoint, the 40-m version of the infrared nulling interferometer is close to the minimum length needed to provide the requisite angular resolution. A smaller, 20-m system would be restricted to resolving the central habitable zones of fewer than 25 stars. From a feasibility standpoint, the structurally connected version will be limited to baselines ≤40 m. The technology panel was confident that lengths up to 25 m could be achieved with two SIM-like structures connected with a single hinge. A larger system might be achieved with deployments of a number of SIM-like structures, but weight, stiffness, and packaging in realistic launch fairings would have to be carefully assessed. The TPF version, of course, will have to operate cold. The design of lightweight, stable, precision-composite structures for cryogenic applications is an active field of development. It is likely that deployable precision structure technology for TPF can be derived from related work for NGST.

4.1.5 Precision Formation Flying

The formation-flying interferometer version of TPF will require a set of additional technologies to establish and control the formation during data acquisition. These technologies include a formation-sensing system to determine the range and bearing of the individual spacecraft. This will likely be a hybrid RF/optical system. The Autonomous Formation Flying (AFF) sensor, a prototype version of the RF system originally intended for StarLight has been developed at JPL. The laser metrology system will be similar to that used on SIM except that only nm-level control is required. The precision formation control algorithms have been under development for several years at JPL in support of StarLight and the NASA Cross Enterprise Technology Development Program. Moderately sophisticated simulators exist for formations of up to five spacecraft.

The final piece of the formation flying technology is precision low-thrust propulsion. Micronewton and millinewton thrusters will be required to control and maneuver the formation. Various versions of small electric propulsion thrusters such as field emission electric propulsion (FEEPs), pulse plasma thrusters (PPTs), and colloidal thrusters are candidates for TPF and are currently under development and use by other missions in the US and Europe. The Terrestrial Planet Finder and ESA’s Darwin project will address the tradeoffs between the precision of spacecraft control and the range of delay lines and beam steering optics. An additional complication of the formation flying version of TPF is the need for stringent control of stray light, thermal radiation, and glints over variable baselines which will require detailed, integrated modeling to understand and correct.

4.1.6 Summary

The largest area of technical risk for the infrared interferometers is not in the performance of the individual components but in the operation of the various elements as a complete system. No insurmountable problems have been identified at the component or assembly level. Most of the required elements are either under development and making good progress or are reasonable extensions of technology being developed for missions and ground observatories that will be in place well before TPF needs them. A major focus of TPF technology development in support of these architectures must be the development of system-level testbeds, simulators and integrated models that will provide the necessary insight into the problems associated with TPF performance at the system level.

4.2. Visible Coronagraph Technology

The technology base for the visible coronagraph architectures for TPF is not as well developed as for the infrared nulling interferometers. While coronagraphs are well developed and understood instruments for solar astronomy and other applications, they have not been exploited at this level of starlight rejection by many orders of magnitude. On the other hand, the coronagraph-based architectures for TPF are functionally simpler than the interferometer architectures, consisting primarily of large visible telescopes with extraordinarily low levels of wavefront error. In this respect, these architectures do have heritage in the efforts of HST and NGST. A set of precision image or pupil plane masks, stops, and/or deformable mirrors, are used to suppress starlight and control scattered and diffracted light sufficiently to darken a suitable region of the image plane where the reflected planet light can be observed. A key development over the past decade has been deformable mirror technology that makes it possible to control the wavefront to the requisite $\lambda/10{,}000$ precision in an active manner on a small optical element, rather than manufacture a large monolithic mirror to such a precise tolerance.

4.2.1 Optics

The single biggest technical challenge for the TPF coronagraph architectures is the requirement for a lightweight primary mirror three to four times the size of the HST mirror with a (corrected) wavefront error (WFE) over the critical mid-spatial frequencies of ~0.1 nm rms and a stability of ≤ 0.1 nm rms over the required integration time of several hours. Two mirror concepts were studied as part of this effort including a 4×10-m elliptical monolith and an 8×8-m square, segmented, deployable mirror. The required WFE performance is achieved by a combination of an as-manufactured WFE of ≤ 5 nm rms (five times better than Hubble), corrected at low spatial frequencies with a grid of primary mirror actuators and at mid spatial frequencies with a high-actuator-density deformable mirror located at a pupil down stream in the optical train (see below). The 10-m monolith, which is actually an off-axis piece of an 11-m parent, exceeds current size capability for optical fabrication anywhere in the world. The largest fabrication facility currently in operation is the Mirror Laboratory at the University of Arizona's Stewart Observatory, which can spin-cast ~8.4-m diameter optics. Manufacture of a large segmented mirror using square, rectangular, or other-shaped segments of 1 to 4 m on a side is within current capabilities and might be suitable for either the ASA or Ball designs. However, manufacturing such segments with the required WFE error performance will be difficult, and controlling diffracted/scattered light from the edges will present a major challenge.

4.2.2 Wavefront Control

The previous section described the requirements for large primary mirrors for the visible coronagraph architectures for TPF. Starting with a very high quality as-manufactured optic, the WFE must be further reduced to < 0.1 nm (λ/5,000) rms and controlled to a fraction of that value for long periods of time. A grid of several hundred actuators on the back of the primary mirror provides the first level of correction. Such technology is similar to that being developed by the Advanced Mirror System Demonstrator Program jointly funded by NASA (NGST), the Air Force, and the National Reconnaissance Organization (NRO). Further correction at the mid-spatial frequencies is achieved by incorporating a high-actuator-density deformable mirror in the optical train. Such a mirror will require 10,000 actuators or more in a compact package operating at low power and low bandwidth (essentially DC). Such technology has been under development for several years at Xinetics, Inc. Prototype mirrors with as many as 1700 actuators on 1-mm centers have been developed and tested at JPL. Precision and stability of ≤ 0.1 nm has been demonstrated for single actuators over hundreds of hours of operation. The modular design of the mirrors enable them to be expandable to whatever size is required. Compact, multiplexed, low power electronics have also been demonstrated to be adequate for a correction bandwidth of a few Hz. This technology is maturing rapidly and represents a major breakthrough leading to serious consideration of coronagraphs for TPF (See Figure 4-2).

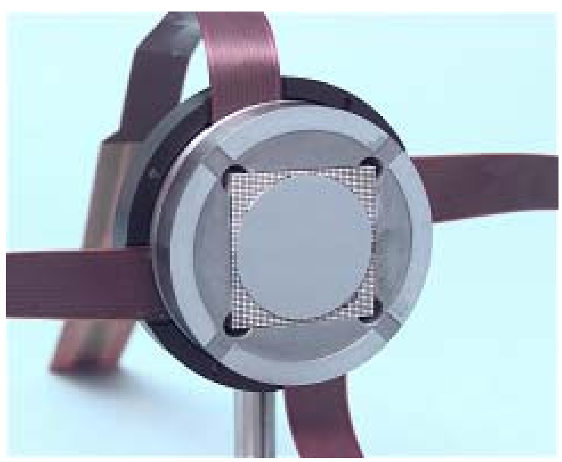

Figure 4-2. A small deformable mirror is capable of sub-Angstrom wavefront correction.

An additional requirement on the quality of the optics is the uniformity of the coatings which, at the primary, must be better than ~0.1% to achieve the requisite stellar rejection. Achieving this uniformity over an 8 to 10-m optical element, or correcting the imperfections downstream in the optical path, will require technology development.

4.2.3 Starlight Suppression

Once a wavefront of adequate quality has been produced (as described above), either coronagraphic image-plane masks or specially-shaped pupil masks must be installed in the system to control the diffraction and scattering to create a sufficiently dark region to search for planets. These masks require high levels of geometric and transmission precision, estimated to be on the order of one part in 10^3 to 10^5, depending on the exact details of the implementation and performance. There are concepts for production of such masks including micro-lithographic and sputter-coating techniques, but these are largely unproven. Work is underway at JPL, Princeton University, and several other facilities, but to date no reliable data from a well-designed and controlled experiment exists to indicate the level of performance that can be achieved. Most of the projected performance has been the result of modeling. While the projected results are encouraging, standard optical modeling tools do not have the necessary dynamic range to deal with this problem and thus approximations and as yet unproven techniques have been applied. The adequacy of the models is currently unknown.

4.2.4 Structural Stability

A large telescope of the size under consideration for a TPF coronagraph will necessarily have to be launched in a stowed configuration and deployed on orbit. Even with a monolithic primary mirror, a secondary mirror structure and various sun shields will also have to be deployed. Concepts involving assembly of large structures in space by astronauts were eliminated from further consideration due to the projected difficulty and cost of such an approach. The basic methodology for precision deployment, alignment and wavefront control should be available from NGST. However, while NGST envisions little if any active control on the optics and the structure during observations, a TPF coronagraph requiring wavefront error stability of ≤ 0.1 nm rms over several hours of integration time will likely require such control to mitigate thermal and dynamic effects. It is possible that such effects can be mitigated with sound design and active control with deformable mirrors and a fast steering mirror to reduce jitter. Development of high-fidelity integrated models, grounded in laboratory testbed experiments, will be necessary to understand the required and achievable performance.

4.2.5 Summary

The principal conclusion with regard to the state of technology for the visible coronagraph is that the greatest technical risk for this architecture is in the development, manufacturing, and implementation of the large, ultra-low wavefront error primary mirror and components associated with the challenging requirements for starlight suppression. The coronagraphs themselves are functionally simple and although the demands for system performance are challenging, none are thought to be insurmountable. Work is in progress on many of the required elements and, in some cases (e.g., the high-actuator-density deformable mirrors), is progressing very well. Studies are underway with regard to possible approaches for mirror fabrication. Mirror development will be a top priority over the next several years. A major focus of TPF technology development in support of this architecture is, and will continue to be, the development of system-level testbeds, simulators, and integrated models that will provide the necessary insight into the achievable levels of performance in the laboratory and problems associated with implementing this architecture in space for TPF.

4.3. Technology Recommendations

Based on careful study of the candidate TPF architectures, the independent TPF Technology Review Board recommended that NASA pursue a sustained and well-funded technology development program for both visible coronagraphs and infrared nulling interferometers until one architecture clearly emerges as the leading concept. The overall approach that was recommended includes a combination of "component-level" developments, comprehensive laboratory testbeds, and integrated software models/simulators. Specific areas of technology development recommended for the two architectures are shown in Table 4-1.

Continued close coordination and monitoring of the technical progress of missions including SIRTF, SIM, and NGST is essential. Technology flight demonstrations should be considered only if laboratory testbeds could not conclusively resolve uncertainty and reduce risk to an acceptable level with adequate margins for development of the TPF flight system.

Table 4-1. Key Areas for Technology Development for TPF

Technology Area	Infrared Interferometers	Visible Coronagraphs
Precision formation flying	●	
Nulling	●	
Beam path control	●	
Cryo-mechanisms	●	
Cryocoolers	●	
Large-precision mirrors		●
Starlight suppression		●
Ultra-high-quality wavefront control		●
High-actuator-density deformable mirror		●
End-to-end system testbeds	●	●

5 Final Architecture Recommendations

Based on the study efforts of the past two years and the inputs of the TPF Science Working Group and the Technology Review Board, the TPF Project has identified two architectural concepts for further study and technology development.

5.1. IR Nulling Interferometer

An IR nulling interferometer operating either on a fixed ~40-m structure or in a separated spacecraft configuration offers good performance. It can achieve the fundamental TPF goals of surveying nearby stars for Earths, carrying out a low spectral resolution characterization of the atmospheres, and searching among the brightest detected planets for ozone, an important biomarker. In these designs, the angular resolution is, of course, limited by the length of the structure. The benefits of a single spacecraft system must, however, be weighed against the inability to resolve habitable zones subtending smaller angles.

Deciding between these two alternatives will require that important scientific, programmatic and technological tradeoffs be made over the next three to four years. The indefinite deferral of the StarLight flight mission makes it unlikely that a separated spacecraft technology demonstration mission can be operational before ~2010, thus calling into question the viability of a formation-flying version of TPF ready for launch by 2015. If a flight validation of the formation flying interferometer is judged to be necessary prior to implementation on TPF, and if work over the next few years demonstrates that a structurally-connected interferometer would be adequate to study a reasonable sample of stars, then NASA may choose to focus *at an early date* on structurally-connected interferometers.

The technical challenges of this concept are distributed between the interferometry, passive cooling, large lightweight booms or formation flying, and overall system complexity. Given the on-going progress in laboratory interferometric nulling, no single issue looks insurmountable, but the overall complexity of this system, which incorporates some of the most difficult aspects of SIRTF, NGST, SIM, and StarLight, cannot be overemphasized. Issues of integration and test will be very important.

The issue of ancillary science is a difficult one for the interferometer. While a cooled interferometer in space offers thousand-fold sensitivity advantages relative to ground-based systems, the angular resolution of a $\leq$ 40-m fixed boom system is modest compared to the Keck or VLT Interferometers. A separated spacecraft version of TPF would offer dramatic gains in both sensitivity and angular resolution for imaging science using baselines out to 1 km. It should be noted that extension to baselines longer than a few 100 m, or operation on sources without a bright ($K \approx 17$ mag) on-axis star to phase the interferometer, would add significant complexity and cost to the system.

5.2. Visible Telescope with a Coronagraph and/or Apodized Aperture

The primary focus of one team and the secondary priority of another team was on a visible light system using a large telescope along with a variety of techniques to reject diffracted and scattered starlight. A coronagraph incorporating a shaped-pupil mask and a deformable mirror operating on a monolithic 4×10-m telescope (shaped to fit into existing launch shrouds) offers good performance and can achieve the fundamental TPF goals of surveying nearby stars for Earths, carrying out a low spectral resolution characterization of the atmospheres, and searching for an important biomarker, molecular oxygen, in the brightest planets detected.

The technical challenges of this concept are: 1) the construction of a telescope of adequate size and quality, and 2) integration of a deformable mirror system with adequate vibration suppression to maintain the required wavefront accuracy. Near-term studies should focus on the critical issue of the feasibility of manufacturing and launching a telescope of the requisite size and smoothness in time for a new start around 2010.

The issue of ancillary science is straightforward. The Ball and Boeing-SVS teams envision incorporating the coronagraphic capability as just one of a number of focal plane instruments. Traditional HST-like visible/UV instruments would offer greatly expanded scientific potential due to operation on a telescope with 20 times the collecting area of HST.

6 Programmatic Considerations

6.1 Strategy Leading to a Formulation Phase by 2007

TPF will be the next major mission in the Origins program following SIRTF, SIM and NGST with a launch date around 2015. In support of this schedule (Figure 6-1), NASA will now enter a 3 to 4 year period of intensive scientific investigation, design study, and technology development leading to the selection of the final TPF architecture no later than mid-FY 2006 in preparation to entering the formulation phase by FY 2007. During the preformulation phase, NASA has allocated $200 M to support three main areas of activities: science, mission studies, and technology development:

- Approximately 10% of the total TPF budget will be allocated on an annual basis to support TPF preparatory science investigations and fellowships with the goal to understand better the nature and, if possible, the frequency of occurrence of Earthlike planets around other stars. These funds will be awarded through competitive processes such as NASA Research Announcements (NRAs).
- JPL will perform detailed mission studies of "point designs" for the coronagraphic and interferometric versions of TPF. The products of these studies will be concepts similar in nature and utility to the NGST "Yardstick" design developed by the Goddard Space Flight Center in the early stages of NGST development.
- The bulk of TPF funding will be targeted to developing the key technologies needed for both architectures. The goal will be to develop the critical technologies to a NASA Technology Readiness Level (TRL) of 5 by the end of FY 2005. Technology development will be performed through a combination of efforts at JPL and major competed efforts in industry or at universities. Several major technology solicitations have already been executed or are in preparation.

Annual reviews will be held to assess the state of knowledge and development through FY 2005 in order to determine if an architecture selection is possible prior to FY 2006.

Following the selection of an architecture, the design will be refined and key technologies developed to TRL 6 during the formulation phase. Additional insight into the scientific or technology issues will be gained from precursor missions such as SIRTF and Kepler as well as any other precursors (Section 6.6). The current start date for TPF is FY 2011 following the launch of NGST. The current TPF schedule is shown in Figure 6-1.

6.2. Cost

The current studies did not attempt to estimate the costs of the various TPF options. The level of risk associated with many of the excluded options (e.g., IR coronagraphs and the NLRA) have led to the conclusion that these options were likely to cost more, in a relative sense, than the visible coronagraphs and IR nulling interferometers. One of the products of the "point design" mission studies JPL will perform over the next several years will be preformulation phase cost estimates that can be factored into the final architecture selection.

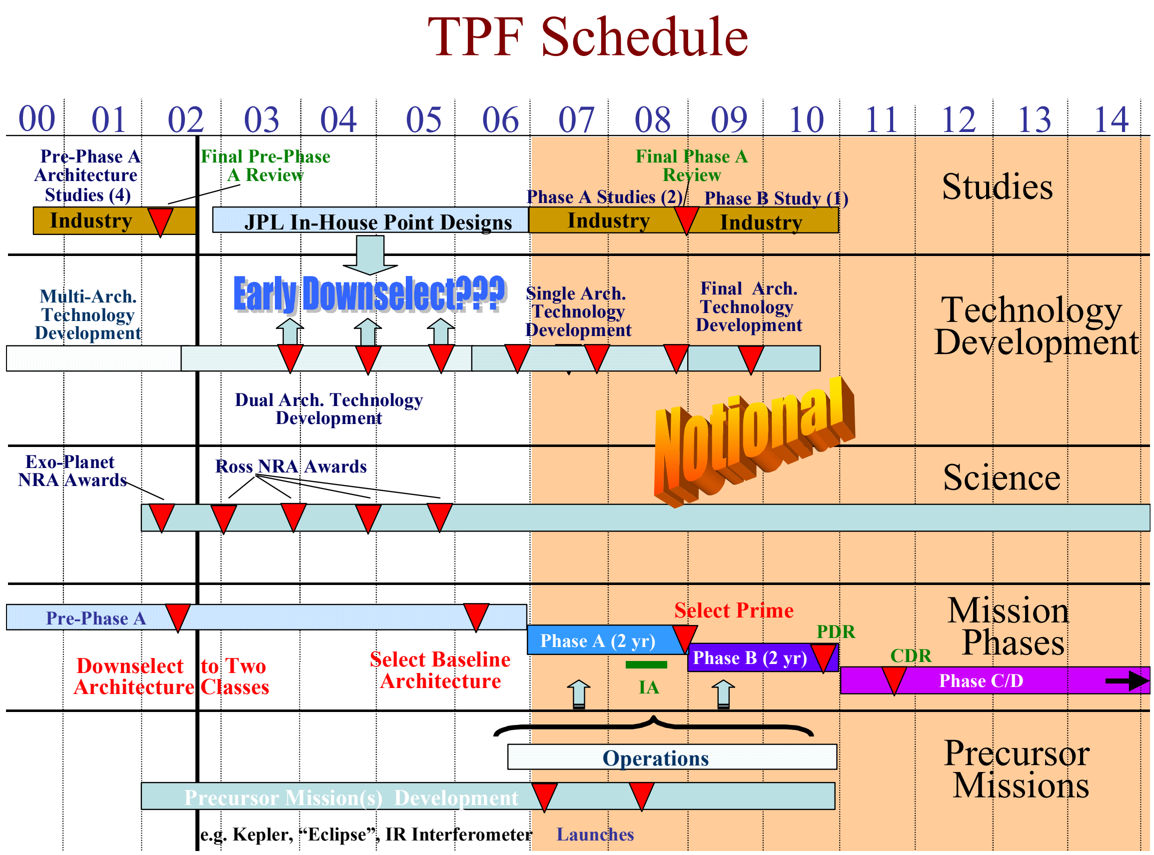

Figure 6-1. A notional schedule for TPF shows downselect between coronagraphic and interferometric architectures occurring by 2006 with a start of development by 2011.

6.3. A Strong Science Program is Critical for TPF

Understanding the formation and evolution of other solar systems and the identification of life on other planets calls for a long-term commitment to basic research across a variety of disciplines and a large suite of supporting observations. The TPF-SWG and other groups have identified a number of these, some of which are already being supported by NASA, others of which might be. Funding through the various grants programs (Astrobiology Institute, Exobiology, Origins of Solar Systems, Theory Program, etc.) is critical to address such key theoretical questions as the following:

- What is the initial mass, structure, motions, composition, and temperature of the solar nebula, and what were the time scales over which planets formed?
- What are the conditions of star formation that lead to a single star surrounded by a protoplanetary disk?
- What was the infall history of material falling onto the young Earth?
- How stable are multi-planet systems?
- What is the effect on terrestrial planets of differing configurations of giant planets and debris belts (asteroid, Kuiper, Oort cloud equivalents, etc.)?
- How do exozodiacal disks form, evolve, and dissipate?
- What determines the chemical fractionation observed in the primitive meteorites, and what determines the abundance of volatiles in the planets?
- How do we model the relative abundances of gaseous by-products of geological and biological processes?

A variety of ground-based observing programs could help establish a firm set of requirements for TPF. Some of these are already being funded by NASA, others might be added to a broad-based attack on the problem of extrasolar planets:

- Dedicated facilities for radial-velocity (Doppler) monitoring of stars.
- Microlensing surveys for giant and terrestrial planets.
- Transits of giant planets from ground-based telescopes.
- Long term astrometry of long-period gas-giant planets from ground-based interferometers.
- Imaging and spectroscopy of circumstellar disks.
- Direct imaging of gas giants using advanced adaptive optics systems on ground-based telescopes.

A vigorous research program will have numerous advantages for the goals of TPF: researchers will be attracted by exciting research with near-term rewards, a broad multi-disciplinary community of scientists and technologists will be created that will be the eventual builders and users of TPF. The already strong public interest in the search for planets will be maintained and even increased by a steady stream of exciting new results. To ensure long-term support for TPF, these results should be conveyed to the public through an active program of public outreach and education.

6.4. A Strong Technology Program is Critical for TPF

Differentiating between the candidate architectures and demonstrating readiness for TPF to enter formulation in the FY 2007 timeframe will require a better understanding of the real-world challenges and limitations for the mission. A strong, well-conceived, well-funded technology development program is required to accomplish these objectives. The Project is currently in the process of planning and implementing such an effort intended to provide the necessary information to enable architecture selection in FY 2006 or sooner.

The content of the effort has been developed from the information gleaned from the current architecture studies with the assistance of the independent TPF Technology Review Board. Current plans call for addressing the topics summarized in Table 6-1.

Table 6-1. Key Areas for Technology Development

Coronagraph Technology
Large lightweight, high-precision optics
Starlight suppression techniques
Image and pupil-plane masks and stops
Wavefront sensing and control
High-actuator-density deformable mirror
Precision deployment mechanisms
System testbeds

Formation Flying Interferometer Technology
Precision formation flying
Formation sensing and metrology
Formation control algorithms
Low-thrust propulsion
Separated-spacecraft interferometry
Beam transport and stray light rejection
System testbeds

Interferometer Core technology
Nulling
Cryogenic mechanisms and beam path
Cryogenic optics & structures (including deployment)
System Testbeds

Structurally Connected Interferometer Technology
Precision deployment mechanisms
Lightweight, cryogenic structures

Observatory Technology
Cryocoolers
Integrated modeling and simulation tools

A strong technology program including contributions from researchers in industry, academia, NASA, and the broader commun ity will generate and validate the best ideas for implementing TPF, facilitate the final architecture selection, and train future TPF builders and users. The results of the technology development, along with those from a strong science program and mission study effort, will position TPF for formulation, implementation, and launch by the middle of the next decade.

6.5. Mission Studies and Potential Precursor Missions

While a visible coronagraph and an infrared interferometer appear to be viable architectures for TPF, there are still many unanswered questions and unexplored details in each system. In order to guide the technology development effort and the ultimate selection of the TPF architecture, it is necessary to delve more deeply into the design concepts. Therefore, NASA will develop point designs for a range of coronagraph and interferometer missions. The goal of this preformulation activity is to perform high- and mid-level trade studies, demonstrate feasibility at the mission level, and provide a solid basis for the technology requirements.

The study teams all highlighted the scientific and technological value of one or more missions smaller than the full scale TPF. Such missions would be smaller, lower risk, less challenging, and lower in cost than TPF. They might be carried out sooner and, while necessarily having reduced capability, would produce high-quality science relevant to TPF. Table 6-2 lists some examples. The Project will evaluate, as part of the mission studies, the cost and risk reduction that could be achieved and the science that could be produced by missions that are reduced in scale and scope relative to the full-scale TPF mission.

Table 6-2. Potential TPF Precursors

Mission	Technology Benefit	Science Return
StarLight	Formation Flying Interferometry	None
IR Interferometer (9-m baseline, two 0.6-m mirrors)	Demonstrate IR nulling; precision, cryogenic structure	Detection of hot Jupiters
IR Interferometer (20 m, four 2-m mirrors)	Demonstrate IR nulling, precision, cryogenic structure	Jupiters, nearest Earths (< 8 pc)
Visible Coronagraph (2-m mirror)	Demonstrate visible coronagraph, apodized apertures	Low-resolution spectroscopy of Jupiters to 25 pc
Visible Coronagraph (4-m mirror)	Demonstrate visible coronagraph, apodized aperture; fabrication of large telescopes	High-resolution spectroscopy of Jupiters to 50 pc, nearest Earths. Strong ancillary astrophysics

6.6. Continuing Involvement with International Partners

The TPF Project has worked closely with other space agencies to lay the groundwork for future collaboration. In Europe, ESA has been studying the Darwin mission which is a nulling IR interferometer similar to the free-flying interferometer studied in the US. Two years ago, NASA and ESA each named scientists to serve on the science team of the other agency's project. A Letter of Agreement is pending between ESA and NASA to lay out plans for collaborative studies and ITAR-compliant technology development in support of the architecture downselect to take place in two to three years. This letter acknowledges the ultimate goal of a collaboration on a joint TPF/Darwin mission. Each agency will continue to have members on both science teams and will have semi-annual management meetings to ensure close coordination between the projects and agencies on technology plans, key decisions, and project milestones.

In addition to its contacts with ESA, the TPF Project has worked with the Inter-Agency Consultative Group (IACG) that advises NASA, ESA, the Japanese (ISAS) and Russian space agencies. In support of the IACG, the TPF Project invited an ISAS scientist to participate in the TPF-SWG activities over the past two years. The IACG has established a working group to advise all four agencies on the opportunities for additional collaborations.

7 The Importance of TPF's Goals

One of mankind's longest standing questions is: "*Are we alone in the universe?*" The successful detection of an Earth-like planet with an environment suitable for life as we know it would have dramatic implications for humanity's view of our place in the universe. The scientific answer to this question builds not only on astronomy and space sciences, but draws on geophysics, atmospheric physics, biophysics and organic chemistry. Observations conducted from space over the next two decades will provide the key to understanding the origin of life and its evolution in the universe by allowing us to detect and study Earth-type planets and to characterize them as possible abodes of life. Although for centuries this question has been the topic of vigorous philosophical and religious debate, we have finally arrived at a time when our technology has advanced to a state that allows us to address this question with the tools of science.

But these questions are deep enough and the observational challenges great enough that this investigation will require a suite of evermore capable observatories. In the sense that observational cosmology, which started with Edwin Hubble's first observations from Mt. Wilson, will be 90-years old by the time that NGST takes its first images, we must recognize that the search for other planets is still in its infancy. It was only in 1995 that Mayor and Queloz (1995) and Marcy and Butler (1996) first identified planets orbiting other stars like the Sun. Since that remarkable breakthrough, ground and space-based observatories have taken a few more small steps with the discoveries of additional planets via radial velocity studies, transits, and the imaging of hot young planets (or brown dwarfs). Within the next decade, approved NASA programs such as SIM, Kepler, and NGST will take the next important steps by carrying out a planetary census and imaging Jupiter-mass planets around the nearest stars. But it will only be with the launch of TPF that we will be able to address the central questions of life and habitability beyond our solar system.

The NAS/NRC Decadal Review of Astronomy and Astrophysics (2001) recognized the long term importance of this research, stating in the endorsement of these goals that TPF should:

> *"Search for life outside of earth and, if it is found, determine its nature and its distribution in the galaxy…[This] is so challenging and of such importance that it could occupy astronomers for the foreseeable future."*

However, the Decadal Review expressed reservations about the complexity of TPF, called for developing increased confidence that terrestrial planets actually exist before initiating TPF, and emphasized the importance of a general astrophysics capability for the mission. NASA's Origins program and the TPF Project have addressed these concerns directly:

– The recently completed TPF studies have shown that *there are credible engineering solutions to the challenges of TPF*. A well-funded program of technology development including ground testbeds and space precursors, as appropriate, will address issues of technology readiness and system complexity.

– Observations from SIRTF, SIM, Kepler, and NGST as well as from ground-based observatories will greatly improve our knowledge of all constituents of planetary systems, from gas giants and debris disks to rocky planets, both in a statistical sense and around the specific nearby stars that will be TPF's targets.

– The teams studying the IR interferometers and visible coronagraphs each identified exciting astrophysical goals that their concepts could address. In the words of the TPF Science Working Group: "An observatory with the power to detect an Earth orbiting a nearby star will be able to collect important new data on many targets of general astrophysical interest."

As the technology matures and the opportunity to start the mission approaches, NASA and the science community will have to reach a consensus on the scientific performance in the areas of planet finding and general astrophysics needed to justify the mission. Some of TPF's observational capabilities will be affordable; others will have to be deferred to subsequent, still more capable missions.

This judgment will demand increased knowledge about all aspects of the frequency, nature and evolution of planetary systems. The missions and investigations outlined above, including SIRTF, SIM, Kepler, and NGST, as well as ground-based activities will provide important scientific background. The technology program, if adequately funded, will provide the engineering basis for choosing a particular design and implementing it in a timely and cost-effective manner. At the end of TPF's preformulation phase, NASA—together with its potential international partners—will be prepared to address the challenge of looking for habitable planets and seeking signs of life beyond the Solar System.

References

J.R.P. Angel and N.J. Woolf, “An imaging nulling interferometer to study extrasolar planets,” *Astrophys. J.* **475**, 373–379 (1997).

Astronomy and Astrophysics in the New Millennium, National Academy Press, Washington, D.C. (2001).

C.A. Beichman, ed., *A Road Map for the Exploration of Neighboring Planetary Systems (ExNPS)*, (Jet Propulsion Laboratory, Pasadena, CA, 1996).

C.A. Beichman, N.J. Woolf, and C.A. Lindensmith, eds., *The Terrestrial Planet Finder: A NASA Origins Program to Search for Habitable Planets*, JPL Publication, 99-3 (Jet Propulsion Laboratory, Pasadena, CA, 1999).

C.A. Beichman, “NASA’s Terrestrial Planet Finder: searching for pale blue dots,” in *Planetary Systems in the Universe: Observation Formation and Evolution*. A. Penny, P. Artymowicz, A.-M. Lagrange, and S. Russell, eds., IAU Symp. 202, ASP Conf. Ser. (Brigham Young University Press: Provo, Utah, 2002)

B. Burke and R. Brown, eds., *TOPS: Toward Other Planetary Systems*, (NASA, Washington, DC, 1992).

A. Burrows et al., “The spectral character of giant planets and brown dwarfs,” in *The Tenth Cambridge Workshop on Cool Stars, Stellar Systems and the Sun*, R. A. Donahue and J. A. Bookbinder, eds., ASP Conf. Ser. **154** (Brigham Young University Press: Provo, Utah, 1998) p.27.

D.J. Des Marais et al., “Remote sensing of planetary properties and biosignatures on extrasolar terrestrial planets,” *Astrobiology*, in press (2002).

D.J. Des Marais et al., *Biosignatures and Planetary Properties to be Investigated by the TPF Mission*, JPL Technical Report 01-008 (Jet Propulsion Laboratory: Pasadena, CA, 2001).

A. Dressler, ed., *HST and Beyond: Exploration and the Search for Origins: A Vision for Ultraviolet-Optical-Infrared Space Astronomy*, (AURA, Washington, DC, 1996).

J.F. Kasting, D.P. Whitemire, and R.T. Reynolds, “Habitable zones around main-sequence stars,” *Icarus* **101**, 108–128 (1993).

J.I. Lunine, “The occurrence of Jovian planets and the habitability of planetary systems,” *Proc. Nat. Acad. Sci.* **98**, 809–814 (2001).

M. Mayor and D. Queloz, “A Jupiter-mass companion to a solar-type star,” *Nature* **378**, 355–359 (1995).

G. Marcy and P. Butler, “A planet orbiting 47 Ursae Majoris,” *Astrophys. J.* **464**, L153–L156 (1996).

P. Nisenson and C. Papaliolios, “Detection of Earth-like planets using apodized telescopes,” *Astrophys. J.* **548**, L201–L205 (2001).

D.N. Spergel, “A new optical coronagraph for terrestrial planet detection,” *Appl. Opt.*, submitted (2001)

N. Woolf and J.R. Angel, “Astronomical searches for Earth-like planets and signs of life,” *Ann. Rev. Astron. Astrophys.* **36**, 507–537 (1998).

Acknowledgements

The editors would like to acknowledge the contributions of the contractor team members in industry and academia for their dedication and hard work in generating the material described in this overall report and in their individual reports. In addition, the TPF Science Working Group and Independent Technology Review Board provided expert guidance to the Project in many areas. Members of the JPL project also made valuable contributions to these studies, including: E. Serabyn, O. Lay, T. Velusamy, R. Morgan, M. Devirian, G. Campbell, K. Miller, C. Davis, P. Dumont, J. Cornish, M. King, K. Lynn, C. Weaver, M. Young, K. Marshall.

The TPF activities were funded by NASA through contracts to the Jet Propulsion Laboratory which is managed for NASA by the California Institute of Technology.

Appendices

APPENDIX A
Study Teams,
Science Working Group,
and Technology Review Panel

Table A-1. Ball Aerospace: University Science Team Members

Ball Aerospace	**Study Lead: Dr. Steve Kilston** **Science Lead: Dr. Bob Brown**		
STScI	**Penn State**	**Carnegie Inst.**	**Joint Astronomy Center**
Dr. Bob Brown	Dr. Jim Kasting	Dr. Alan Boss	Dr. Tim Hawarden
Dr. Ron Allen			
Dr. Pierre Bely	**Smithsonian Astrophysical Obs.**	**Rutherford-Appleton Laboratory**	**Univ. of Hawaii**
Dr. Chris Burrows			Dr. Christ Ftaclas
Dr. Torsten Böker	Dr. Wes Traub	Dr. Alan Penny	
Dr. Steve Lubow	Dr. Ken Tucks		**Naval Research Lab**
Dr. Richard Miles	Dr. Marc Kuchner	**Univ. of Florida**	Dr. D. Mozurkewich
		Dr. Charlie Telesco	
Princeton Univ.	**UCSD**		**Inst. for Advanced Studies**
Dr. Ed Turner	Dr. A. Quirrenbach	**Univ. of Colorado**	
Dr. David Spergel	Dr. Ed Stephan	Dr. John Bally	Dr. Sara Seager
Dr. Russ Arrell		Dr. Peter Bender	
Dr. Edgar Choueiri	**UCSC**	Dr. Tim Brown	
Dr. Pini Gurfil	Dr. Jerry Nelson	Dr. Web Cash	
Dr. Norm Jarosik		Dr. Tuck Stebbins	
Dr. Jeremy Kasdin		Dr. Robin Stebbins	
Dr. Mike Littman		Dr. Webster Cash	
		Dr. Greg Kopp	

Table A-2. Lockheed Martin: University Science Team Members

Lockheed Martin	**Study Lead: Dr. Domenick Tenerelli** **Science Lead: Dr. Neville Woolf**		
Univ. of Arizona	**Lockheed**	**Princeton Univ.**	**MIT**
Dr. Neville Woolf	Dr. Adrian Roche	Dr. James Gunn	Dr. Dave Miller (Lead)
Dr. Roger Angel	Dr. Alan Title		Dr. Jonathan How
Dr. Jonathan Lunine		**Caltech**	Dr. Brian Makins
Dr. Phil Hinz	**NASA-Ames**	Prof. J. Westphal	Dr. Cyrus Jilla
Dr. Tom Connors	Dr. Dave Des Marais		Dr. Edmund Kong
Dr. Tom McMahon		**STScI**	
Dr. Jim Burge	**NASA/GSFC**	Dr. Peter Stockman	**Busek**
	Dr. John Mather		Dr. Vlad Hruby

Table A-3. TRW: University Science Team Members

TRW	**Study Lead: Dr. Chuck Lillie** **Science Leads: Dr. Ned Wright and Dr. S. Casement**		
UCLA	**UC Berkeley**	**CWRU**	**MPI**
Dr. Ned Wright (PI)	Dr. Frank Shu	Dr. Craig Copi	Dr. Thomas Herbst
Dr. James Larkin	Dr. James Graham	Dr. Glenn Starkman	
			USNO
TRW	**UCSC**	**NRAO**	Dr. Ken Johnston
Dr. S. Casement	Dr. Douglas Lin	Dr. Richard Simon	
	Dr. Steve Vogt		**JPL**
Carnegie Inst.		**Obs. de Paris**	Dr. John Trauger
Dr. Alan Dressler	**LLNL**	Dr. V. Coudé du Foresto	Dr. B. Mennesson
	Dr. Charles Bennett		
			Consultant
			Dr. Dan Weedman

Table A-4. Boeing-SVS University Science Team Members

Boeing-SVS	Study Leads: Mr. Mike Kaplan and Dr. Ed Friedman Science Lead: Dr. Steve Ridgway

NOAO
Dr. Steve Ridgway

Montpellier
Dr. Michel Faucherre

Franklin & Marshall
Dr. Dana Backman

Obs. de Haute-Provence
Dr. Antoine Labeyrie
Dr. Sophie Gillet
Dr. Olivier Lardiere
Dr. Luc Arnold

Laboratoire d'Astrophysique de Marseille
Dr. Roger Malina
Dr. Pascal Dargent
Dr. Pierre Barge
Dr. Magali Deleuil
Dr. Kjetil Dohlen

Obs. de Paris
Dr. Pierre Riaud
Dr. Daniel Rouan
Dr. Jean Schneider

NASA/GSFC
Dr. Bill Danchi
Dr. Dan Gezari
Dr. Richard Lyon
Dr. Harvey Moseley
Dr. Daesoo Han
Dr. Tim Murphy

Caltech
Dr. Anthony Boccaletti

CNRS
Dr. Robin Kaiser

UC Berkeley
Prof. Charles Townes

Smithsonian Astrophysical Observatory
Dr. Peter Nisenson
Dr. Cos Papaliolios
Dr. Gary Melnick

Univ. of Hawaii
Dr. Olivier Guyon
Dr. F. Roddier
Dr. C. Roddier
Dr. Pierre Baudoz

Cornell
Dr. Martin Harwit

Testex
Dr. Bob Stachnik

Univ. of Maryland
Dr. J. Staguhn

Univ. de Nice
Dr. Claude Aime
Dr. Remi Soummer

Univ. de Rennes
Dr. Yann Legrand

Observatoire de la Côte d'Azur
Dr. Bruno Lopez
Dr. Farrokh Vakili
Dr. Lyu Abe

Digiphase
Dr. Lawrence Mertz

Phillips Lab
Dr. Sergio Restaino

Rowland Institute
Dr. Jean Marc Fournier

Table A-5. TPF Science Working Group (2000–2002)

TPF Science Working Group		
Name	**Institution**	**Team Affiliation**
Charles Beichman	Jet Propulsion Laboratory	TPF-SWG co-chair
Frank Shu	University of California, Berkeley	TPF-SWG co-chair, TRW
Roger Angel	University of Arizona	Lockheed Martin
Robert Brown	Space Telescope Science Institute	Ball Aerospace
Dave Des Marais	NASA Ames Research Center	Lockheed Martin
Suzan Edwards	Smith College	
Malcolm Fridlund	ESA/ESTEC	
Dan Gezari	NASA Goddard Space Flight Center	Boeing-SVS
Martin Harwit	Cornell University	Boeing-SVS
James Kasting	Penn State University	Ball Aerospace
Doug Lin	University of California, Santa Cruz	TRW
Jonathan Lunine	University of Arizona	Lockheed Martin
Geoff Marcy	University of California, Berkeley	
Ken Nealson	University of Southern California	
Steve Ridgway	National Optical Astronomy Observatory	Boeing-SVS
Huub Röttgering	University of Leiden	
Anneila Sargent	California Institute of Technology	
Mike Shao	Jet Propulsion Laboratory	
David Spergel	Princeton	Ball Aerospace
Robert Stachnik	Testex	Boeing-SVS
Glenn Starkman	Case Western Reserve University	TRW
Motohide Tamura	National Astronomical Observatory of Japan	
Wes Traub	Smithsonian Astrophysical Observatory	Ball Aerospace
Nick Woolf	University of Arizona	Lockheed Martin
Ned Wright	University of California, Los Angeles	TRW

Table A-6. TPF Independent Technology Review Board

TPF Independent Technology Review Board		
Name	**Institution**	**Area of Expertise**
Pierre Bely	Space Telescope Science Institute	Large optical systems
Rich Capps	Jet Propulsion Laboratory	Origins theme technologist
Mark Colavita	Jet Propulsion Laboratory	Interferometry systems
Dick Dyer	Schafer Corporation	Large optical systems, precisions wavefront control
Dave Hyland	University of Michigan	Precision formation flying
Ken Johnston	US Naval Observatory	Interferometry systems
Michael Krim	Perkin-Elmer	Large optical systems
John Lipa	Stanford University	Cryogenic systems
Michael Lou	Jet Propulsion Laboratory	Mechanical systems & structures

APPENDIX B
Reference Observations

The TPF Project asked each study team to describe, in a uniform way for easy comparison, the configuration and basic parameters of each architecture, the observing scenario, and the performance on a specific set of targets. This appendix describes the request to the teams in more detail. The subsequent appendices contain the responses to these questions.

B.1. INSTRUMENT CONFIGURATION

As a minimum for each configuration, provide the following critical instrument parameters:

B.1.1 Telescopes and Coronagraphs

1. Optical architecture (apodized aperture, coronagraph, other)
2. Optical layout drawing (if a deformable mirror is used, where is it?)
3. Primary aperture shape, dimensions, actual area, and effective area.
4. Primary aperture optical figure
5. Operational wavelength range
6. Amplitude uniformity requirement
7. Corrected optical figure (after AO, if an deformable mirror is used)
8. Aperture mask shape including intensity and phase tolerances
9. Coronagraph mask shape including intensity and phase tolerances
10. Lyot mask shape including intensity and phase tolerances
11. Angular resolution at planet position, in the final image (after Lyot, etc).
12. Inner and outer radius of effective field-of-view within which planets might be detected (instantaneous and after observations at multiple roll angles)
13. Operating temperatures and thermal stability for key optical components
14. Effects of spacecraft parameters (vibration, pointing jitter, etc) on stability of PSF
15. Spectrometer design
16. Operations scenario (e.g. does the coronagraphic spot or apodized aperture mask change for each target?
17. Specify Q, defined as the operational ratio planet light/scattered starlight. What is the needed stability in the PSF/scattered light to see a planet for a given Q? Justify why you feel the instrument PSF is that stable (not necessary for configurations working at a Q of 1). The value of Q should be consistent with the properties of the optical system given above.

18. Total optical efficiency for planetary light including reflection and transmission losses, effective vs. total collection area, Lyot mask loss, filters, etc. for both broadband and spectroscopic measurements
19. Specify detected average count rates, in the effective planetary diffraction spot size (FWHM), from planet, diffracted star, scattered star, exozodi, local zodi, instrument thermal emission, and detector dark counts. Assume the solar system at 10 pc.

B.1.2 Interferometers

1. Optical architecture ($\theta^{2 \text{ or } 4}$ null, chopping, hypertelescope, densified pupil, etc.)
2. Optical layout drawing (if a deformable mirror is used, where is it?)
3. Primary aperture shapes, dimensions, actual area, effective area, and baselines.
4. Primary aperture optical figure
5. Operational wavelength range
6. Amplitude matching requirement
7. Corrected wavefront (after AO or spatial filtering)
8. Properties of null, including depth and leakage due to finite stellar diameter
9. Assumptions needed to achieve null depth, including optical path accuracy (piston) and pointing accuracy (tip/tilt).
10. Properties of spatial filter, if any.
11. Angular resolution at planet position, in the final image.
12. Inner and outer radius of effective field-of-view within which planets might be detected (instantaneous and after observations at multiple roll angles).
13. Operating temperatures and thermal stability for key optical components
14. Effects of spacecraft parameters (vibration, pointing jitter, etc) on stability of null.
15. Spectrometer design
16. Operations scenario (e.g. does the baseline change for each target?)
17. Specify *Q*, defined as the operational ratio planet light/scattered starlight.
18. Total optical efficiency for planetary light including reflection and transmission losses, effective vs. total collection area, , filters etc. for both broadband and spectroscopic measurements.
19. Specify detected average count rates, in the effective planetary diffraction spot size (FWHM), from planet, diffracted star, scattered star, exozodi, local zodi, instrument thermal emission, detector dark count, and any other source. Assume the solar system at 10 pc.

B.2. CONFIGURATION INFORMATION AND SAMPLE OBSERVING PROGRAM

B.2.1 Photometric Detection

Using a standard Earth spectrum (G2V star, 1 R_e, standard atmosphere, 1 AU; Traub, private communication), each team should describe how long a particular configuration would take to detect an Earth located at 1 AU from a solar type (G2V) at distances of 3, 5, 10 and 15 pc. Assume that the system has only 1 planet, is oriented at 45 deg to the line-of-sight but that the planet is observed at projected separation of 1 AU. The effect of exozodiacal dust emission/scattering should be accounted for by noting the effect on integration time due to shot noise of 0.5, 1,2, 5, and 10 times the level of dust emission/scattering in our own solar system as based on a standard COBE model for our zodiacal cloud. The unit of time to report for each instrument is T_{basic}, the total of integration time to achieve SNR = 5 on the planet *plus* any spacecraft maneuvering time needed to accomplish any motions (rotations) to a survey the full area at 1 AU. *The entire 1 AU zone around the star should be observed with less than a factor of ~2* *variation relative to the quoted sensitivity.* An "observation" may consist of measurements at multiple roll angles or spectral channels that can be averaged to achieve this SNR. As the target stars move to greater distances, achieving the required angular resolution will become more challenging. Each team should specify how the necessity of working at a smaller angular separation quantitatively affects the performance of a particular configuration, e.g., less favorable Q, greater leakage, etc.

While performance at other wavelengths may be specified, please include values at 0.7 μm (visible systems) and 12 μm (IR systems) for easy inter-comparison between different architectures.

All instruments will have to make observations at 2 to 3 different epochs to confirm common proper motions and to detect planets at different orbital positions. Therefore we will multiply the basic observing time by a repeat factor as appropriate to determine the necessary duration of the planet survey portion of the mission. Each team should specify the number of repeats they feel is appropriate.

B.2.2 Spectroscopic Characterization

The second step concerns the spectroscopy for any planets detected as per step 1. Based on the work of Dave Des Marais (Des Marais et al. 2002), each team should determine the observing time (integration time plus spacecraft maneuvering time as required for a source at a *known* position) needed for a particular configuration to detect the following. (a) One or two lines characterizing the planet's atmosphere, e.g. CO_2 or H_2O. (b) One or two lines indicative of the presence of photosynthetic life, e.g. O_2 or O_3.

The teams should highlight all key assumptions, including any spatial or spectral multiplex advantages inherent in each configuration. To put these measurements on a common footing, the teams should use the spectral information in Appendix C (Des Marais et al. 2002) to determine the wavelengths and approximate spectral resolution for their observations. Traub has added a column giving the depth of each feature. The observing time estimate should include the time necessary to detect the line plus any overheads needed for reconfiguring the spacecraft. It is up to each team to describe how it will ensure a minimum SNR = 5 on the presence of the line of a specific species. The description of the line detection algorithm should be quite specific, e.g. detect 6 channels, 2 continuum on each side of the line and two elements across the line. The SNR estimate should include the effect of the narrow bandwidth (R = 5–100 depending on species, wavelength, band) used within each spectral channel, the depth or equivalent width of each spectral signature, and the efficiency of the dispersing element used to make the measurement (prism, grating, etc). Appendix C lists the minimum acceptable resolving power that each instrument should use in calculating the integration time for each spectral line. *For convenience, the strength and shape of each spectroscopic feature in the terrestrial spectrum is given (Appendix C).*

B.2.3 Survey of Nearby Stars

The final step is to assess the performance of each architecture on the list of 150 stars of various spectral types (F5–K5) and distances to assess the ability of TPF to detect an Earth at SNR = 5. This calculation will highlight the trade-offs between sensitivity versus angular resolution of the different instruments. To simplify the problem, each team should investigate a search radius at the habitable zone, R_{HZ}, defined by the luminosity of the star, $R_{HZ} = 1.0 \times L^{0.5}$ AU, and a visible spectrum defined by $B_\nu(T_*)/B_\nu(T_{sun}) \times F_\nu(Traub)$. These assumptions will keep the planet at a constant temperature for the IR instruments, while still accounting for the changing reflection spectrum for the visible light instruments. Each team should give the basic observing time (integration time plus maneuvering time for each star) plus a grand total for the time required to observe all stars *one time* to SNR = 5. Each group should list any criteria they used to winnow the list, for example the constraints on ecliptic or galactic latitude, presence or absence of companions within a certain radius, etc.

APPENDIX C
Terrestrial Spectral Lines

Table C-1. Representative Spectral Lines in the Earth's Atmosphere

Species	Wavelength(μm) Min	Max	Avg.	Resolution ($\lambda/\Delta\lambda$)	Line Depth
CH_4	0.72	0.73	0.73	57	0.002
CH_4	0.78	0.81	0.79	29	0.0009
CH_4	0.88	0.91	0.89	32	0.002
CH_4	0.97	1.02	1.00	20	0.011
CH_4	1.62	1.78	1.69	10	0.012
CH_4	7.37	7.96	7.65	13	0.095
CO_2	1.04	1.06	1.05	40	0.0006
CO_2	1.20	1.23	1.21	34	0.012
CO_2	1.52	1.66	1.59	11	0.030
CO_2	9.56	9.07	9.31	19	0.022
CO_2	10.75	10.10	10.42	16	0.014
CO_2	13.33	17.04	14.96	4	0.374
H_2O	0.71	0.73	0.72	37	0.238
H_2O	0.81	0.83	0.82	35	0.220
H_2O	0.91	0.97	0.94	17	0.628
H_2O	1.10	1.17	1.13	19	0.734
H_2O	1.34	1.48	1.41	10	0.948
H_2O	1.79	1.97	1.88	11	0.969
H_2O	6.67	7.37	7.00	10	0.707
H_2O	17.36	25.00	20.49	3	0.248
H_2O	25.00	33.30	28.57	4	0.353
H_2O	33.33	50.00	40.00	2	0.346
O_3	0.31	0.33	0.32	16	0.692
O_3	0.53	0.66	0.58	5	0.195
O_3	9.37	9.95	9.65	17	0.449
O_2	0.68	0.70	0.69	54	0.124
O_2	0.76	0.77	0.76	69	0.474
O_2	1.26	1.28	1.27	72	0.153
N_2O	7.57	7.55	7.56	18	0.095

APPENDIX D
Ball Team
Design Reference Mission Analysis

D.1. INSTRUMENT CONFIGURATION FOR TPF VISIBLE-LIGHT CORONAGRAPH

D.1.1 SHAPED PUPIL CORONAGRAPH

1. The optical architecture is a coronagraph with a nonapodized primary mirror, and a binary mask at the first pupil image. There is a binary image plane mask, whose purpose is to block the bulk of the excess light, rather than acting as a filter in a classical coronagraph. There is no Lyot stop. Wavefront corrections are made with actuators on the back surface of the primary mirror (low spatial frequencies only), and with a 256×100 actuator deformable mirror at a later pupil image.
2. Optical layout drawing—pages II-13 and II-15 from our Final Architecture Review presentation.
3. The primary mirror is a 4×10 m ellipse with a 14.9-m focal length. It is an off-axis segment of an 11-m diameter paraboloid.
4. The requirements for the optical figure of the primary mirror, after correction with mirror actuators but before the deformable mirror, are wavefront accuracies of:

   8 nm rms at low spatial frequencies: 0–3 Cycles Per Aperture (CPA)

   5 nm rms at critical spatial frequencies: 3–80 CPA

   5 nm rms at mid spatial frequencies: 80–10^4 CPA

   1.5 nm rms at high spatial frequencies: > 10^4 CPA

These requirements are along the major axis (10 m) of the mirror. Our accuracy requirements along the minor axis are a factor of several looser.

If we fail to meet the low or critical spatial frequency requirements (along the major axis) by a small factor, more precise correction with mirror actuators and a deformable mirror can compensate. However, a very accurate wavefront is an essential feature of a high-performance coronagraph.

5. The operational wavelength range is 400–1100 nm, but various effects limit our useful instantaneous bandwidth to approximately 20%.

6. The goal for intensity uniformity of the starlight beam profile at the DM is 3×10^{-5} *rms* in the critical spatial frequency range. If we can achieve this goal, then the DM will be used only for correcting wavefront phase, and we will be able to perform planet searches in two opposite regions (approximately quadrants) of the image plane. If we fail to achieve this level of intensity uniformity at the DM, adjustments with the DM can be used to correct the intensity over half the image plane, giving one usable quadrant. In this latter case, our search times for planets will increase by a factor of two.

7. The requirements for the optical wavefront accuracy, after correction with mirror actuators and the deformable mirror, are:

   1 nm rms at low spatial frequencies: 0–3 Cycles Per Aperture (CPA)

   0.07 nm rms at critical spatial frequencies: 3–80 CPA

   5 nm rms at mid spatial frequencies: 80–10^4 CPA

   1.5 nm rms at high spatial frequencies: > 10^4 CPA

   Note that no corrections are possible at > 80 CPA.

These requirements are along the major axis (10 m) of the mirror. Our accuracy requirements along the minor axis are a factor of several looser.

8. The aperture (pupil plane) mask has a prolate spheroidal function shape. It is a binary mask, with an opaque outer region, and one or more transparent (empty) inner regions. The intensity requirements are that the opaque portions must have transmission < 10^{-7}. If this requirement is achieved, there are no phase requirements. The requirement on the shape is a boundary accuracy of < 1 micron for a 10-cm mask. We are investigating the option of using actuators to control the shape of the mask, in order to mitigate the effect of small amplitude errors (see #6 above).

9. The image plane mask (CFO) is also a binary mask. The rejection of diffracted starlight is achieved entirely with the pupil plane mask: starlight is diffracted into two regions (roughly opposite quadrants) of the image plane. The purpose of the image plane mask is only to remove most of this light, to avoid problems with stray light and detector saturation downstream. Therefore, the requirements for shape and intensity are rather loose: several microns for shape and transmission < 10^{-4}.

10. There is no Lyot mask in this design.

11. With a 4×10 m aperture and a 700 nm reference wavelength, our angular resolution would be 14×36 mas. The pupil mask will degrade the resolution to approximately 20×50 mas. Because of the orientation of our shaped-pupil mask, the direction of highest angular resolution will be approximately along the star-planet separation axis (it would be exactly along that direction if the planet were in the middle of the search cone on the sky).

12. The outer radius of the effective field-of-view is set by the number of actuators on the deformable mirror. It is approximately 1.5 arcseconds at a wavelength of 700 nm. The inner radius is set by the ability to suppress diffracted starlight in our search quadrants. For a wavelength of 700 nm, this is 70 mas. Both radii scale with wavelength, so that we can achieve 50 mas inner radius in our preferred observing band of 450–550 nm.

13. Our operating temperature is 50°C for the optical bench, and 0°C for the primary mirror. During exposures of multiple hours, the front-to-back temperature difference in our primary mirror must remain constant to 1 mK.

14. Our requirements for pointing jitter are 14 mas in body pointing, with control by a fine steering mirror to 1 mas. Our requirements on vibrations depends on their frequency and location. Their effect on the wavefront must be controlled to < 50 pm rms.

15. For spectroscopy, the same optical system will be used, but a spectrograph with a radial entrance slit will be placed in the image plane. This entrance slit will range from the Inner Working Distance (IWD) to the Outer Working Distance (OWD). We will rotate either the telescope or the spectrograph so that the planet lies on the entrance slit. A prism will be used to achieve R = 20–80 on the image of the planet.

16. For our operations scenario, we have the option of a small number of pupil plane and image plane masks which can be chosen for different types of targets/observations. Our design does not require changing the

pupil mask, but a selection of field occulting masks allows us to optimize the IWD for a given wavelength.

17. We approach Q in different ways for different types of noise sources. For sources that we know are statistical in nature, averaging via a long integration will ease our requirement on Q. For the most demanding case specified here, exozodi level of ×10 and a star at 15 pc, we have $Q = 0.05$ for these statistical noise sources. For residual diffracted light, which should be fairly constant in time, we estimate $Q = 1$ as a requirement for planet detection. For cases in this assignment where our numerical simulations yield $Q < 1$, we have stated that planet detection is not possible. For residual scattered light, we set a requirement of $Q = 1$ for planet detection or characterization, and specify corrected wavefront accuracies small enough to allow $Q = 1$. We estimate that the stability of scattered light during an integration will be approximately 20% of the total scattered light level. The Q values for diffracted and scattered light refer to the ratio between the planet flux and the DC background signal level in that region of the image.

18. The optical efficiency is determined by three main items: the pupil mask, mirror reflectivity, and detector quantum efficiency. Our pupil mask has a 50% throughput (geometrical coverage factor). Our plan for mirror coatings is to have the primary and secondary mirrors coated with aluminum, have a pick-off mirror for UV observations, and have downstream mirrors in the coronagraph coated with silver. Two aluminum-coated mirrors, each with 88% reflectivity at 700 nm, and eight silver-coated mirrors, each with 98.8% reflectivity at 700 nm, give a throughput of 70%. Finally, our CCD quantum efficiency at 700 nm is 80%, for a total throughput of 28% in broadband (detection) observations. For spectroscopy, the importance of measuring continuum channels longward of the 940 nm water line leads us to the choice of an InGaAs detector, with quantum efficiencies of 60% at 700 nm and 80% at 1100 nm.

19. The average count rates for a sun-earth combination at 10 pc in the 650–750 nm band are: 0.15 s^{-1} from the planet, 0.09 s^{-1} from the local zodi, 0.12 s^{-1} from the exozodi, 0.01 s^{-1} from diffracted starlight, and 0.15 s^{-1} from scattered starlight. (As stated above in #17, the diffracted starlight level is calculated via numerical simulations. The level of scattered starlight is specified, and the wavefront accuracy requirements are derived to meet this level.) The detector read noise and dark current are 2 electrons and 0.001 s^{-1} for each pixel. The above count rates are for one diffraction spot size, and we assume 9 pixels per diffraction beam. The instrument thermal emission is negligible.

D.1.2 CLASSICAL CORONAGRAPH

1. The optical architecture is a coronagraph with a non-apodized primary mirror, and no pupil mask. There is a graded image plane mask, plus a Lyot stop. Wavefront corrections are made with actuators on the back surface of the primary mirror (low spatial frequencies only), and with a 256×100 actuator deformable mirror at a pupil image.

2. Optical layout drawing—pages II-13 and II-15 from our Final Architecture Review presentation.

3. The primary mirror is a 4×10-m ellipse with a 14.9 m focal length. It is an off-axis segment of an 11 m diameter paraboloid.

4. The requirements for the optical figure of the primary mirror, after correction with mirror actuators but before the deformable mirror, are wavefront accuracies of:

   8 nm rms at low spatial frequencies: 0–3 Cycles Per Aperture (CPA)

   5 nm rms at critical spatial frequencies: 3–80 CPA

   5 nm rms at mid spatial frequencies: 80–10^4 CPA

   1.5 nm rms at high spatial frequencies: > 10^4 CPA

These requirements are along the major axis (10 m) of the mirror. Our accuracy requirements along the minor axis are a factor of several looser.

If we fail to meet the low or critical spatial frequency requirements (along the major axis) by a small factor, more precise correction with mirror actuators and a deformable mirror can compensate. However, a very accurate wavefront is an essential feature of a high performance coronagraph.

5. The operational wavelength range is 400–1100 nm, but various effects limit our useful instantaneous bandwidth to approximately 20%.
6. The goal for intensity uniformity of the starlight beam profile at the DM is 3×10^{-5} *rms* in the critical spatial frequency range. If we can achieve this goal, then the DM will be used only for correcting wavefront phase, and we will be able to perform planet searches in two opposite regions (approximately quadrants) of the image plane. If we fail to achieve this level of intensity uniformity at the DM, adjustments with the DM can be used to correct the intensity over half the image plane, giving one usable quadrant. In this latter case, our search times for planets will increase by a factor of two.
7. The requirements for the optical wavefront accuracy, after correction with mirror actuators and the deformable mirror, are:

   1 nm rms at low spatial frequencies: 0–3 Cycles Per Aperture (CPA)

   0.07 nm rms at critical spatial frequencies: 3–80 CPA

   5 nm rms at mid spatial frequencies: 80–10^4 CPA

   1.5 nm rms at high spatial frequencies: > 10^4 CPA

   Note that no corrections are possible at > 80 CPA.

These requirements are along the major axis (10 m) of the mirror. Our accuracy requirements along the minor axis are a factor of several looser.

8. There is no aperture mask in this design.
9. The image plane mask will be very long in one direction (so it has zero bandwidth in that direction). This choice provides ~15% greater throughput than the spot-like mask case, and makes the instrument insensitive to pointing errors and wavefront intensity and phase errors along that direction. The cost is a small fraction of the search area (reducing it from 100% to 85%).

In the other direction, the mask will be band-limited to a ~20% bandwidth, with a Gaussian mask as a backup in case the band-limited mask proves to be too hard to manufacture. The attenuation for the mask must be > 10^6 at the center over the core of the stellar image, assuming that we use a graded Lyot stop. The *rms* transmission error must be < 10^{-8} over the core of the stellar image at critical spatial frequencies. Elsewhere on the mask, the tolerances are two to fix orders of magnitude less severe. The design is completely insensitive to high spatial frequency transmission errors (< $\lambda/(2D)$).

As illustrated in the results from Step 1 (broadband) and Step 2 (spectroscopy) calculations, the classical coronagraph can achieve a smaller Inner Working Distance than a shaped-pupil coronagraph. However, a variable transmission mask (required for the classical coronagraph) is more challenging to produce, whereas the binary masks of the shaped-pupil coronagraph are comparatively easy to manufacture.

10. The Lyot mask is opaque exterior to the mask band, and graded interior to the mask band (or the Gaussian -40 dB band) with a mild apodizing function (like a Hanning function) to suppress low frequency transmission errors in the image plane mask. Since 99.9999% of the starlight is outside the mask band, the grading transmission need only be accurate at the ~5% level.
11. With a 4×10 m aperature and a 700 nm reference wavelength, our angular resolution is 14×36 mas. The Lyot stop will degrade the resolution at the location of the planet. With our nominal Lyot stop (50% throughput), the solid angle of the beam will be increased by a factor of two. Because of the orientation of our image plane mask, the direction of highest angular resolution will be approximately along the star-planet separation axis (it would be exactly along that direction if the planet were in the middle of the search cone on the sky).
12. The outer radius of the effective field-of-view is set by the number of actuators on the deformable mirror, and is approximately 1.5 arcseconds at 700 nm wavelength. The inner radius depends on our image plane

mask-Lyot stop pair, and is a soft limit—the transmission of a Gaussian mask drops as the angular radius decreases (note that a planet's brightness *increases* with decreasing orbital radius). Our nominal image plane mask-Lyot stop pair (which was used for the calculations reported here) consists of an attenuation HWHM of 3.3 Airy radii, and a Lyot stop that blocks 50% of the light. If we define the 30% transmission point through such an image plane mask as our IWD, then IWD = 59 mas × λ (μm).

13. Our operating temperature is 50°C for the optical bench, and 0°C for the primary mirror. During exposures of multiple hours, the front-to-back temperature difference in our primary mirror must remain constant to 1 mK.

14. Our requirements for pointing jitter are 14 mas in body pointing, with control by a fine steering mirror to 0.5 mas. Our requirements on vibrations depends on their frequency and location. Their effect on the wavefront must be controlled to < 50 pm rms.

15. For spectroscopy, the same optical system will be used, but a spectrograph with a radial entrance slit will be placed in the image plane. This entrance slit will range from the Inner Working Distance (IWD) to the Outer Working Distance (OWD). We will rotate either the telescope or the spectrograph so that the planet lies on the entrance slit. A prism will be used to achieve R = 20–80 on the image of the planet.

16. For our operations scenario, we have the option of a small number of image plane and Lyot masks which can be chosen for different types of targets/observations. By using a smaller (sharper falloff) image plane mask, we can achieve a smaller IWD. However, we then need to block more of the light with the Lyot stop, reducing the total throughput.

17. We approach Q in different ways for different types of noise sources. For sources that we know are statistical in nature, averaging via a long integration will ease our requirement on Q. For the most demanding case specified here, exozodi level of ×10 and a star at 15 pc, we have $Q = 0.05$ for these statistical noise sources. For residual diffracted light, which should be fairly constant in time, we estimate $Q = 1$ as a requirement for planet detection. For cases in this assignment where our numerical simulations yield $Q < 1$, we have stated that planet detection is not possible. For residual scattered light, we set a requirement of $Q = 1$ for planet detection or characterization, and specify corrected wavefront accuracies small enough to allow $Q = 1$. We estimate that the stability of scattered light during an integration will be approximately 20% of the total scattered light level. The Q values for diffracted and scattered light refer to the ratio between the planet flux and the DC background signal level in that region of the image

18. The optical efficiency is determined by four main items: the Lyot stop, mirror reflectivity, detector quantum efficiency, and image plane mask. Our nominal Lyot stop has a 50% throughput (geometrical coverage factor). Our plan for mirror coatings is to have the primary and secondary mirrors coated with aluminum, have a pick-off mirror for UV observations, and have downstream mirrors in the coronagraph coated with silver. Two aluminum-coated mirrors, each with 88% reflectivity at 700 nm, and eight silver-coated mirrors, each with 98.8% reflectivity at 700 nm, give a throughput of 70%. Finally, our CCD quantum efficiency at 700 nm is 80%, for a total throughput (exclusive of the image plane mask) of 28% in broadband (detection) observations. For spectroscopy, the importance of measuring continuum channels longward of the 940 nm water line leads us to the choice of an InGaAs detector, with quantum efficiencies of 60% at 700 nm and 80% at 1100 nm.

The throughput factor for the image plane mask will depend on the separation angle between the star and the planet (see #12 above). We specify a Gaussian mask, with a HWHM of 3.3 Airy radii. In practice, this has almost no effect for 1 AU planets at 3 or 5 pc, but a substantial effect for 1 AU planets at 10 or 15 pc.

19. The average count rates for a Sun-Earth combination at 10 pc in the 650 to 750 nm band are: 0.13 s^{-1} from the planet, 0.08 s^{-1} from the local zodi, 0.11 s^{-1} from the exozodi, 0.04 s^{-1} from diffracted starlight, and 0.13 s^{-1} from scattered starlight. (As stated above in #17, the diffracted starlight level is calculated via numerical simulations. The level of scattered starlight is specified and the wavefront accuracy requirements are derived to meet this level.) The detector-read noise and dark current are 2 electrons and 0.001 s^{-1} for each pixel. The above count rates are for one diffraction spot size, and we assume 9 pixels per diffraction beam. The instrument thermal emission is negligible.

D.2. Photometric Detection Calculations for TPF Visible Light Coronagraph

D.2.1 CALCULATION OF SIGNAL

Calculation of the count rate from the planet requires only the input spectral flux (supplied with our assignment), the instrument throughput, and the instrument passband. We have chosen a passband of 650–750 nm, with the reference wavelength from JPL's assignment (700 nm) at its center, and the approximate bandwidth for which we get the optimum combination of sensitivity and rejection of starlight. The instrument throughput consists of the area of the primary mirror (31.4 m^2), the fraction of light passed by the various masks (0.44 for the shaped-pupil coronagraph; < 0.50 for the classical coronagraph, depending on angular distance from the star), two reflections off aluminum-coated mirrors and eight reflections off silver-coated mirrors ($0.882^2 \times 0.988^8 = 0.71$), and the quantum efficiency of the detector (0.80 at 700 nm).

D.2.2 CALCULATION OF NOISE

There are several noise sources for observations with the visible-light coronagraph. The statistical noise sources can be readily calculated with a spreadsheet.

At visible wavelengths, the statistical noise sources are: local zodiacal light, exozodiacal light, detector-read noise, and detector dark current. The table from JPL's assignment gives the spectral flux from 1.0 zodi. The flux is specified as the value for a 0.1 AU diameter circular patch, 1 AU from the star, and 10 pc from Earth, for a system that is viewed face-on. A note for this table reminds us that this value also applies to the local zodi, when we are looking out at the "average view angle" from Earth (30° from the ecliptic plane). From the note we infer that this average view angle should be assumed in our calculation. The distant solar system has its orbital plane inclined 45° to the plane of the sky, so we get an extra factor of $\sqrt{2}$ in the exozodi contribution. The total received zodi flux is thus proportional to $1+Z\sqrt{2}$, where Z is the exozodi level, in units of the level in our solar system. In addition to this algebraic factor and the specified spectral flux density, an additional multiplicative parameter is the ratio of the coronagraph beam footprint area to the reference footprint (0.1 AU diameter at 10 pc). This ratio depends quadratically on the observing wavelength. Because surface brightness is independent of (noncosmological) distance, the received zodiacal flux is also independent of distance. (With the classical coronagraph, the graded image plane mask introduces an angle-dependent sensitivity).

A level of two electron read noise and 0.001/s dark current has been assumed, per pixel. We assume nine pixels per diffraction beam.

The residual diffracted starlight level was calculated with numerical simulations. The ratio of planet flux to calculated residual diffracted flux is given in the tables below.

The scattered light level has been set equal to the planet flux level ($Q_{scattered} = 1$). We then derive the required wavefront accuracy levels.

We then calculated the integration time required to reach S/N of 5, for the combination of statistical noise sources and diffracted plus scattered starlight.

For the classical coronagraph, our search area is two full (opposite) quadrants in the image plane. For the shaped-pupil coronagraph, the azimuth range is an increasing function of the star-planet angular separation. We have multiplied each of the calculated integration times by the number of separate pointings needed to cover the full 360° of azimuth. In addition, a slew+settling time of 1500 seconds has been added for each repointing.

If we are unable to achieve our 3×10^{-5} intensity uniformity before the DM and are forced to use the DM to modify the intensity, our search times will all increase by a factor of two.

The integration times are less than one hour for the 3 and 5 pc cases. At 10 pc, the total integration times are in the 5 to 9 hour range. For observations at 500 nm, the azimuth search range at 100 mas star-planet separation is substantially larger, and the total integration times at 10 pc are a factor of ~2 smaller than in the table below.

The shaped-pupil coronagraph (Table D-1) is not able to detect planets at angular separations < 70 mas at 700 nm wavelength with a 10 m primary mirror. Therefore, we fail the 15 pc case. However, we could detect a planet in 1 AU orbit around a 15 pc distant star at a wavelength of 500 nm.

Table D-1. Results for 650 to 750 nm Shaped Pupil

Total counts from local + exozodi in beam footprint (s^{-1})									
0.1503	0.2126	0.3371	0.7106	1.3332					
Z = 0.5	**Z = 1**	**Z = 2**	**Z = 5**	**Z = 10**					
Total Integration time to get S/N = 5 with slews and repointings (s)					**d (pc)**	**Counts from planet (s^{-1})**	**Number of pointings**	***Q* from diffraction**	***Q* from scattering**
1592	1593	1595	1603	1616	3	1.4482	2	200	1
3406	3421	3450	3542	3702	5	0.5213	3	150	1
18327	19080	20621	25391	33515	10	0.1303	9	20	1
Detection not possible					15	0.0579			1

For the classical coronagraph (Table D-2), we assumed an image plane mask whose HWHM is 3.3 times the Airy radius. The integration times are less than one hour for the 3 and 5 pc cases and 1 to 2 hours for the 10 pc case.

Table D-2. Results for 650 to 750 nm Classical Coronagraph

Total counts from local + exozodi in beam footprint (s^{-1})									
Z = 0.5	**Z = 1**	**Z = 2**	**Z = 5**	**Z = 10**	**d (pc)**				
0.150	0.213	0.337	0.711	1.333	3				
0.150	0.213	0.337	0.710	1.333	5				
0.133	0.187	0.297	0.627	1.176	10				
0.092	0.130	0.207	0.436	0.817	15				
Integration time to get S/N = 5, including multiple pointings and slews (seconds)					**d (pc)**	**Counts from planet (s^{-1})**	**Number of pointings**	***Q* from diffraction**	***Q* from scattering**
1582	1582	1584	1590	1600	3	1.6457	2	20	1
1742	1750	1765	1813	1895	5	0.5923	2	10	1
2953	3101	3402	4331	5913	10	0.1306	2	3	1
8041	9163	11441	18380	30044	15	0.0404	2	2	1

D.2.3 NUMBER OF EPOCHS TO CONFIRM PLANET DETECTIONS

We think that the estimate of three total epochs per star for planet searches is reasonable in order to confirm any detections.

D.3. Spectroscopic Characterization Calculations for TPF Visible Light Coronagraph

D.3.1 ABSTRACT

Spectroscopic detection of H_20 and O_2 at terrestrial levels in an Earth mass planet is possible with both our shaped-pupil coronagraph and classical coronagraph designs, for distances up through 10 pc. At 15 pc, detection is precluded by either our Inner Working Distance (shaped-pupil coronagraph) or excessive integration times (classical coronagraph). At a distance of 10 pc, we can detect H_20 with integration times < 15 hours, even for the case of a ×10 exozodi level. The corresponding integration times at 10 pc for O_2 are less than two days in most cases.

D.3.2 CALCULATION OF SIGNAL

Calculation of the spectral count rate from the planet requires only the input spectral flux (supplied with our assignment), the instrument throughput, and the instrument passband. The instrument throughput consists of the area of the primary mirror (31.4 m^2), the fraction of light passed by the various masks (0.50 for the shaped-pupil coronagraph; < 0.50 for the classical coronagraph, depending on angular distance from the star), two reflections off aluminum-coated mirrors and eight reflections off silver-coated mirrors ($0.882^2 \times 0.988^8 = 0.71$), and the quantum efficiency of the InGaAs detector (60% at 700 nm, 70% at 900 nm, 80% at 1100 nm). For atmospheric detection, the 940 nm water line will be observed, with a spectral resolution of 24. For a biomarker search, the 760 nm molecular oxygen line will be observed, with a spectral resolution of 70. A dispersing prism is assumed, with a throughput of 90%. We are searching for only one spectral line of each of these two molecules.

For the 940 nm H_20 line, we measure two continuum channels: 1.010–1.057 microns, and 0.858–0.891 microns. These are not adjacent to our line channel—we "skip" one channel on either side of our line channel, in order to avoid the wings of the line. For the O_2 line, we measure four continuum channels (spanning 0.769–0.791 microns and 0.738–0.758 microns), two on either side of the line. These channels are adjacent to our line channel. Our algorithm for determining a detection is simple—we subtract the flux in the line channel from the average flux in the continuum channels.

D.3.3 CALCULATION OF NOISE

There are several noise sources for observations with the visible-light coronagraph. These are described in the Step 1 (broadband) writeup.

The statistical noise sources can be readily calculated with a spreadsheet. At visible and near-IR wavelengths, the statistical noise sources are: local zodiacal light, exozodiacal light, detector-read noise, and detector dark current. The table from JPL's assignment gives the spectral flux from 1.0 zodi. The flux is specified as the value for a 0.1 AU diameter circular patch, 1 AU from the star, and 10 pc from Earth, for a system that is viewed face-on. A note for this table reminds us that this value also applies to the local zodi, when we are looking out at the "average view angle" from Earth (30° from the ecliptic plane). The distant solar system has its orbital plane inclined 45° to the plane of the sky, so we get an extra factor of $\sqrt{2}$ in the exozodi contribution. The total received zodi flux is thus proportional to $1+Z\sqrt{2}$, where Z is the exozodi level, in units of the level in our solar system. In addition to this algebraic factor and the specified spectral flux density, an additional multiplicative parameter is the ratio of the coronagraph beam footprint area to the reference footprint (0.1 AU diameter at 10 pc). This ratio depends quadratically on the observing wavelength. Because surface brightness is independent of (non-cosmological) distance, the received zodiacal flux is also independent of distance. (With the classical coronagraph, the graded image plane mask introduces an angle-dependent sensitivity.)

A level of two electron read noise and 0.001 s^{-1} dark current has been assumed, per pixel. We assume nine pixels per diffraction beam.

The residual diffracted starlight level was calculated with numerical simulations. The ratio of planet flux to calculated residual diffracted flux is given in the tables below.

The scattered light level has been set equal to the planet flux level ($Q_{scattered} = 1$). We then derive the required wavefront accuracy levels.

We calculated the integration time required to reach S/N of 5, including all our noise sources: statistical plus diffracted and scattered starlight.

The table below gives the integration times required to reach S/N of 5 for the 940 nm H_2O line, with the shaped-pupil coronagraph. For distances of 3 and 5 pc, the integration times are less than one hour. At 15 pc, the Inner Working Distance of the shaped-pupil coronagraph is larger than the star-planet angular separation (67 mas), and we cannot do the measurement.

Table D-7. Results for 940 nm H_2O line, Shaped-pupil Coronagraph

Total counts per channel from local + exozodi in beam footprint (s^{-1})					**Number of continuum channels**	**Spectral Resolution**			
Z = 0.5	**Z = 1**	**Z = 2**	**Z = 5**	**Z = 10**					
0.078	0.110	0.175	0.369	0.693	2	24			
Integration time to get S/N = 5 (seconds) with R = 24					**d (pc)**	**Counts from planet (s^{-1}) in line**	**Counts from planet in continuum (avg)**	***Q* from diffraction**	***Q* from scattering**
301	310	329	388	488	3	0.1201	0.4802	100	1
965	1041	1194	1665	2468	5	0.0432	0.1729	50	1
6465	7742	10324	18148	31257	10	0.0108	0.0432	10	1
detection not possible					15	0.0048	0.0192		1

The second table gives the integration times required to reach S/N of 5 for the 760 nm O_2 line, again with the shaped pupil. As with the 940 nm H_20 line, we cannot achieve adequate suppression of diffracted starlight to make the measurement for the 15 pc case.

Table D-8. Results for 760 nm O_2 line, Shaped-pupil Coronagraph

Total counts per channel from local + exozodi in beam footprint (s^{-1})					Number of continuum channels	Spectral Resolution			
Z = 0.5	Z = 1	Z = 2	Z = 5	Z = 10					
0.013	0.018	0.029	0.061	0.114	4	70			
Integration time to get S/N = 5 (seconds) with R = 70					d (pc)	Counts from planet (s^{-1}) in line	Counts from planet in continuum (avg)	*Q* from diffraction	*Q* from scattering
2553	2600	2696	2986	3473	3	0.0558	0.1187	200	1
8071	8445	9196	11468	15292	5	0.0201	0.0427	150	1
51476	57599	69890	106940	168895	10	0.0050	0.0107	20	1
detection not possible					15	0.0022	0.0047		1

The third and fourth tables give the same results for the classical coronagraph.

Table D-9. Results for 940 nm H_2O line, Classical Coronagraph

Total counts per channel from local + exozodi in beam footprint (s^{-1})					d (pc)	Number of continuum channels	Spectral Resolution		
Z = 0.5	Z = 1	Z = 2	Z = 5	Z = 10					
0.078	0.110	0.175	0.369	0.693	3	2	24		
0.077	0.109	0.174	0.366	0.686	5				
0.054	0.076	0.121	0.255	0.478	10				
0.032	0.045	0.071	0.150	0.281	15				
Integration time to get S/N = 5 (seconds) with R = 24					d (pc)	Counts from planet (s^{-1}) in line	Counts from planet in continuum (avg)	*Q* from diffraction	*Q* from scattering
266	273	288	333	410	3	0.1364	0.5456	20	1
858	918	1038	1409	2041	5	0.0487	0.1946	10	1
9835	11933	16161	28939	50309	10	0.0085	0.0339	3	1
100458	131724	194335	382337	695779	15	0.0022	0.0088	2	1

Table D-10. Results for 760 nm O_2 line, Classical Coronagraph

Total counts per channel from local + exozodi in beam footprint (s^{-1})					**d (pc)**	**Number of continuum channels**	**Spectral Resolution**		
Z = 0.5	**Z = 1**	**Z = 2**	**Z = 5**	**Z = 10**					
0.013	0.018	0.029	0.061	0.114	3	4	70		
0.013	0.018	0.029	0.061	0.114	5				
0.011	0.015	0.024	0.051	0.095	10				
0.007	0.010	0.016	0.033	0.063	15				
Integration time to get S/N = 5 (seconds) with R = 70 with CCD detector					**d (pc)**	**Counts from planet (s^{-1}) in line**	**Counts from planet in continuum (avg)**	***Q* from diffraction**	***Q* from scattering**
2267	2304	2378	2603	2979	3	0.0634	0.1349	20	1
7189	7479	8061	9822	12784	5	0.0228	0.0485	10	1
59350	66176	79869	121113	190045	10	0.0048	0.0101	3	1
441967	522169	682707	1164727	1968453	15	0.0014	0.0030	2	1

D.4. Survey of Nearby Stars for Terrestrial Planets Visible Light Coronagraph

D.4.1 BASIC ASSUMPTIONS AND CALCULATIONS

Most of the details of our coronagraph design have been given in the writeups for Step 1 (broadband detection) and Step 2 (spectroscopic characterization). For the survey calculations, we assumed one hour to slew to a new star and prepare for observations, and 25 minutes to slew between azimuths on the same star.

Three key parameters were not stated explicitly in the assignment for Step 3. For the exozodi level, we chose a multiplier of 1 (i.e., equal to that of our solar system). For the inclination angle of the other solar systems, we chose 30° (i.e., 30° from edge-on), the median value. For the elongation angle of the target planet, we chose 90° (the most favorable case, but the same value as for Steps 1 and 2).

We did not exclude stars based on their ecliptic latitude. However, we accounted for the ecliptic latitude in our calculations of the noise contribution from local zodiacal dust (pathlength proportional to 1/sin (ecliptic latitude), an increase towards the ecliptic that is at least as steep as the observed dependence). Therefore, stars lying very close to the ecliptic require very long integration times. Such stars are therefore far down on the lists given in this document, which are sorted by total observing time required to give SNR = 5.

We adopt the standard definition of Q as the ratio of the planet flux to the sum of all non-planetary fluxes (residual diffracted light from the star, scattered light, local zodi and exozodi, and detector noise). We group the zodi and detector noise contributions into one term: $Q_{statistical}$, because they average down with increasing integration time.

$$Q = \frac{1}{1/Q_{diffract} + 1/Q_{scatter} + 1/Q_{statistical}}$$

We *calculated* $Q_{diffract}$. Specifically, we determined the stellar leakage, or residual diffracted light from the star, as a function of position in the final image plane. Our leakage term *L* is the fraction of central stellar brightness at the planet's position in the image plane. The diffracted light contribution to *Q* was then:

$$Q_{diffract} = \frac{S_{planet}}{S_{star} L}$$

Here S represents the flux from the star or planet. We required $Q_{diffract} > 1$ in order to detect the planet.

As in the calculations presented in Step 1 and Step 2, we *assumed* that we could control the scattered light well enough to achieve $Q_{scatter} = 1$. We define the scattered light as arising from wavefront imperfections, due to mirror surface errors.

By construction, whereby each of our target planets has the same effective temperature and albedo as does the Earth, it receives the same total (integrated over frequency) stellar flux as does the Earth. However, the spectral distribution of this flux depends on the temperature of the star. We multiplied the reflected spectral flux specified for the Earth by the factor

$$\left(\frac{T_{sun}}{T_{star}}\right)^4 \frac{B_\nu(T_{star})}{B_\nu(T_{sun})}$$

This factor was also used in calculating the spectral flux of the exozodi (the local zodi was of course independent of properties of the distant star).

D.4.2 STARS THAT WERE NOT DETECTABLE

With the shaped-pupil coronagraph, we excluded all stars for which the angular separation between the star and the planet was less than 50 mas. This is the Inner Working Distance for the shaped-pupil coronagraph at 500 nm wavelength. The Inner Working Distance for the classical coronagraph is smaller than any of the angular separations studied here, although the throughput decreases at smaller separations.

With the classical coronagraph, the light leakage does not fall off as quickly at large angular separations as for the shaped-pupil coronagraph. There were a small number of hot stars for which the $Q_{diffract} < 1$. We excluded those stars.

D.4.3 SUMMARY OF RESULTS

The table below gives the total observing time (with setup and slews) for the 50, 100, 150, or 200 stars that require the *shortest* total time to achieve SNR = 5 on an Earth analog. This represents the most favorable case (but a realistic one, since the parameters which determine the total integration time are known in advance, and we can select the most favorable stars for our observing program). The factor of 2–3 advantage in integration time of the classical coronagraph is due primarily to its larger azimuth range for starlight suppression, so that fewer telescope repointing are needed per star. Note that the results in this document are for a dual-shaped pupil, which was presented at the FAR. The use of a higher number of shaped pupils (each one long and narrow) will widen the azimuth range of heavy starlight suppression. This has not yet been quantified for the 50–100 mas separation range of interest here, and we do not know the resulting improvement in search efficiency.

As stated at the FAR, our primary concern with the classical coronagraph architecture (compared to the shaped-pupil architecture) is the difficulty in manufacturing precise graded image plane masks. The tradeoff between the two architectures could be characterized as higher performance (classical coronagraph) vs. lower technical risk (shaped-pupil coronagraph).

Table D-11. Total Observing Time for Stars for SNR = 5

Number of stars	Total Observing Time (days) with Shaped-pupil Coronagraph	Total Observing Time (days) with Classical Coronagraph
50	7	3.5
100	22	9
150	50	15
200	105	25

With an allocation for the survey phase of six months, we could observe 150 stars *12 times each* with the classical coronagraph!

D.4.4 RESULTS LISTED BY STAR

In the tables below, the stars are sorted by increasing total observing time.

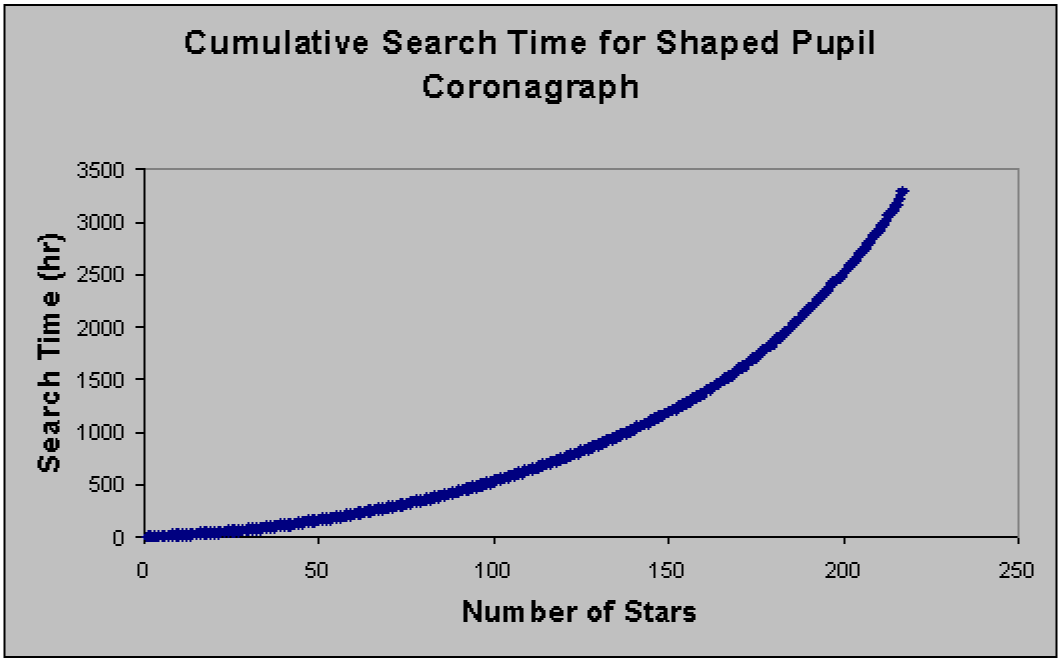

Table D-12. Results for Shaped-pupil Coronagraph

HIP catalog number	Target Planet Sep. (mas)	Local Zodi Counts/s (450–550 nm)	Exozodi Counts/s (450–550 nm)	Planet counts/s (450–550 nm)	$Q_{diffract}$	$Q_{scatter}$	Basic Integ Time (s)	# of pointings	Total Detect. Time (hr)	# of stars searched	Cumulative Search Time (hr)
71683	915	0.026	0.066	5.587	901	1	12	3	1.84	1	2
71681	522	0.026	0.056	4.674	2776	1	14	3	1.84	2	4
37279	746	0.065	0.077	0.980	214	1	69	3	1.89	3	6
16537	174	0.038	0.057	0.836	982	1	80	3	1.90	4	7
8102	183	0.042	0.065	0.752	774	1	90	3	1.91	5	9
108870	123	0.027	0.047	0.543	641	1	124	3	1.94	6	11
19849	122	0.037	0.060	0.361	329	1	195	3	2.00	7	13
3821	182	0.024	0.072	0.314	290	1	226	3	2.02	8	15
15510	128	0.021	0.066	0.276	237	1	259	3	2.05	9	17
99240	179	0.025	0.064	0.263	275	1	274	3	2.06	10	19
2021	245	0.020	0.071	0.195	181	1	384	3	2.15	11	22
89937	174	0.018	0.076	0.181	157	1	422	3	2.18	12	24
22449	206	0.067	0.076	0.183	161	1	449	3	2.21	13	26
61317	127	0.027	0.072	0.159	123	1	497	3	2.25	14	28
1599	128	0.021	0.073	0.152	117	1	518	3	2.27	15	31
27072	171	0.025	0.076	0.146	126	1	548	3	2.29	16	33
105858	129	0.024	0.076	0.138	103	1	589	3	2.32	17	35
64394	128	0.033	0.073	0.134	103	1	617	3	2.35	18	37
104214	108	0.023	0.040	0.498	610	1	135	4	2.40	19	40

HIP catalog number	Target Planet Sep. (mas)	Local Zodi Counts/s (450–550 nm)	Exozodi Counts/s (450–550 nm)	Planet counts/s (450–550 nm)	$Q_{diffract}$	$Q_{scatter}$	Basic Integ Time (s)	# of pointings	Total Detect. Time (hr)	# of stars searched	Cumulative Search Time (hr)
96100	108	0.018	0.062	0.285	224	1	248	4	2.53	20	42
14632	139	0.035	0.072	0.100	83	1	897	3	2.58	21	45
72659	113	0.032	0.066	0.224	173	1	331	4	2.62	22	48
78072	152	0.031	0.076	0.095	78	1	952	3	2.63	23	50
12777	135	0.034	0.075	0.092	72	1	1003	3	2.67	24	53
109176	158	0.032	0.077	0.087	71	1	1084	3	2.74	25	56
46853	208	0.031	0.076	0.065	57	1	1602	3	3.17	26	59
7513	135	0.037	0.074	0.063	50	1	1684	3	3.24	27	62
70497	139	0.021	0.076	0.055	43	1	1939	3	3.45	28	65
16852	124	0.056	0.073	0.060	45	1	1953	3	3.46	29	69
28103	164	0.029	0.078	0.054	44	1	2092	3	3.58	30	73
64924	103	0.110	0.066	0.140	97	1	667	5	3.59	31	76
59199	143	0.048	0.078	0.056	43	1	2125	3	3.60	32	80
77257	117	0.040	0.071	0.080	58	1	1224	4	3.61	33	83
95501	194	0.042	0.078	0.052	44	1	2343	3	3.79	34	87
116771	133	0.143	0.075	0.061	47	1	2443	3	3.87	35	91
50954	144	0.019	0.078	0.046	36	1	2510	3	3.93	36	95
23693	102	0.018	0.075	0.085	52	1	1065	5	4.15	37	99
102485	134	0.146	0.078	0.056	42	1	2874	3	4.23	38	103
12843	114	0.033	0.076	0.060	40	1	1790	4	4.24	39	108
112447	129	0.056	0.075	0.044	33	1	3103	3	4.42	40	112
104217	84	0.023	0.033	0.408	445	1	165	9	4.75	41	117
71284	115	0.027	0.078	0.051	33	1	2253	4	4.75	42	121
57443	95	0.029	0.069	0.123	75	1	672	7	4.81	43	126
17651	128	0.027	0.077	0.037	27	1	3579	3	4.82	44	131
15457	98	0.071	0.068	0.124	79	1	728	7	4.92	45	136
24813	104	0.061	0.070	0.068	45	1	1639	5	4.94	46	141
105090	71	0.048	0.028	0.271	264	1	261	9	4.99	47	146
67275	113	0.040	0.075	0.048	32	1	2573	4	5.11	48	151
99461	83	0.066	0.057	0.239	145	1	317	9	5.13	49	156
114622	79	0.022	0.050	0.179	116	1	412	9	5.36	50	162
73184	75	0.235	0.049	0.213	131	1	443	9	5.44	51	167
10644	97	0.054	0.071	0.093	56	1	1027	7	5.50	52	172
92043	130	0.026	0.076	0.032	24	1	4443	3	5.54	53	178
32362	192	0.101	0.077	0.039	34	1	4547	3	5.62	54	184
7981	85	0.114	0.059	0.162	99	1	545	9	5.70	55	189
57757	171	1.472	0.075	0.097	85	1	4638	3	5.70	56	195
49908	67	0.031	0.032	0.204	157	1	350	10	5.72	57	201
114046	59	0.039	0.023	0.316	275	1	218	11	5.83	58	207
61174	124	0.088	0.078	0.037	26	1	4810	3	5.84	59	212
67153	128	0.051	0.078	0.033	23	1	4966	3	5.97	60	218
54035	57	0.039	0.022	0.498	428	1	134	12	6.03	61	224
46509	109	0.062	0.078	0.041	26	1	3572	4	6.22	62	231
77760	108	0.021	0.073	0.045	30	1	2578	5	6.25	63	237
36366	134	0.105	0.078	0.036	26	1	5342	3	6.29	64	243
56997	79	0.036	0.065	0.110	55	1	781	9	6.29	65	249
51459	97	0.026	0.074	0.069	40	1	1433	7	6.29	66	256
84478	62	0.295	0.042	0.180	91	1	594	10	6.40	67	262

HIP catalog number	Target Planet Sep. (mas)	Local Zodi Counts/s (450–550 nm)	Exozodi Counts/s (450–550 nm)	Planet counts/s (450–550 nm)	$Q_{diffract}$	$Q_{scatter}$	Basic Integ Time (s)	# of pointings	Total Detect. Time (hr)	# of stars searched	Cumulative Search Time (hr)
7751	68	0.021	0.057	0.130	58	1	602	10	6.42	68	269
96441	114	0.019	0.078	0.035	23	1	3816	4	6.49	69	275
29271	88	0.018	0.066	0.098	56	1	863	9	6.49	70	282
80686	94	0.024	0.074	0.077	43	1	1222	8	6.63	71	288
56452	60	0.033	0.061	0.102	34	1	848	10	7.11	72	295
7918	91	0.036	0.071	0.068	38	1	1497	8	7.24	73	302
8362	70	0.024	0.061	0.094	41	1	919	10	7.30	74	310
23311	61	0.038	0.047	0.093	40	1	931	10	7.34	75	317
99825	69	0.146	0.057	0.111	50	1	954	10	7.40	76	325
15371	80	0.019	0.072	0.076	35	1	1234	9	7.42	77	332
81300	66	0.053	0.060	0.095	38	1	967	10	7.44	78	339
15330	71	0.019	0.070	0.073	28	1	1287	9	7.55	79	347
47080	77	0.051	0.063	0.077	38	1	1294	9	7.57	80	355
82860	95	0.018	0.076	0.052	28	1	2107	7	7.60	81	362
76829	106	0.043	0.078	0.039	24	1	3569	5	7.62	82	370
21770	117	0.020	0.078	0.030	20	1	4879	4	7.67	83	377
27072	59	0.025	0.053	0.101	36	1	821	11	7.68	84	385
46733	168	0.025	0.078	0.023	19	1	7932	3	8.44	85	394
113283	56	0.046	0.045	0.117	44	1	707	13	8.55	86	402
34834	115	0.019	0.078	0.027	18	1	5709	4	8.59	87	411
22263	72	0.028	0.070	0.061	24	1	1708	9	8.60	88	419
80337	76	0.060	0.070	0.065	28	1	1715	9	8.62	89	428
13402	59	0.038	0.058	0.082	27	1	1132	11	8.63	90	437
110109	76	0.028	0.071	0.059	25	1	1787	9	8.80	91	445
47592	92	0.031	0.074	0.052	28	1	2199	8	8.80	92	454
3093	63	0.066	0.058	0.072	27	1	1460	10	8.81	93	463
53721	89	0.035	0.070	0.055	30	1	2029	9	9.41	94	472
84862	75	0.022	0.071	0.053	22	1	2050	9	9.46	95	482
72848	60	0.032	0.059	0.068	23	1	1437	11	9.56	96	491
86614	109	0.018	0.077	0.025	16	1	6598	4	9.58	97	501
5862	91	0.024	0.073	0.050	27	1	2266	9	10.00	98	511
32984	52	0.038	0.046	0.093	30	1	932	14	10.04	99	521
58576	72	0.108	0.063	0.058	26	1	2314	9	10.12	100	531
10138	56	0.021	0.061	0.078	22	1	1161	13	10.19	101	541
37853	76	0.022	0.072	0.048	20	1	2347	9	10.20	102	551
40693	59	0.034	0.064	0.062	19	1	1676	11	10.29	103	562
42438	67	0.025	0.071	0.053	18	1	2035	10	10.40	104	572
79672	72	0.081	0.069	0.054	22	1	2437	9	10.43	105	583
117712	54	0.020	0.051	0.067	21	1	1355	13	10.89	106	593
16245	103	0.019	0.078	0.026	15	1	6008	5	11.01	107	604
75181	67	0.037	0.070	0.051	18	1	2298	10	11.13	108	616
49081	76	0.056	0.068	0.047	21	1	2742	9	11.19	109	627
68184	53	0.020	0.048	0.071	23	1	1236	14	11.23	110	638
3583	62	0.024	0.070	0.048	15	1	2351	10	11.28	111	649
86796	86	0.037	0.067	0.044	24	1	2786	9	11.30	112	661
43587	62	0.099	0.057	0.056	20	1	2370	10	11.33	113	672
113357	73	0.042	0.068	0.045	19	1	2816	9	11.37	114	683
3909	83	0.070	0.075	0.049	22	1	2825	9	11.40	115	695

HIP catalog number	Target Planet Sep. (mas)	Local Zodi Counts/s (450–550 nm)	Exozodi Counts/s (450–550 nm)	Planet counts/s (450–550 nm)	$Q_{diffract}$	$Q_{scatter}$	Basic Integ Time (s)	# of pointings	Total Detect. Time (hr)	# of stars searched	Cumulative Search Time (hr)
4151	98	0.023	0.074	0.033	19	1	4165	7	11.60	116	706
77052	61	0.048	0.067	0.048	15	1	2570	10	11.89	117	718
26779	54	0.036	0.059	0.060	16	1	1717	13	12.20	118	730
88972	51	0.020	0.057	0.071	17	1	1299	15	12.25	119	743
107649	69	0.034	0.072	0.045	16	1	2715	10	12.29	120	755
38908	68	0.018	0.073	0.043	15	1	2754	10	12.40	121	767
12653	74	0.020	0.073	0.038	15	1	3322	9	12.64	122	780
25278	89	0.176	0.074	0.053	28	1	3356	9	12.72	123	793
32480	80	0.051	0.073	0.041	19	1	3371	9	12.76	124	805
7978	70	0.021	0.074	0.038	14	1	3382	9	12.79	125	818
114570	113	0.024	0.078	0.020	13	1	9518	4	12.83	126	831
34065	69	0.020	0.070	0.041	15	1	2910	10	12.83	127	844
544	56	0.041	0.064	0.052	14	1	2192	12	12.89	128	857
39903	101	0.018	0.077	0.026	15	1	6019	6	13.12	129	870
78459	75	0.022	0.071	0.036	15	1	3605	9	13.35	130	883
32439	73	0.021	0.075	0.036	14	1	3629	9	13.40	131	897
910	94	0.068	0.076	0.033	18	1	5242	7	13.69	132	910
84893	119	0.503	0.078	0.040	27	1	10549	4	13.97	133	924
89042	72	0.029	0.072	0.035	14	1	3878	9	14.03	134	938
35136	70	0.043	0.073	0.039	14	1	3483	10	14.43	135	953
109422	92	0.053	0.076	0.033	18	1	4788	8	14.56	136	967
73996	93	0.027	0.077	0.031	16	1	4860	8	14.72	137	982
27435	58	0.039	0.070	0.044	12	1	2836	12	15.04	138	997
86486	100	0.041	0.078	0.025	14	1	7271	6	15.20	139	1012
98819	62	0.030	0.072	0.035	10	1	3885	10	15.54	140	1028
88175	107	0.053	0.078	0.023	14	1	9386	5	15.70	141	1044
72567	60	0.029	0.073	0.035	9	1	3984	10	15.82	142	1059
26394	66	0.018	0.072	0.033	11	1	4011	10	15.89	143	1075
77358	57	0.059	0.066	0.043	12	1	3125	12	16.00	144	1091
64792	82	0.064	0.072	0.035	16	1	4690	9	16.06	145	1107
100017	59	0.018	0.071	0.036	9	1	3613	11	16.21	146	1124
86201	100	0.018	0.077	0.022	12	1	8113	6	16.60	147	1140
51523	94	0.022	0.076	0.024	13	1	6801	7	16.72	148	1157
97675	85	0.035	0.073	0.030	15	1	5162	9	17.24	149	1174
62207	58	0.028	0.073	0.038	9	1	3540	12	17.38	150	1191
91438	61	0.488	0.068	0.062	19	1	4553	10	17.40	151	1209
18859	75	0.051	0.075	0.031	12	1	5269	9	17.51	152	1226
36439	76	0.039	0.076	0.030	12	1	5409	9	17.86	153	1244
97295	89	0.022	0.076	0.027	14	1	5776	9	18.77	154	1263
50564	99	0.121	0.077	0.027	15	1	9417	6	18.78	155	1282
43726	57	0.048	0.069	0.036	9	1	4034	12	19.03	156	1301
40843	84	0.137	0.076	0.036	17	1	5909	9	19.11	157	1320
25110	86	0.022	0.075	0.026	13	1	5966	9	19.25	158	1339
88694	58	0.082	0.071	0.036	9	1	4691	11	19.50	159	1359
51502	80	0.020	0.078	0.026	11	1	6110	9	19.61	160	1378
77801	55	0.033	0.072	0.036	8	1	3814	13	19.77	161	1398
69965	60	0.091	0.075	0.037	10	1	4848	11	19.98	162	1418
114924	68	0.023	0.073	0.028	9	1	5590	10	20.28	163	1438

HIP catalog number	Target Planet Sep. (mas)	Local Zodi Counts/s (450–550 nm)	Exozodi Counts/s (450–550 nm)	Planet counts/s (450–550 nm)	$Q_{diffract}$	$Q_{scatter}$	Basic Integ Time (s)	# of pointings	Total Detect. Time (hr)	# of stars searched	Cumulative Search Time (hr)
29800	88	0.092	0.077	0.031	15	1	6396	9	20.32	164	1459
114948	67	0.023	0.075	0.027	9	1	5733	10	20.68	165	1479
107350	58	0.040	0.072	0.033	8	1	4593	12	20.89	166	1500
950	80	0.033	0.077	0.025	11	1	7052	9	21.96	167	1522
44075	62	0.034	0.075	0.025	7	1	6863	10	23.81	168	1546
19335	70	0.062	0.075	0.025	9	1	7903	9	24.09	169	1570
86620	62	0.018	0.074	0.024	7	1	6983	10	24.15	170	1594
40035	70	0.033	0.076	0.023	8	1	7958	9	24.23	171	1618
11783	101	0.037	0.077	0.018	10	1	12822	6	24.45	172	1643
89348	90	0.018	0.077	0.022	11	1	8195	9	24.82	173	1668
44897	58	0.062	0.072	0.030	8	1	5799	12	24.91	174	1693
12444	62	0.044	0.075	0.025	7	1	7523	10	25.65	175	1718
73165	116	0.086	0.078	0.016	10	1	21189	4	25.79	176	1744
98470	66	0.080	0.076	0.027	8	1	7862	10	26.59	177	1771
33302	106	0.026	0.078	0.014	9	1	18013	5	27.68	178	1798
82020	97	0.018	0.078	0.017	9	1	12482	7	27.77	179	1826
58803	84	0.029	0.078	0.021	9	1	9631	9	28.41	180	1855
86736	95	0.597	0.076	0.038	21	1	12918	7	28.62	181	1883
34017	58	0.154	0.072	0.030	8	1	8246	11	30.36	182	1914
43797	65	0.019	0.076	0.020	6	1	9333	10	30.67	183	1944
62512	61	0.021	0.077	0.020	5	1	9414	10	30.90	184	1975
103389	65	0.118	0.075	0.026	8	1	9434	10	30.95	185	2006
111449	81	0.094	0.077	0.023	10	1	10901	9	31.59	186	2038
33277	64	0.405	0.073	0.038	11	1	10058	10	32.69	187	2070
23783	91	0.037	0.078	0.018	9	1	13113	8	33.06	188	2103
23941	85	0.039	0.077	0.019	9	1	11609	9	33.36	189	2137
44143	83	0.019	0.078	0.018	8	1	11845	9	33.95	190	2171
23482	76	0.019	0.078	0.018	7	1	11877	9	34.03	191	2205
63121	69	0.028	0.078	0.019	6	1	10600	10	34.19	192	2239
80179	99	0.047	0.078	0.016	9	1	16113	7	34.83	193	2274
32366	59	0.022	0.076	0.020	5	1	9740	11	34.93	194	2309
33202	103	0.106	0.078	0.016	9	1	23268	5	34.98	195	2344
50384	62	0.088	0.076	0.023	6	1	11011	10	35.34	196	2379
5799	84	0.071	0.077	0.020	9	1	12547	9	35.70	197	2415
51814	84	0.026	0.078	0.017	8	1	12629	9	35.91	198	2451
96258	65	0.019	0.076	0.018	5	1	11295	10	36.13	199	2487
6813	97	0.032	0.078	0.015	8	1	16979	7	36.51	200	2523
80008	72	0.021	0.078	0.017	6	1	13028	9	36.90	201	2560
2711	69	0.023	0.076	0.018	6	1	11637	10	37.07	202	2597
29650	82	0.241	0.077	0.027	12	1	13357	9	37.73	203	2635
69989	75	0.042	0.078	0.018	7	1	13376	9	37.77	204	2673
3810	87	0.096	0.075	0.020	10	1	13572	9	38.26	205	2711
21861	88	0.021	0.078	0.016	8	1	14376	9	40.27	206	2751
13665	68	0.026	0.077	0.017	6	1	13125	10	41.21	207	2792
3765	69	12.246	0.056	0.154	71	1	13299	10	41.69	208	2834
107975	71	0.028	0.078	0.016	5	1	15391	9	42.81	209	2877
49809	79	0.047	0.078	0.016	7	1	16117	9	44.63	210	2922
79822	92	0.018	0.078	0.014	7	1	18428	8	44.87	211	2966

HIP catalog number	Target Planet Sep. (mas)	Local Zodi Counts/s (450–550 nm)	Exozodi Counts/s (450–550 nm)	Planet counts/s (450–550 nm)	$Q_{diffract}$	$Q_{scatter}$	Basic Integ Time (s)	# of pointings	Total Detect. Time (hr)	# of stars searched	Cumulative Search Time (hr)
3505	82	0.043	0.078	0.016	7	1	16821	9	46.39	212	3013
6706	77	0.109	0.078	0.018	7	1	18651	9	50.96	213	3064
97650	76	0.102	0.078	0.017	7	1	19001	9	51.84	214	3116
59750	54	0.129	0.076	0.023	5	1	12421	14	54.72	215	3170
19076	59	0.888	0.071	0.039	11	1	17381	11	58.28	216	3229
11029	74	0.045	0.078	0.014	5	1	22008	9	59.35	217	3288
19205	82	0.129	0.078	0.016	7	1	24610	9	65.86	218	3354
32851	63	0.045	0.078	0.014	4	1	22403	10	66.98	219	3421
102805	56	0.037	0.078	0.014	3	1	20762	12	74.79	220	3496
35550	180	5.415	0.078	0.037	32	1	99968	3	85.14	221	3581
106559	65	0.190	0.078	0.016	5	1	29412	10	86.45	222	3667

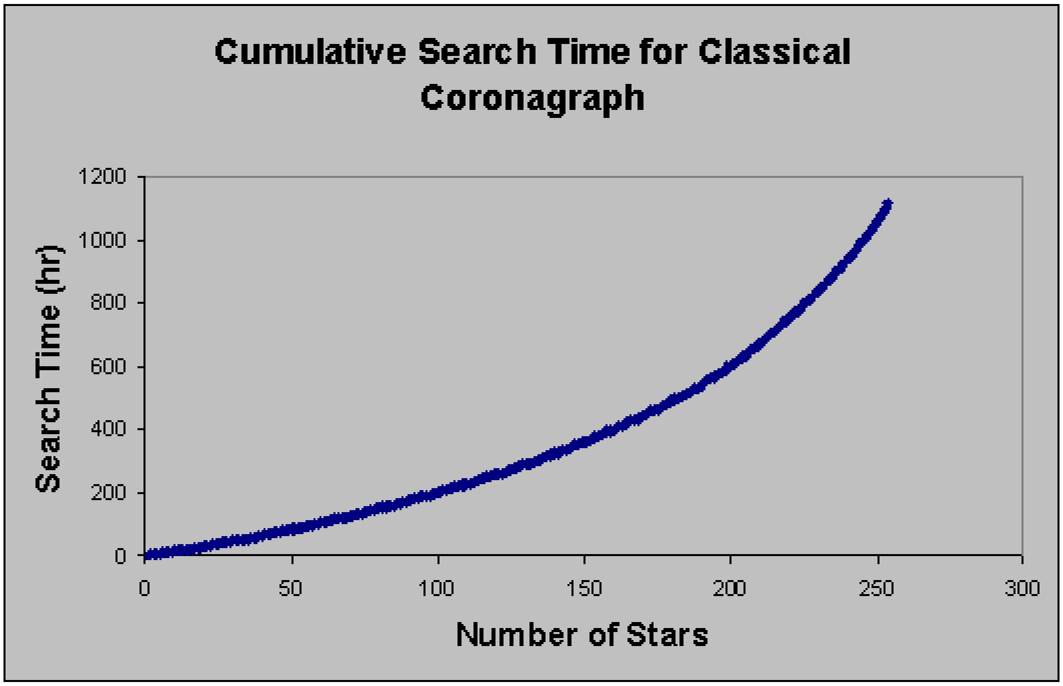

Table D-13. Results for Classical Coronagraph

HIP Catalog number	Target Planet Sep. (mas)	Local Zodi Counts/s (450–550 nm)	ExoZodi Counts/s (450–550 nm)	Planet Counts/s (450–550 nm)	$Q_{diffract}$	$Q_{scatter}$	Basic Integ Time (s)	# of Pointings	Total Detect. Time (hr)	# of stars searched	Cumulative Search Time (hr)
71683	915	0.030	0.075	6.349	34.5	1	10	2	1.42	1	1
71681	522	0.030	0.063	5.311	103.6	1	12	2	1.42	2	3
37279	746	0.073	0.088	1.114	8.1	1	63	2	1.45	3	4
16537	174	0.044	0.064	0.950	55.9	1	71	2	1.46	4	6
8102	183	0.048	0.074	0.854	42.1	1	79	2	1.46	5	7
108870	123	0.031	0.053	0.617	53.3	1	110	2	1.48	6	9
104214	108	0.026	0.046	0.563	60.9	1	120	2	1.48	7	10
104217	84	0.024	0.036	0.441	68.4	1	153	2	1.50	8	12
54035	57	0.033	0.019	0.427	156.3	1	157	2	1.50	9	13
19849	122	0.042	0.068	0.410	27.6	1	173	2	1.51	10	15
3821	182	0.028	0.082	0.357	15.9	1	203	2	1.53	11	16
96100	108	0.020	0.070	0.322	22.4	1	222	2	1.54	12	18
15510	128	0.024	0.075	0.313	18.7	1	231	2	1.54	13	19
99240	179	0.029	0.073	0.298	15.2	1	245	2	1.55	14	21
114046	59	0.034	0.020	0.279	92.1	1	247	2	1.55	15	22
105090	71	0.048	0.028	0.271	58.6	1	262	2	1.56	16	24
72659	113	0.036	0.074	0.254	16.3	1	297	2	1.58	17	26
99461	83	0.071	0.062	0.257	23.1	1	298	2	1.58	18	27
87937	25	0.010	0.005	0.209	571.0	1	318	2	1.59	19	29
2021	245	0.022	0.080	0.221	8.1	1	349	2	1.61	20	30
49908	67	0.030	0.031	0.198	39.5	1	364	2	1.62	21	32
89937	174	0.020	0.086	0.205	8.9	1	382	2	1.63	22	34
114622	79	0.023	0.053	0.189	20.3	1	394	2	1.64	23	35
22449	206	0.076	0.086	0.207	8.0	1	407	2	1.64	24	37

HIP Catalog number	Target Planet Sep. (mas)	Local Zodi Counts/s (450–550 nm)	ExoZodi Counts/s (450–550 nm)	Planet Counts/s (450–550 nm)	$Q_{diffract}$	$Q_{scatter}$	Basic Integ Time (s)	# of Pointings	Total Detect. Time (hr)	# of stars searched	Cumulative Search Time (hr)
73184	75	0.242	0.050	0.220	25.4	1	432	2	1.66	25	39
61317	127	0.031	0.082	0.180	9.8	1	448	2	1.67	26	40
1599	128	0.024	0.082	0.172	9.3	1	468	2	1.68	27	42
27072	171	0.028	0.087	0.166	7.3	1	499	2	1.69	28	44
7981	85	0.123	0.064	0.176	15.0	1	510	2	1.70	29	45
105858	129	0.028	0.086	0.156	8.1	1	534	2	1.71	30	47
64394	128	0.038	0.083	0.152	8.2	1	558	2	1.73	31	49
64924	103	0.124	0.074	0.157	10.5	1	605	2	1.75	32	50
57443	95	0.032	0.076	0.137	9.3	1	618	2	1.76	33	52
7751	68	0.020	0.055	0.127	14.0	1	626	2	1.76	34	54
84478	62	0.270	0.039	0.165	27.3	1	651	2	1.78	35	56
15457	98	0.080	0.076	0.138	9.3	1	666	2	1.79	36	58
56997	79	0.039	0.069	0.117	9.5	1	754	2	1.84	37	59
91768	30	0.006	0.008	0.089	127.2	1	779	2	1.85	38	61
29271	88	0.020	0.072	0.107	8.0	1	810	2	1.87	39	63
14632	139	0.040	0.082	0.113	5.9	1	819	2	1.87	40	65
113283	56	0.038	0.037	0.097	17.7	1	862	2	1.90	41	67
78072	152	0.035	0.087	0.108	5.1	1	874	2	1.90	42	69
439	33	0.013	0.010	0.080	77.6	1	913	2	1.92	43	71
12777	135	0.039	0.085	0.104	5.3	1	919	2	1.93	44	73
8362	70	0.024	0.061	0.093	9.2	1	944	2	1.94	45	75
10644	97	0.060	0.079	0.104	6.7	1	948	2	1.94	46	77
27072	59	0.022	0.047	0.089	12.4	1	953	2	1.95	47	78
56452	60	0.030	0.054	0.091	10.9	1	967	2	1.95	48	80
23693	102	0.020	0.084	0.095	5.6	1	983	2	1.96	49	82
99825	69	0.143	0.056	0.110	11.9	1	983	2	1.96	50	84
109176	158	0.036	0.088	0.098	4.4	1	1000	2	1.97	51	86
81300	66	0.051	0.057	0.092	9.9	1	1028	2	1.99	52	88
23311	61	0.034	0.043	0.083	12.7	1	1054	2	2.00	53	90
45343	46	0.021	0.019	0.073	30.0	1	1081	2	2.02	54	92
77257	117	0.045	0.081	0.090	5.2	1	1122	2	2.04	55	94
80686	94	0.027	0.082	0.086	5.5	1	1141	2	2.05	56	96
120005	46	0.021	0.018	0.068	29.5	1	1163	2	2.06	57	98
15371	80	0.020	0.076	0.080	5.9	1	1198	2	2.08	58	101
32984	52	0.030	0.036	0.072	14.2	1	1215	2	2.09	59	103
47080	77	0.054	0.066	0.080	7.0	1	1270	2	2.12	60	105
13402	59	0.033	0.051	0.072	9.3	1	1318	2	2.15	61	107
15330	71	0.019	0.070	0.073	6.2	1	1326	2	2.15	62	109
51459	97	0.029	0.083	0.077	4.8	1	1336	2	2.16	63	111
99701	41	0.025	0.015	0.059	32.3	1	1392	2	2.19	64	113
7918	91	0.040	0.078	0.075	5.1	1	1405	2	2.20	65	116
10138	56	0.018	0.051	0.065	8.6	1	1419	2	2.21	66	118
54211	31	0.012	0.008	0.053	67.3	1	1421	2	2.21	67	120
67155	33	0.018	0.011	0.055	49.8	1	1429	2	2.21	68	122
24813	104	0.069	0.079	0.076	4.8	1	1510	2	2.26	69	124
46853	208	0.035	0.087	0.074	2.8	1	1510	2	2.26	70	127
7513	135	0.042	0.084	0.072	3.7	1	1559	2	2.28	71	129
68184	53	0.016	0.038	0.057	10.4	1	1589	2	2.30	72	131

HIP Catalog number	Target Planet Sep. (mas)	Local Zodi Counts/s (450–550 nm)	ExoZodi Counts/s (450–550 nm)	Planet Counts/s (450–550 nm)	$Q_{diffract}$	$Q_{scatter}$	Basic Integ Time (s)	# of Pointings	Total Detect. Time (hr)	# of stars searched	Cumulative Search Time (hr)
3093	63	0.062	0.054	0.067	7.8	1	1603	2	2.31	73	134
72848	60	0.028	0.052	0.060	7.5	1	1659	2	2.34	74	136
12843	114	0.037	0.086	0.068	3.7	1	1659	2	2.34	75	138
80337	76	0.062	0.073	0.068	5.3	1	1703	2	2.36	76	141
117712	54	0.016	0.042	0.054	9.0	1	1712	2	2.37	77	143
22263	72	0.029	0.071	0.061	5.1	1	1749	2	2.39	78	145
88972	51	0.015	0.043	0.054	8.8	1	1752	2	2.39	79	148
85295	45	0.028	0.020	0.051	19.6	1	1764	2	2.40	80	150
110109	76	0.029	0.074	0.061	4.8	1	1781	2	2.41	81	153
16852	124	0.064	0.082	0.068	3.7	1	1801	2	2.42	82	155
70497	139	0.023	0.086	0.063	3.1	1	1811	2	2.42	83	157
53721	89	0.038	0.077	0.060	4.1	1	1926	2	2.49	84	160
86400	50	0.029	0.039	0.051	9.6	1	1935	2	2.49	85	162
40693	59	0.030	0.056	0.055	6.3	1	1949	2	2.50	86	165
28103	164	0.033	0.089	0.061	2.6	1	1969	2	2.51	87	167
59199	143	0.055	0.089	0.064	3.0	1	1979	2	2.52	88	170
82860	95	0.020	0.085	0.057	3.5	1	1991	2	2.52	89	172
42808	47	0.015	0.038	0.047	9.2	1	2033	2	2.55	90	175
84862	75	0.022	0.073	0.054	4.3	1	2059	2	2.56	91	178
47592	92	0.034	0.082	0.057	3.6	1	2079	2	2.57	92	180
71284	115	0.030	0.089	0.058	3.0	1	2104	2	2.59	93	183
64797	50	0.033	0.040	0.049	8.8	1	2135	2	2.60	94	185
41926	49	0.017	0.045	0.047	7.5	1	2140	2	2.61	95	188
5862	91	0.026	0.080	0.055	3.6	1	2152	2	2.61	96	191
26779	54	0.029	0.048	0.049	7.0	1	2171	2	2.62	97	193
42438	67	0.025	0.069	0.052	4.6	1	2173	2	2.62	98	196
95501	194	0.048	0.089	0.059	2.3	1	2221	2	2.65	99	198
116771	133	0.162	0.086	0.069	3.5	1	2236	2	2.66	100	201
10798	50	0.022	0.048	0.046	6.9	1	2288	2	2.69	101	204
58576	72	0.109	0.064	0.059	5.4	1	2348	2	2.72	102	207
37853	76	0.023	0.075	0.050	3.8	1	2357	2	2.73	103	209
50954	144	0.022	0.089	0.053	2.5	1	2369	2	2.73	104	212
67275	113	0.045	0.085	0.054	3.0	1	2397	2	2.75	105	215
58345	45	0.027	0.029	0.042	11.3	1	2405	2	2.75	106	217
77760	108	0.023	0.083	0.051	3.0	1	2415	2	2.76	107	220
85235	48	0.013	0.045	0.042	6.9	1	2451	2	2.78	108	223
75181	67	0.036	0.067	0.049	4.4	1	2464	2	2.79	109	226
79672	72	0.082	0.070	0.055	4.6	1	2485	2	2.80	110	229
102485	134	0.166	0.088	0.063	3.1	1	2636	2	2.88	111	231
3583	62	0.022	0.064	0.044	4.4	1	2655	2	2.89	112	234
43587	62	0.090	0.052	0.051	6.2	1	2664	2	2.90	113	237
86796	86	0.041	0.073	0.048	3.6	1	2673	2	2.90	114	240
544	56	0.034	0.054	0.044	5.5	1	2686	2	2.91	115	243
69972	48	0.019	0.035	0.038	8.0	1	2696	2	2.91	116	246
49081	76	0.058	0.071	0.049	4.0	1	2729	2	2.93	117	249
3909	83	0.075	0.081	0.052	3.5	1	2733	2	2.93	118	252
113576	40	0.039	0.016	0.037	19.2	1	2809	2	2.98	119	255
107649	69	0.033	0.071	0.044	3.8	1	2862	2	3.01	120	258

HIP Catalog number	Target Planet Sep. (mas)	Local Zodi Counts/s (450–550 nm)	ExoZodi Counts/s (450–550 nm)	Planet Counts/s (450–550 nm)	$Q_{diffract}$	$Q_{scatter}$	Basic Integ Time (s)	# of Pointings	Total Detect. Time (hr)	# of stars searched	Cumulative Search Time (hr)
113357	73	0.043	0.070	0.046	3.8	1	2863	2	3.01	121	261
112447	129	0.064	0.086	0.050	2.6	1	2891	2	3.02	122	264
38908	68	0.018	0.071	0.042	3.5	1	2935	2	3.05	123	267
77052	61	0.044	0.061	0.043	4.6	1	2938	2	3.05	124	270
34065	69	0.019	0.070	0.041	3.5	1	3067	2	3.12	125	273
116745	39	0.011	0.027	0.032	10.0	1	3071	2	3.12	126	276
25278	89	0.194	0.081	0.058	3.8	1	3143	2	3.16	127	279
32480	80	0.054	0.077	0.044	3.2	1	3310	2	3.26	128	283
46509	109	0.070	0.088	0.047	2.5	1	3334	2	3.27	129	286
76829	106	0.049	0.088	0.044	2.5	1	3351	2	3.28	130	289
17651	128	0.030	0.088	0.042	2.1	1	3380	2	3.29	131	292
12653	74	0.021	0.075	0.039	3.0	1	3388	2	3.30	132	296
27435	58	0.033	0.060	0.038	4.2	1	3415	2	3.31	133	299
7978	70	0.021	0.074	0.038	3.0	1	3549	2	3.39	134	302
96441	114	0.022	0.088	0.040	2.1	1	3613	2	3.42	135	306
35136	70	0.042	0.072	0.039	3.2	1	3653	2	3.45	136	309
78459	75	0.023	0.073	0.037	2.9	1	3662	2	3.45	137	313
32439	73	0.022	0.076	0.037	2.8	1	3741	2	3.50	138	316
77358	57	0.051	0.056	0.037	4.4	1	3769	2	3.51	139	320
78775	43	0.013	0.040	0.029	5.9	1	3875	2	3.57	140	323
4151	98	0.026	0.083	0.037	2.3	1	3961	2	3.62	141	327
89042	72	0.029	0.073	0.036	2.9	1	4013	2	3.65	142	331
57757	171	1.673	0.085	0.111	4.9	1	4122	2	3.71	143	334
92043	130	0.029	0.086	0.037	1.9	1	4214	2	3.76	144	338
62207	58	0.024	0.063	0.032	3.4	1	4278	2	3.79	145	342
32362	192	0.115	0.088	0.044	1.8	1	4282	2	3.80	146	346
100017	59	0.016	0.063	0.031	3.2	1	4297	2	3.80	147	350
95319	50	0.016	0.045	0.029	4.6	1	4308	2	3.81	148	353
26394	66	0.018	0.069	0.032	2.8	1	4369	2	3.84	149	357
98819	62	0.027	0.066	0.032	3.1	1	4427	2	3.88	150	361
82003	33	0.009	0.014	0.022	15.5	1	4447	2	3.89	151	365
61174	124	0.100	0.089	0.041	2.1	1	4478	2	3.90	152	369
109422	92	0.058	0.084	0.037	2.3	1	4563	2	3.95	153	373
64792	82	0.068	0.077	0.037	2.6	1	4572	2	3.96	154	377
48331	34	0.010	0.018	0.022	11.6	1	4604	2	3.97	155	381
21770	117	0.023	0.089	0.034	1.8	1	4644	2	4.00	156	385
72567	60	0.026	0.065	0.031	3.1	1	4650	2	4.00	157	389
73996	93	0.030	0.086	0.034	2.1	1	4669	2	4.01	158	393
67153	128	0.058	0.089	0.037	1.8	1	4678	2	4.02	159	397
77801	55	0.027	0.059	0.030	3.4	1	4837	2	4.10	160	401
83591	32	0.023	0.018	0.023	13.1	1	4859	2	4.12	161	405
43726	57	0.040	0.058	0.031	3.5	1	4935	2	4.16	162	409
910	94	0.075	0.084	0.037	2.2	1	4964	2	4.17	163	413
36366	134	0.119	0.089	0.040	2.0	1	4970	2	4.18	164	417
97675	85	0.038	0.079	0.032	2.2	1	5035	2	4.21	165	422
91438	61	0.442	0.062	0.056	5.8	1	5089	2	4.24	166	426
34069	40	0.011	0.035	0.023	5.6	1	5125	2	4.26	167	430
18859	75	0.052	0.077	0.032	2.4	1	5346	2	4.39	168	435

HIP Catalog number	Target Planet Sep. (mas)	Local Zodi Counts/s (450–550 nm)	ExoZodi Counts/s (450–550 nm)	Planet Counts/s (450–550 nm)	$Q_{diffract}$	$Q_{scatter}$	Basic Integ Time (s)	# of Pointings	Total Detect. Time (hr)	# of stars searched	Cumulative Search Time (hr)
34834	115	0.022	0.089	0.031	1.6	1	5453	2	4.45	169	439
36439	76	0.040	0.080	0.031	2.2	1	5476	2	4.46	170	443
107350	58	0.034	0.062	0.028	3.0	1	5566	2	4.51	171	448
88694	58	0.071	0.062	0.031	3.3	1	5582	2	4.52	172	452
97295	89	0.024	0.084	0.030	1.9	1	5606	2	4.53	173	457
69965	60	0.081	0.067	0.033	3.1	1	5635	2	4.55	174	462
40843	84	0.148	0.082	0.039	2.6	1	5665	2	4.56	175	466
16245	103	0.021	0.087	0.029	1.7	1	5755	2	4.61	176	471
39903	101	0.021	0.087	0.029	1.7	1	5771	2	4.62	177	475
25110	86	0.023	0.082	0.029	1.9	1	5840	2	4.66	178	480
114924	68	0.022	0.072	0.027	2.3	1	6000	2	4.75	179	485
101997	49	0.142	0.048	0.034	5.2	1	6033	2	4.77	180	490
29800	88	0.101	0.085	0.034	2.1	1	6114	2	4.81	181	494
51502	80	0.021	0.083	0.028	1.9	1	6120	2	4.82	182	499
114948	67	0.022	0.072	0.026	2.2	1	6267	2	4.90	183	504
86614	109	0.020	0.087	0.028	1.5	1	6319	2	4.93	184	509
51523	94	0.024	0.084	0.027	1.7	1	6564	2	5.06	185	514
86486	100	0.046	0.087	0.028	1.6	1	6929	2	5.27	186	519
44897	58	0.054	0.062	0.026	2.8	1	6982	2	5.30	187	525
950	80	0.035	0.082	0.027	1.8	1	7038	2	5.33	188	530
74702	39	0.031	0.032	0.020	5.3	1	7367	2	5.51	189	535
46733	168	0.029	0.089	0.026	1.1	1	7743	2	5.72	190	541
86201	100	0.020	0.087	0.024	1.4	1	7828	2	5.77	191	547
44075	62	0.031	0.068	0.023	2.1	1	7891	2	5.80	192	553
89348	90	0.020	0.085	0.024	1.5	1	8008	2	5.87	193	559
86620	62	0.016	0.068	0.022	2.0	1	8091	2	5.91	194	565
19335	70	0.062	0.075	0.025	2.0	1	8292	2	6.02	195	571
28954	42	0.077	0.036	0.023	5.2	1	8353	2	6.06	196	577
40035	70	0.033	0.076	0.023	1.8	1	8445	2	6.11	197	583
98470	66	0.077	0.073	0.026	2.2	1	8520	2	6.15	198	589
12444	62	0.040	0.068	0.023	2.1	1	8602	2	6.20	199	595
50564	99	0.136	0.086	0.030	1.7	1	8808	2	6.31	200	601
88175	107	0.059	0.088	0.025	1.4	1	8901	2	6.36	201	608
114570	113	0.027	0.089	0.023	1.2	1	9150	2	6.50	202	614
84893	119	0.570	0.088	0.045	2.4	1	9504	2	6.70	203	621
58803	84	0.031	0.084	0.022	1.4	1	9537	2	6.71	204	628
34017	58	0.134	0.062	0.026	2.8	1	9736	2	6.83	205	634
103389	65	0.112	0.071	0.025	2.2	1	10329	2	7.16	206	642
43797	65	0.018	0.072	0.019	1.6	1	10468	2	7.23	207	649
54646	28	0.015	0.012	0.012	12.0	1	10541	2	7.27	208	656
111449	81	0.101	0.082	0.025	1.7	1	10685	2	7.35	209	663
33277	64	0.378	0.068	0.035	3.2	1	10941	2	7.50	210	671
62512	61	0.019	0.069	0.018	1.7	1	11020	2	7.54	211	679
23941	85	0.042	0.083	0.021	1.3	1	11420	2	7.76	212	686
63121	69	0.027	0.077	0.019	1.5	1	11464	2	7.79	213	694
86736	95	0.664	0.085	0.043	2.6	1	11793	2	7.97	214	702
32366	59	0.019	0.066	0.017	1.7	1	11801	2	7.97	215	710
44143	83	0.021	0.084	0.019	1.2	1	11847	2	8.00	216	718

HIP Catalog number	Target Planet Sep. (mas)	Local Zodi Counts/s (450–550 nm)	ExoZodi Counts/s (450–550 nm)	Planet Counts/s (450–550 nm)	$Q_{diffract}$	$Q_{scatter}$	Basic Integ Time (s)	# of Pointings	Total Detect. Time (hr)	# of stars searched	Cumulative Search Time (hr)
82020	97	0.020	0.087	0.019	1.1	1	12153	2	8.17	217	726
5799	84	0.076	0.083	0.022	1.4	1	12261	2	8.23	218	734
23482	76	0.020	0.081	0.018	1.3	1	12272	2	8.23	219	743
11783	101	0.042	0.086	0.020	1.2	1	12310	2	8.26	220	751
16134	30	0.010	0.011	0.011	10.1	1	12342	2	8.27	221	759
51814	84	0.028	0.085	0.019	1.2	1	12559	2	8.39	222	768
2711	69	0.023	0.075	0.018	1.4	1	12576	2	8.40	223	776
50384	62	0.081	0.069	0.021	1.9	1	12587	2	8.41	224	784
96258	65	0.018	0.072	0.017	1.5	1	12738	2	8.49	225	793
23783	91	0.041	0.087	0.020	1.2	1	12745	2	8.50	226	801
29650	82	0.258	0.083	0.029	1.9	1	12836	2	8.55	227	810
3810	87	0.104	0.082	0.022	1.4	1	13073	2	8.68	228	819
3765	69	12.060	0.055	0.152	16.6	1	13512	2	8.92	229	828
80008	72	0.021	0.079	0.017	1.3	1	13776	2	9.07	230	837
69989	75	0.043	0.081	0.018	1.3	1	13790	2	9.08	231	846
21861	88	0.023	0.086	0.017	1.1	1	14187	2	9.30	232	855
13665	68	0.026	0.076	0.017	1.3	1	14250	2	9.33	233	864
66459	24	0.006	0.007	0.009	17.2	1	14414	2	9.42	234	874
23708	24	0.005	0.007	0.008	14.9	1	15038	2	9.77	235	883
80179	99	0.053	0.088	0.018	1.0	1	15480	2	10.02	236	894
59750	54	0.103	0.061	0.019	2.1	1	15955	2	10.28	237	904
49809	79	0.049	0.083	0.017	1.2	1	16258	2	10.45	238	914
107975	71	0.028	0.078	0.016	1.2	1	16407	2	10.53	239	925
6813	97	0.036	0.087	0.017	1.0	1	16449	2	10.56	240	935
102186	24	0.008	0.008	0.008	13.7	1	16597	2	10.64	241	946
3505	82	0.046	0.084	0.017	1.1	1	16776	2	10.74	242	957
6706	77	0.114	0.081	0.019	1.3	1	18697	2	11.80	243	991
76602	44	0.062	0.047	0.014	2.3	1	19100	2	12.03	244	1003
97650	76	0.106	0.081	0.018	1.3	1	19197	2	12.08	245	1015
19076	59	0.783	0.062	0.034	3.6	1	19851	2	12.45	246	1028
33202	103	0.120	0.088	0.018	1.0	1	21893	2	13.58	247	1054
11029	74	0.046	0.080	0.014	1.0	1	22820	2	14.09	248	1068
19205	82	0.138	0.084	0.017	1.1	1	23994	2	14.75	249	1083
32851	63	0.042	0.072	0.013	1.1	1	25625	2	15.65	250	1098
102805	56	0.031	0.065	0.012	1.2	1	26015	2	15.87	251	1114
106559	65	0.180	0.074	0.015	1.3	1	31966	2	19.18	252	1133

APPENDIX E
Boeing-SVS Team
ASA Design Reference Mission Analysis

E.1. The Apodized Square Aperture

1. Optical architecture (apodized aperture, coronagraph, other)

The optical architecture is an off-axis apodized coronagraph. A fast-steering mirror folds the beam behind the primary for compact packaging and fine-pointing control. The Cassegrain field focus that follows is reimaged by the tertiary mirror through the deformable mirror to the field mask. The deformable mirror corrects low- and critical mid-spatial frequency wavefront errors in the optical path. The field mask blocks the core of the parent star and directs it to a light trap. After the field mask, the light from the planet is reimaged through selectable spectral filters on a filter wheel to the focal plane. A Lyot stop lies at the primary mirror image before the filter wheel.

2. Optical layout drawing (If a deformable mirror is used, where is it?)

The following two figures opposite illustrate the overall optical layout and the focal plane details.

3. Primary aperture shape, dimensions, actual area, and effective area

The primary aperture's collecting area is an 8×8-m square, for a total collecting area of 64 m^2. The effective transmission/quantum efficiency of the entire optical train including detectors is 30%, making the effective area 19.2 m^2.

4. Primary aperture optical figure

The primary mirror is an off-axis ellipse that will be figured as well as technology allows, facilitating fine correction by the deformable mirror. Our current error budgets allocate primary mirror surface figure accuracy to be $\lambda/1800$ or 0.35 nm rms over the critical spatial frequency range (3 to 30 cycles per aperture). The low-spatial frequency range, up to 3 cycles per aperture is allocated 1.17 nm rms. The allocations over the remaining mid-spatial frequency range (30 to 104 cycles per aperture) and high-spatial frequency range are 4.0 nm rms, and 1.0 nm rms respectively.

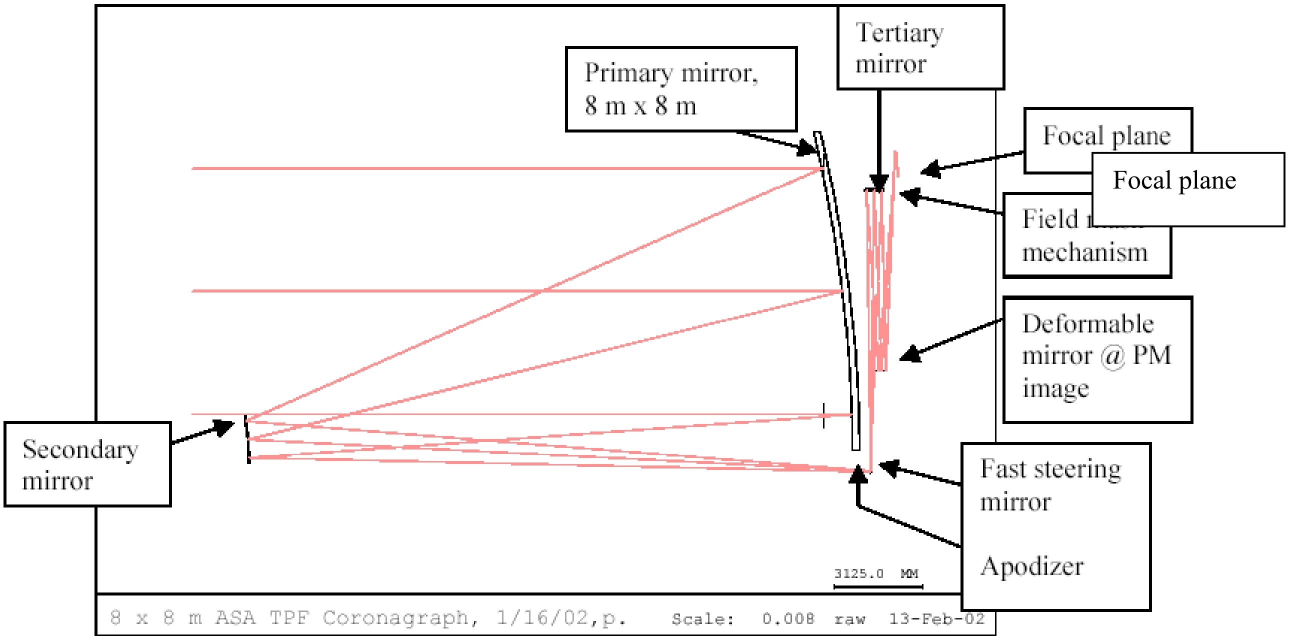
Tertiary mirror
Primary mirror, 8 m x 8 m
Focal plane
Focal plane
Field
mechanism
Deformable mirror @ PM image
Secondary mirror
Fast steering mirror
Apodizer
3125.0 MM
8 x 8 m ASA TPF Coronagraph, 1/16/02,p. Scale: 0.008 raw 13-Feb-02

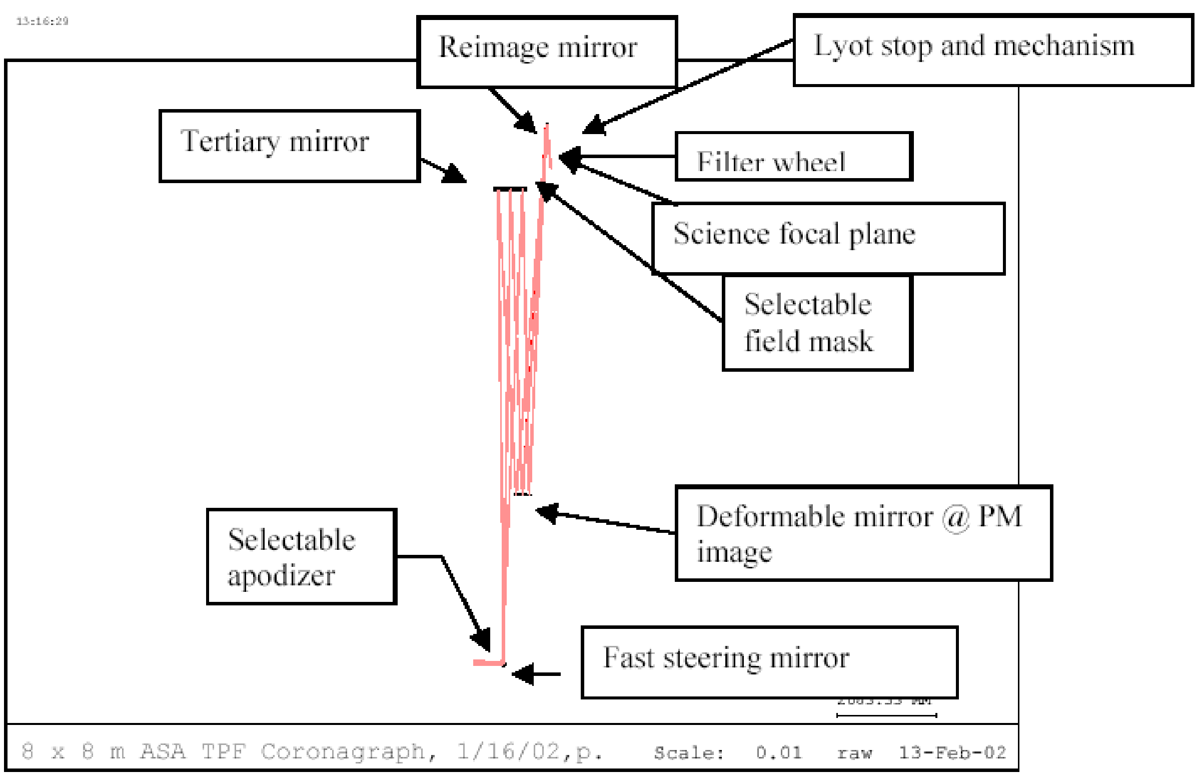
13:16:29
Reimage mirror
Lyot stop and mechanism
Tertiary mirror
Filter wheel
Science focal plane
Selectable field mask
Deformable mirror @ PM image
Selectable apodizer
Fast steering mirror
8 x 8 m ASA TPF Coronagraph, 1/16/02,p. Scale: 0.01 raw 13-Feb-02

5. Operational wavelength range

The operational wavelength range is 400 to 1000 nm.

6. Amplitude uniformity requirement

The overall system amplitude uniformity requirement is 1%.

7. Corrected optical figure (after AO, if a deformable mirror is used)

The Boeing-SVS ASA design balances wavefront control with long-term system stability. If our DM enables us to achieve wavefront control for $Q = 1$ operation, we will correct the critical spatial frequency wavefront to 0.064 nm rms using the DM and maintain it to better than 0.090 nm rms over the relatively short integration period (nominally 70 seconds) by control of the pointing, temperature, mechanical, and optical stability. If we operate at $Q = 0.1$, we will correct the wavefront to 0.20 nm rms and maintain it to better than 0.29 nm rms over a longer integration period (nominally 1350 seconds). For purposes of the present response, we assume a Q value of about 0.01 as presented at the San Diego final architecture review.

8. Aperture mask shape including intensity and phase tolerances

The aperture mask shape is square, with a Jacquinot-function profile. The intensity tolerance falls within the system amplitude tolerance of 1%. The phase tolerance is within the overall wavefront error budget of $\lambda/900$.

9. Coronagraph mask shape including intensity and phase tolerances

The coronagraphic field mask is cross-shaped with a central disk. The bar widths and disk radius are each $3\lambda/D$, or 46 mas. This blocking mask has no phase or intensity taper.

10. Lyot mask shape including intensity and phase tolerances

The Lyot mask is a square hole that is oversized by 10% compared to the pupil image.

11. Angular resolution at planet position, in the final image (after Lyot, etc).

The ASA images terrestrial planets as close as $3\lambda/D$ or 39 mas at 500 nm to the target star. The focal plane pixel spacing is 10 mas.

12. Inner and outer radius of effective field-of-view within which planets might be detected (instantaneous and after observations at multiple roll angles)

The inner and radius of the field-of-view within which a planet can be detected are 39 mas to 1 arcsec.

13. Operating temperatures and thermal stability for key optical components

The ASA system operates near 0°C so it "flies-as-we test," but further system work is needed to quantify this. The current error budget allocations for $Q = 1$ operation allow a primary mirror ΔT of 0.2 K, a DM ΔT of 10 mK and an optical bench ΔT of 1 K. These conditions must be maintained for each nominal 70-second exposure. For $Q = 0.01$, we allocate a primary mirror ΔT of 1 K, a DM ΔT of 0.1 K and an optical bench ΔT of 5 K.

14. Effects of spacecraft parameters (vibration, pointing jitter, etc) on stability of PSF

The spacecraft maintains the telescope body line-of-sight stability over an integration period to 10 mas ($Q = 1$) to 200 mas ($Q = 0.01$). The internal fast-steering mirror and its sensor accomplish the fine pointing correction of the line-of-sight to 1 mas.

15. Spectrometer design

The spectrometer is a prism system that operates between 400 and 1000 nm and has a transmission of 90%. The light from the planet falls on a pixel-sized square slot and is refracted and re-imaged onto a separate array. The entire spectrum is observed simultaneously. The nominal resolving power is 20.

16. Operations scenario (e.g., Does the coronagraphic spot or apodized aperture mask change for each target?)

The apodized mask does not have to change for different targets.

17. Specify *Q*, defined as the operational ratio planet light/scattered starlight. What is the needed stability in the PSF/scattered light to see a planet for a given *Q*? Justify why you feel the instrument PSF is that stable (not necessary for configurations working at a *Q* of 1). The value of *Q* should be consistent with the properties of the optical system given above.

The Q of the ASA instrument is as low as 0.01. See the answer to question 7 above for DM and optical surface performance allocations.

18. Total optical efficiency for planetary light including reflection and transmission losses, effective vs. total collection area, Lyot mask loss, filters, etc. for both broadband and spectroscopic measurements

The total optical efficiency is 30% in the planet survey mode and 27% in spectroscopy mode.

19. Specify detected average count rates, in the effective planetary diffraction spot size (FWHM), from planet, diffracted star, scattered star, exozodi, local zodi, instrument thermal emission, and detector dark counts. Assume the solar system at 10 pc.

- Planet's light: 0.32 photoelectrons per second per pixel
- Diffracted starlight: negligible (by orders of magnitude) relative to scattered starlight
- Scattered starlight: 44.7 photoelectrons per second per pixel
- Exozodiacal light: even at 100 times the local zodiacal light the exozodiacal light is negligible compared to the scattered starlight
- Local zodiacal light: 0.011 photoelectrons per second per pixel
- Thermal emission: negligible in the 400 to 10000 nm wavelength range
- Detector dark counts: readout noise ≤ 3 electrons; pixel dark current ≤ 5 electrons per hour

E.2. The Observing Program

E.2.1 Photometric Detection

The ASA system requires two bore-sight orientations to survey all habitable zones around a target star since the coronagraphic mask blocks part of the field around the target star. This is true for all distances beyond 4λ/E, where λ is the longest wavelength used and E is the square edge, or 8 meters. For the nominal survey bandpass of 500 to 700 nm two bore-sight orientations will fully survey a target star habitable zone down to 72 mas. The ASA system requires three bore-sight orientations to survey habitable zones between 3λ/E and 4λ/E. For three of the four test cases (an Earth-Sun pair at 3, 5, 10 and 15 pc), two orientations with a 500 to 700 nm bandpass will survey the entire habitable zone of the target star. At 15 pc we can either use three bore-sight orientations and the nominal bandpass of 500 to 700 nm, or we can use two bore-sight orientations and a slightly shorter bandpass 400 to 600 nm. The time to survey a target star at 15 pc is slightly shorter (20.5 versus 21.2 hours) for the combination of 2 orientations and shorter bandpass.

Table E-1. Summary of Photometric Detection Results

Distance (parsecs)	Detection time including 1 boresight rotation (hours)
3	0.66
5	1.7
10	6.3
15	20.5

Wavelength range for 3, 5 and 10 pc is 500 to 700 nm and for 15 pc is 400 to 600 nm.

E.2.2 Spectroscopic Characterization

To characterize a planet at a known position the ASA system is rotated to ensure that the field mask does not block the exoplanet position. The light from the planet falls on a pixel-sized slot that is then refracted by a prism with a spectral resolving power of 20.

Table E-2. The Time to Characterize the Atmosphere of an Earth-Twin at 10 pc

	CO_2 or H_2O	O_2 or O_3
Time to characterize an Earth twin at 10 pc with an SNR $\geq$ 5	H_2O in 24.3 hours	O_3 in 92.5 hours

E.2.3 Survey of Nearby Stars

From the list of 259 candidate target stars all stars, with habitable zones $\leq$ 60 mas were removed. Then the time required for a 5-σ detection was computed. The 500 to 700 nm bandpass was used for habitable zones larger than 100 mas and a 400 to 600 nm bandpass was used for habitable zones between 60 and 100 mas. The total observing time for the 150 planets that could be detected most rapidly was 6287 hours, as shown in Table 6 on the following page. Assuming that the total observing efficiency is 90% to take inefficiencies due to slews and boresight rotations explicitly into account, the total search time is 6985 hours or 291 days for one visit to each to each of 150 target stars.

E.2.4. Appendix Star Data

Table 6. List of 150 Planetary Systems to be Searched

Hipparcos Catalog Entry	HD + Bayer Catalog Entry	RA	DEC	distance pc	Sp Type	V mag	L*/Lsun	Angular Distance from Star	5-sigma Detection Hours
71681	ξ Boo A	14 39 39.39	-60 50 22.1	1.35	K1V, K4V	1.35	0.49	522.0024965	0.26212577
71683	α Cen A	14 39 40.90	-60 50 06.5	1.35	G2V	-0.01	1.52	915.3793067	0.368961366
104214	201091	21 06 55.31	+38 44 31.4	3.50	K5V	5.2	0.14	108.3573175	0.378752529
104217	201092	21 06 52.19	+38 44 03.9	3.50	K7V	6.05	0.09	84.32996122	0.409337104
108870	ε Ind	22 03 17.44	-56 46 47.3	3.63	K5V	4.69	0.20	123.1983418	0.41572079
16537	ε Eri	03 32 56.42	-09 27 29.9	3.22	K2V	3.72	0.31	173.7202543	0.41744684
105090	202560	21 17 17.7	-38 51 52.5	3.95	M1/M2V	6.69	0.08	70.60449391	0.497746342
8102	τ Cet	01 44 05.13	-15 56 22.4	3.65	G8V	3.49	0.45	183.3339973	0.560547033
49908	88230	10 11 23.36	+49 27 19.7	4.87	K8V	6.6	0.11	66.86932387	0.712568859
19849	o2 Eri	04 15 17.64	-07 38 40.4	5.04	K1V	4.43	0.38	122.2255536	0.816617899
84478	156026	17 16 13.68	-26 32 36.3	5.97	K5V	6.33	0.14	62.20392205	0.87432473
73184	131977	14 57 27.35	-21 24 40.6	5.91	K4V	5.72	0.20	74.9478061	0.979361007
96100	σ Dra	19 32 20.59	+69 39 55.4	5.77	K0V	4.67	0.39	108.1962381	1.005732579
99461	191408	20 11 11.61	-36 05 50.6	6.05	K2V	5.32	0.25	82.67465456	1.081838025
114622	219134	23 13 14.74	+57 10 03.5	6.53	K3Vvar	5.57	0.27	79.04601856	1.452784697
15510	e Eri	03 19 53.22	-43 04 17.6	6.06	G8V, G5V	4.26	0.60	128.1425226	1.527731248
3765	4628	00 48 22.53	+05 17 00.2	7.46	K2V G8II?	5.74	0.26	68.80675352	1.635758535
72659	ξ Boo A	14 51 23.28	+19 06 02.3	6.70	G8eV	4.7	0.57	112.8572196	1.986461376
7751	P Eri A	01 39 47.24	-56 11 47.2	8.15	K2V	5.8	0.31	67.83858775	2.241309437
7981	10476	01 42 29.95	+20 16 12.5	7.47	K1V	5.24	0.40	84.67145635	2.29035905
3821	η Cas A	00 49 05.10	+57 48 59.6	5.95	G3V	3.45	1.17	182.1503972	2.598503613
23311	32147	05 00 48.68	-05 45 03.5	8.81	K3V	6.22	0.29	60.58767839	2.810190157
99240	δ Pav	20 08 41.86	-66 10 45.6	6.11	G5IV, G8V	3.55	1.20	179.4056599	2.946486935
56452	100623	11 34 29.95	-32 50 00.0	9.54	K0V + M V	5.96	0.33	60.22589612	2.954651423
99825	192310	20 15 16.58	-27 01 57.1	8.82	K3V. K0V	5.73	0.37	68.74937926	2.974667738
64924	115617	13 18 24.97	-18 18 31.0	8.53	G5V	4.74	0.77	102.6855794	3.529204081
81300	149661	16 36 21.18	-02 19 25.8	9.78	K2V	5.77	0.42	66.11027389	3.911212452
8362	10780	01 47 44.06	+63 51 11.2	9.98	K0V	5.63	0.49	69.94315608	4.631370711
56997	101501	11 41 03.03	+34 12 09.2	9.54	G8Vvar	5.31	0.57	79.22135974	4.751335978
61317	β CVn	12 33 45.09	+41 21 24.4	8.37	G0V	4.24	1.13	127.1335958	4.79913238
37279	α Cmi	07 39 18.54	+05 13 39.0	3.50	F5IV-V	0.4	6.81	746.1913078	5.129431576
1599	ζ Tuc	00 20 01.91	-64 52 39.4	8.59	F9V	4.23	1.20	127.6242645	5.337653705
57443	102365	11 46 32.25	-40 30 04.8	9.24	G3/G5V + M	4.89	0.77	95.04762442	5.844431937
15457	κ Cet	03 19 21.54	+03 22 11.9	9.16	G5Vvar	4.84	0.80	97.53557772	5.973360676
3093	3651	00 39 22.09	+21 15 04.9	11.11	K0V	5.88	0.50	63.4047884	5.982899506
64394	β Com	13 11 52.92	+27 52 33.7	9.15	G0V	4.23	1.36	127.5965672	6.815054967
105858	γ Pav	21 26 26.49	-65 22 05.3	9.22	F6V, F8V	4.21	1.41	128.6504507	7.094657946
29271	α Men	06 10 14.20	-74 45 09.1	10.15	G5V	5.08	0.80	87.89680573	7.349843695
89937	χ Dra	18 21 02.34	+72 44 01.3	8.06	F7Vvar	3.55	1.97	174.3698942	7.623435475
47080	82885	09 35 40.03	+35 48 38.8	11.18	G8IV-V + M V	5.4	0.74	76.93479117	8.486381977
43587	ρ Cnc	08 52 36.13	+28 19 53.0	12.53	G8V + M3.5V	5.96	0.60	61.59693404	9.179795255
91438	172051	18 38 53.45	-21 03 05.4	12.98	G5V	5.85	0.63	61.17433991	9.301884622
15330	ζ (1)Ret	03 17 44.47	-62 34 36.8	12.12	G2V	5.53	0.73	70.55460694	9.320162389
22449	π3 Ori	04 49 50.14	+06 57 40.5	8.03	F6V	3.19	2.73	205.8456886	10.40428435
10644	δ Tri	02 17 02.42	+34 13 29.4	10.85	G0V	4.84	1.10	96.5864739	11.11667469
27072	γ Lep A	05 44 27.97	-22 26 51.0	8.97	F7V + K2	3.59	2.36	171.2335032	11.19701785
2021	β Hyi	00 25 39.20	-77 15 18.1	7.47	G2IV	2.82	3.36	245.1178663	11.19980336
23693	ζ Dor	05 05 30.69	-57 28 22.8	11.65	F7V	4.71	1.42	102.1574711	11.2682897
15371	ζ (2)Ret	03 18 11.14	-62 30 28.6	12.08	G1V	5.24	0.94	80.28875434	11.76730428
58576	104304	12 00 44.37	-10 26 41.4	12.91	K0IV	5.54	0.86	71.92721001	12.98560325
80337	147513	16 24 01.24	-39 11 34.8	12.87	G3/G5V + DA	5.37	0.95	75.80493173	13.55323123
22263	30495	04 47 36.21	-16 56 05.5	13.32	G3V, G4V	5.49	0.91	71.78670771	13.92859866

14632	ι Per	03 09 02.88	+49 36 48.6	10.53	G0V	4.05	2.14	138.8296213	13.9794112
77052	ψ Ser	15 44 01.85	+02 30 55.9	14.67	G5V + MV	5.86	0.80	61.00907148	15.0151806
77257	λ Ser	15 46 26.75	+07 21 11.7	11.75	G0Vvar	4.42	1.90	117.1659276	15.40719964
42438	π 1 UMa	08 39 11.74	+65 01 14.5	14.27	G1.5Vb	5.63	0.92	67.20088113	16.01586006
80686	ζ TrA	16 28 27.80	-70 05 04.8	12.11	F9V, G0V	4.9	1.29	93.65251806	16.01876426
24813	λ Aur	05 19 08.08	+40 06 02.4	12.65	G0V	4.69	1.72	103.7391163	16.23618909
3583	4391	00 45 45.43	-47 33 07.8	14.94	G5IV	5.8	0.87	62.25869246	16.56618545
110109	211415	22 18 15.18	-53 37 31.9	13.61	G1V + M V	5.36	1.07	76.06789741	16.97424957
12777	θ Per A	02 44 11.69	+49 13 43.2	11.23	F7V + M1	4.1	2.31	135.2922615	17.01741962
75181	ν Lup	15 21 49.57	-48 19 01.1	14.56	G2V	5.65	0.94	66.74441268	17.16340102
79672	146233	16 15 37.13	-08 22 05.7	14.03	G1V	5.49	1.02	71.97288863	17.27369138
7918	10307	01 41 46.52	+42 36 49.7	12.64	G2V	4.96	1.34	91.49028227	18.31820527
78072	γ Ser	15 56 26.99	+15 39 53.0	11.12	F6V	3.85	2.85	151.9285141	20.63901653
84862	157214	17 20 39.47	+32 28 13.0	14.39	G0V, G2V	5.38	1.18	75.40837325	20.82887103
51459	90839	10 30 37.76	+55 58 50.2	12.85	F8V	4.82	1.56	97.12996691	21.7992198
57757	β Vir	11 50 41.29	+01 45 55.4	10.90	F8V, F9V	3.59	3.48	171.1060043	24.11606252
107649	207129	21 48 15.61	-47 18 10.4	15.64	G2V	5.57	1.16	68.97483327	24.14668796
49081	86728	10 01 01.02	+31 55 29.0	14.89	G1V, G2V	5.37	1.29	76.34630406	24.83109584
113357	217014	22 57 27.85	+20 46 07.3	15.36	G5V	5.45	1.27	73.4644436	25.90851745
37853	63077	07 45 35.18	-34 10 35.6	15.20	G0V + M V	5.36	1.33	75.90853501	26.07024284
53721	95128	10 59 28.22	+40 25 48.4	14.08	G0V	5.03	1.56	88.6441176	26.35443137
38908	65907	07 57 46.30	-60 18 12.1	16.19	G2V...	5.59	1.22	68.21217047	27.01773772
109176	ι Peg	22 07 00.47	+25 20 42.2	11.76	F5V	3.77	3.45	158.0326832	27.97019745
34065	53705	07 03 57.4	-43 36 32.3	16.25	G3V...	5.56	1.27	69.44642939	28.6338279
12843	τ Eri	02 45 05.98	-18 34 21.5	13.97	F5/F6V	4.47	2.55	114.1796591	28.88959859
33277	50692	06 55 18.69	+25 22 32.3	17.27	G0V	5.74	1.21	63.65930146	30.43626141
25278	35296	05 24 25.31	+17 23 00.8	14.66	F8V	5	1.72	89.40907236	31.22150063
72567	130948	14 50 15.72	+23 54 42.4	17.94	G2V	5.86	1.17	60.24669846	31.72277579
98819	190406	20 04 06.47	+17 04 16.2	17.67	G1V	5.8	1.20	62.03756168	31.73002901
16852	22484	03 36 52.52	+00 24 10.2	13.72	F9V, F8V	4.29	2.90	124.1392162	31.77808764
3909	φ Cet	00 50 07.72	-10 38 37.6	15.46	F7IV-V	5.17	1.63	82.65572819	32.88979752
35136	55575	07 15 50.11	+47 14 25.5	16.86	G0V	5.54	1.39	69.81250995	33.24670216
7513	ν And D	01 36 47.98	+41 24 23.0	13.47	F8V	4.1	3.32	135.3052735	34.97651758
86796	μ Ara	17 44 08.72	-51 50 00.9	15.28	G5V	5.12	1.72	85.94094625	35.00715523
47592	84117	09 42 14.67	-23 54 58.4	14.88	G0V	4.93	1.89	92.32139473	35.28764907
5862	ν Phe	01 15 10.57	-45 31 55.5	15.05	F8V	4.97	1.87	90.74371797	35.75414795
116771	ι Psc	23 39 56.82	+05 37 38.5	13.79	F7V	4.13	3.39	133.4450794	37.38517814
7978	10647	01 42 29.15	-53 44 26.1	17.35	F8V	5.52	1.49	70.38224664	37.80157505
82860	153597	16 56 01.36	+65 08 04.8	15.09	F6Vvar	4.88	2.03	94.53415397	39.11270088
32480	ψ Aur	06 46 44.34	+43 34 37.3	16.51	G0V	5.24	1.75	80.15100994	40.32521205
26394	π Men	05 37 08.79	-80 28 18.0	18.21	G3IV, G1V	5.65	1.47	66.47444499	41.06739727
12653	ι Hor	02 42 33.16	-50 48 03.0	17.24	G3IV	5.4	1.65	74.40760948	41.21593777
77760	χ Her	15 52 40.19	+42 27 00.0	15.85	F9V	4.6	2.91	107.560689	42.35320458
67275	τ Boo	13 47 16.04	+17 27 24.4	15.60	F7V + M2V	4.5	3.08	112.5374538	43.37211423
89042	ι Pav	18 10 26.26	-62 00 10.0	17.76	G0V, G3V	5.47	1.64	72.17457899	43.74491675
78459	ρ CrB	16 01 02.80	+33 18 19.4	17.43	G2V, G0V	5.39	1.71	75.00971976	44.01711784
71284	σ Boo	14 34 40.69	+29 44 41.3	15.47	F3Vwvar, F2V	4.47	3.18	115.3561975	45.04063539
32439	46588	06 46 14.47	+79 33 58.6	17.85	F8V	5.44	1.70	72.99078505	45.47021247
102485	ψ Cap	20 46 05.77	-25 16 13.9	14.67	F5V	4.13	3.86	133.988214	48.6060109
70497	θ Boo A	14 25 12.02	+51 51 06.2	14.57	F7V + M3	4.04	4.11	139.1169567	50.59656154
59199	α Crv	12 08 24.75	-24 43 43.6	14.77	F0IV/V	4.02	4.43	142.5391068	57.75760378
46509	τ Hyd A	09 29 08.84	-02 46 08.2	17.10	F6V + K0	4.59	3.45	108.5586356	58.87210676
64792	115383	13 16 46.71	+09 25 25.3	17.95	G0Vs	5.19	2.17	82.06770607	59.02803653
76829	139664	15 41 11.52	-44 39 38.0	17.52	F5IV-V	4.64	3.45	106.0669406	61.82836273
40843	χ Cnc	08 20 03.87	+27 13 07.0	18.13	F6V	5.13	2.33	84.23613028	64.45887292
18859	25457	04 02 36.66	-00 16 05.9	19.23	F5V, F6V	5.38	2.08	75.03575586	64.66085827
44075	76932	08 58 43.78	-16 07 59.7	21.32	F7/F8IV/V, F6V	5.8	1.74	61.8392051	66.22910913

114948	219482	23 16 57.47	-62 00 04.1	20.58	F7V	5.64	1.88	66.56775313	66.60661302
114924	219623	23 16 42.19	+53 12 50.6	20.28	F7V	5.58	1.93	68.47541225	66.60840132
112447	ξ Peg A	22 46 41.44	+12 10 26.7	16.25	F7V + M1V	4.2	4.41	129.2219146	67.39264665
103389	199260	20 56 47.27	-26 17 46.4	21.00	F7V , F8V	5.7	1.85	64.75936244	68.43304398
12444	16673	02 40 12.50	-09 27 09.7	21.54	F6V	5.79	1.79	62.12499438	69.64431851
98470	189245	20 00 20.16	-33 42 09.9	20.88	F7V, F8V	5.65	1.91	66.27816406	69.99431338
86736	160915	17 43 25.85	-21 40 59.1	17.54	F6/F7V	4.86	2.80	95.45798224	72.82015725
86620	ψ Dra B	17 41 58.35	+72 09 24.0	22.00	F8V	5.81	1.84	61.6588804	74.84897981
84893	ξ Oph A	17 21 00.21	-21 06 44.8	17.40	F2/F3V + K3	4.39	4.30	119.2442987	76.39019551
36439	58855	07 29 55.86	+49 40 21.6	19.90	F6V	5.35	2.30	76.17131673	76.56947395
28103	40136	05 56 24.32	-14 10 04.9	15.04	F1V	3.71	6.11	164.3357995	82.62186512
46853	θ UMa A	09 32 52.33	+51 40 43.0	13.49	F6IV + M	3.17	7.86	207.822901	83.19612393
50954	l Car	10 24 23.74	-74 01 53.6	16.22	F2IV	3.99	5.44	143.7980894	84.4861656
50384	89125	10 17 14.80	+23 06 23.2	22.72	F8Vw + M1V	5.81	1.96	61.56763906	84.64134476
97675	ο Aql	19 51 01.50	+10 24 57.8	19.39	F8V + M3V	5.12	2.69	84.6551874	85.27418266
19335	25998	04 08 36.49	+38 02 24.8	21.34	F7V	5.52	2.25	70.34997149	85.98747823
109422	τ PsA	22 10 08.48	-32 32 54.4	18.74	F6V	4.94	2.97	91.93301517	87.73173573
96441	θ Cyg A	19 36 26.54	+50 13 13.7	18.59	F4V + M	4.49	4.48	113.8647706	90.79076829
910	693	00 11 15.91	-15 28 02.4	18.89	F5V	4.89	3.16	94.08023804	94.84631067
4151	5015	00 53 04.28	+61 07 24.8	18.57	F8V	4.8	3.31	98.02676397	96.15487417
29800	43386	06 16 26.57	+12 16 18.2	19.61	F5IV-V	5.04	2.98	88.08163	97.0718237
17651	τ Eri	03 46 50.99	-23 14 54.4	17.92	F3/F5V	4.22	5.30	128.463861	99.16104359
61174	η Crv	12 32 04.48	-16 11 45.1	18.21	F2V , F0IV	4.3	5.13	124.3753341	99.83592508
40035	68146	08 10 39.98	-13 47 57.7	22.49	F7V + M3V	5.53	2.48	70.06235879	105.2988378
62512	111456	12 48 39.34	+60 19 11.6	24.16	F5V, F6V	5.83	2.18	61.07380727	106.6504954
73996	134083	15 07 17.95	+24 52 10.5	19.72	F5V	4.93	3.34	92.67375344	110.0901035
29650	43042	06 14 50.94	+19 09 24.8	21.13	F6V	5.2	2.99	81.83156661	112.8534909
51502	90089	10 31 05.02	+82 33 30.7	21.49	F2V	5.25	2.97	80.20469857	116.6120504
43797	76653	08 55 11.76	-54 57 56.0	24.15	F6V	5.7	2.45	64.80204955	119.7394518
25110	33564	05 22 33.78	+79 13 50.7	20.98	F6V	5.08	3.27	86.16054924	120.8346565
950	θ Scl	00 11 43.89	-35 08 00.2	21.81	F3/F5V	5.24	3.06	80.17546243	122.4737817
39903	68456	08 09 00.86	-61 18 06.1	21.39	F5V	4.74	4.68	101.0834149	124.104704
36366	ρ Gem	07 29 06.61	+31 47 02.7	18.50	F0V + M	4.16	6.14	133.9404399	125.7544609
95501	δ Aql	19 25 29.75	+03 06 52.5	15.37	F0IV	3.36	8.86	193.6349633	125.8849652
97295	187013	19 46 25.58	+33 43 43.3	20.86	F5 + K6V	5	3.48	89.46949177	127.5288952
92043	173667	18 45 39.73	+20 32 49.6	19.09	F6V	4.19	6.15	129.8844117	129.776266
16245	κ Ret A	03 29 22.19	-62 56 18.4	21.44	F5IV-V + M	4.71	4.85	102.7323145	129.9113956
67153	119756	13 45 41.57	-33 02 36.1	19.26	F3V	4.23	6.12	128.4204017	133.2690974
86486	λ Ara	17 40 23.73	-49 24 54.6	21.87	F3IV	4.76	4.82	100.3453202	134.1729253
21770	α Cae A	04 40 33.82	-41 51 48.9	20.13	F2V + M	4.44	5.58	117.3280523	134.2736511
111449	υ Aqr	22 34 41.50	-20 42 28.3	22.74	F7V, F3 V	5.21	3.42	81.35733735	149.3240377

5-Sigma Search Time	6287 hr
Correcting for a 90% Duty Cycle	6985 hr
Total Search Period Required	291 days

APPENDIX F
Lockheed Martin Team
Design Reference Mission Analysis

F.1. Introduction

The reference mission that follows is patterned on the assignment from JPL. Because of the length of the document, there are five Appendices, including an optics report, an optics diagram, and two lists of different stars, with the SNR obtainable for each, using the most appropriate baseline for each. The 167 stars are of the following spectral types: 37 F, 86 G, 41 K, and one M star. This distribution arose naturally by attempting to minimize the observing time. The results in the target lists are entirely for the 40-m truss, 4×3.5-m telescope interferometer. The complete list of stars can be observed once for planet searching.

In addition to the reference mission for the 40-m interferometer, the material below also shows how the performance of the devices would suffer from photon noise in examining dusty planetary systems at various distances. Finally, there is a comparison for a solar system twin of the performance of different interferometers.

F.2. Instrument Configuration

A number of interferometers have been compared. Four that could look at terrestrial planets have had some quantitative comparisons of performance. These are:

(A) 4 telescopes, 11.43 to 17.14 to 11.43-m spacing, 40-m truss

(B) 4 telescopes, 8.57 to 12.86 to 8.57-m spacing, 30-m truss

(C) 4 telescopes, 6 to 9 to 6-m spacing, 2-m truss

(D) 2 telescopes, 18-m spacing, 18-m truss

The complete set of stars and observing times have only been calculated for system A, the 40-m truss with 4×3.5-m telescopes. Assorted lesser information (such as observing time for Sun-like stars) has been calculated for the other systems for comparison and is presented in Appendix F-1.

F.2.1. Interferometers

1. *Optical architecture.*
All are θ^2 nulls. The measured signal varies as θ^3. Both outputs go to the spectrometer. Configurations A, B and C have two options whereby either the telescopes are combined in pairs 1 to 2, 3 to 4 or in pairs 1 to 3, 2 to 4. The combined pairs are then combined again, with phase chopping, and both outputs of the final combination are observed.
2. *Optical layout drawing.*
The length of this material requires it to be attached as a separate appendix. Appendix F-4 describes the optical system. Appendix F-5 has diagrams and shows optical paths.
3. *All apertures are circular*. A: 3.5 m. B: 2.5 m, C: 1.7m, D: 1.4 m. All are Cassegrain telescopes with a tertiary flat. The secondary/tertiary obscuration is ~2%. The areas are A: 37.7square m. total effective, B: 19.2, C: 9.0, D 3.08. Baselines are A: 28.54 and 11.43 m, B: 21.43 and 8.57 m, C: 15 and 6 m, D: 18 m.
4. *Primary aperture optical figure.*
Paraboloid on a circular substrate. Some active optics, preferably acting on the primary are assumed necessary for 3.5-m apertures, but not for smaller ones.
5. *Operational wavelength range.*
A, B and C: 7 to 19 µm, D: 7.5 to 12.5 µm
6. *Amplitude matching requirement.*
Intensity matching is to better than 2.1% in the observation wavelength range (produces a leak of 2.8×10^{-5}). The beamsplitters to achieve this have a single high index 1/2 wave layer in the middle of the range.
7. *Corrected wavefront (after AO or spatial filtering).*
Strehl ratio from telescopes better than 60% at 2 µm (= 98.4 at 10 µm). The corresponding wavefront error is no greater than 200 nm rms.
8. *Properties of null.*
Null depth depends on configuration and distance of star. Max depth is 4×10^{-5}. The DRM assigns the stars to one or other of the configurations for the discovery phase, and uses the minimum necessary angular resolution to achieve observations to 12.5 µm. The leak is calculated from the formula $T = \pi^2(\theta_S/\theta_p)^2/64$.
9. *Assumptions needed to achieve null depth, including optical path accuracy (piston) and pointing accuracy.*
There are four different phase precisions: a) The allowable phase error variation from wavelength to wavelength, b) the allowable starting phase error (set at the short wavelength end), c) The precision with which the phase error is measured with respect to time, and d) the precision of correction of the phase error with time.
   a) It is assumed that the starting error at the short wavelength end of the spectrum is ± 5 nm.
   b) It is a range of ± 11.8 nm near the 7 µm end of the spectrum, and broadens to 30 nm at the long wavelength end.
   c) To reduce the random variation to a planet signal per integration or $\sim 10^{-7}$ of the star, a phase error of 6×10^{-4} radians in the band, or 2.4×10^{-3} at 2 µm or 0.75 nm would be adequate. The flux from the star at 2 µm is ~20 Jy in the worst case, giving $\sim 10^9$ detected photons per square meter in the time. In principle the phase can be measured to better than 3×10^{-5} of 300 nm, or 0.01 nm in this time. Thus, the phase error can be measured adequately.
   d) The precision with which phase can be corrected can be worse than just given because the signal versus phase error will be recorded and the statistical effect of signal versus phase can be removed from the result. It is expected that the phase correction will be no worse than ~3 nm.
10. *Properties of spatial filter, if any.*
The spectrograph slit and the detector edges will provide the filtering that selects the planet radiation.
11. *Angular resolution at planet position, in the final image.*
It is assumed that the "resolution" is the smallest separation that can be resolved from circumstellar dust. For the longest wavelength for systems A to C, it is assumed that a wavelength where one is at 0.8 of resolved spacing is observable at a position angle defined by the short wavelength observations.
   - System A: wide spaced 10 µm 0.036 arcseconds 18 µm 0.053 arcseconds close spaced 10 µm 0.093 arcseconds, 18 µm 0.13 arcsec.
   - System B: wide spaced 10 µm 0.047 arcseconds, 18 µm 0.070 arcseconds. close spaced 10 µm 0.12 arcseconds 18 µm 0.175 arcsec.
   - System C: wide spacing 10 microns 0.068 arcseconds, 18 microns 0.10 arcseconds close spaced 10 µm 0.17 arc sec, 18 µm 0.25 arcsec.

- System D: 10 µm 0.080 arc sec, 12.5 µm 0.10 arcsec.

12. *Inner and outer radius of effective field-of-view within which planets might be detected (instantaneous and after observations at multiple roll angles).*
All position angles are available from an integration with the interferometer completing a 180 degree rotation. The minimum observation that has information about statistical errors is 1.5 rotations (3×180 degree observations), which takes 11 hours. The inner radius of the FOV is given by the resolution of the telescope and the shortest wavelength observable. For a wavelength of 7.5 µm, for example, it is 0.027 arcseconds with the 40-m truss, wide-spaced. The outer radius is 40 times the resolution limit, thus it increases with increasing wavelength. Also, for systems A, B and C, the short baseline permits observations to 2.5 times larger radii than the wide baseline. For system A at 10 µm, the inner and outermost radii are 0.036 and 3.6 arcseconds. For B they are 0.047 arcseconds and 4.7 arcseconds, for C they are 0.069 arcseconds and 6.9 arcseconds, and for D they are 0.080 arcseconds and 2.3 arcseconds.

13. *Operating temperatures and thermal stability for key optical components.*
The telescopes must be cooler than 45 K throughout observations for systems A to C, and 60 K for system D. It is required that direct sunlight never reach either the telescopes or the beams that carry the radiation to the beam combiner. The beam combiner outer part has a similar requirement to the telescopes. Inside the beam combiner, there are two regions. The beam combiner itself and associated optics must be at ~17 K, and the detector and spectrometer must be at 7 K. The cryogen will maintain the necessary stability for the optical components.

14. *Effects of spacecraft parameters (vibration, pointing jitter, etc.) on stability of null.*
The vibration frequencies of the trusses are expected to fall into the range 5 to 15 Hz. The position and phase will be measured 200 times-per-second and corrections applied to small mirrors inside the dewar. Calculations show a wide safety margin for vibration and pointing before they start to compromise the inner loop. However there is a second line of defense in that the measured signal variation with error will allow the signals to be corrected for pointing and vibration errors.

15. *Spectrometer design.*
This is a straightforward R = 20 prism spectrograph. The beam expander, collimator and camera are all mirrors. Baseline designs have explored a few different prism materials, however the long wavelength transmission measurements when cold are not available and need to be measured. A likely candidate material is NaCl.

16. *Operations scenario (e.g., does the baseline change for each target?).*
There will be two configurations for any one interferometer. For about 25% of the stars there will be a need to observe short wavelengths with the short baseline and long wavelengths with the long baseline.

17. *Specify Q, defined as the operational ratio planet light/scattered starlight*. In general the local zodiacal dust signal will dominate. Thus Q will vary with star/planet distance from the sun. For the 40-m system with the star at 10 pc, and at 12 µm, $Q = 7.1 \times 10^{-4}$.

18. *Total optical efficiency for planetary light including reflection and transmission losses, effective vs. total collection area, filters etc. for both broadband and spectroscopic measurements.*
The calculated optical efficiencies are for the planet signal averaged over the band and with allowance for modulation 6.7% for systems A to C. For system D, it is 8.6% with allowance for modulation. The effective collection areas have been given with the definitions of A to D. All types of observation are made together and use the same instrumentation.

19. *Specify detected average count rates, in the effective planetary diffraction spot size (FWHM), from planet, diffracted star, scattered star, exozodi, local zodi, instrument thermal emission, detector dark count, and any other source. Assume the solar system at 10 pc.*
Table F-2 shows the results for the 40-m truss. These are, for the first 8 lines-per-pixel, in one minute. The penultimate line is the SNR at R = 20, and the last line is the total SNR in 24 hours of integration.

Table F-1. Efficiency of Sequence of Optical Components in 4 Element TPF Interferometers

Telescope primary (passive)	0.99
Telescope secondary (focussing)	0.99
Telescope tertiary (tip tilt)	0.99
Dewar window, AR-coated	0.96
Gold beamsplitter to send visible to pointing/focus control detector also active as preset path length adjustor	0.99
High speed pathlength adjustor mirror	0.99
phase plate (1 is enough for 8 to 13 µm)	0.92
pathlength adjustor (high speed)	0.99
Beamsplitter #1 (1/2 wave high index coating)	
Reflector to direct beams to beamsplitter #2	0.99
Beamsplitter #2 (1/2 wave high index coating)	> 0.8
Dichroic to separate 2 µm radiation for phase control	0.8
pathlength adjusto	0.99
Beamsplitter #3 (1/2 wave high index coating)	Parallel
Reflector to direct beams to beamsplitter #2	0.99
Beamsplitter #4. (1/2 wave high index coating)	> 0.8
Spectrograph entrance slit (and detector pixel limits)	0.6
Beam expander	0.99
Collimator lens or mirror	0.99
Prism	0.8
Camera lens or mirror	0.99
Detector	0.7

Efficiency 0.134 for star, planet loses half through interference 0.067 for planet, 0.281 for background, all split among 6 pixels.

Table F-2. Results for 40-m Truss

1 minute integration	**8 µm**	**10 µm**	**12 µm**
Earth	3.86	6.92	9.33
Exozodi after	1530	2790	3744
Sun after	5172	3420	2424
Zodi	1950.5	4122	6510
Dark current	228	228	228
Read equivalent counts	117	117	117
Noise	95.3	103.5	114.6
SNR 1 pixel	0.041	0.0673	0.0814
1 day integration	**8 µm**	**10 µm**	**12 µm**
SNR 6 pixels 1 day	3.81	6.26	7.57
SNR 8–12.5 µm		17.49	

Table F-3. 12-μm Effects of Exozodi Amount on Observing Time for 40-m Truss System

Exozodi Distance	0	0.5	1	2	5	10
3pc	0.852	0.926	1.0	1.148	1.592	2.342
5	0.521	0.761	1.0	1.478	2.914	5.307
10	0.715	0.875	1.0	1.285	2.140	3.565
15	0.831	0.916	1.0	1.169	1.676	2.561

Note: the survey time is part of the total for all other uses. Thus, for example, the minimum survey time (11 hours, or 1.5 interferometer rotations) for 61 of our 167 stars will already characterize temperature and size of the planet. That minimum observation will already have done a fair job in searching for atmospheric constituents and search for ozone on eight of the stars. We feel that the optimum number of repeats is four, made at consecutive 1/8 intervals of the period of a planet in the middle of the HZ. The logistics of this are complex, but our method of cooling ensures that almost every part of the sky has a 6-month consecutive interval in which observations can be made. The preferred scenario guarantees to see a planet at least once with a separation of > 0.92 of greatest elongation, regardless of the inclination of the planetary system.

F.2.2. Spectroscopic Characterization

Because of the difference between optical and IR, a somewhat different observing strategy is proposed. Following detection, the next key observation is to determine the planet temperature and size. Also there will be a mass estimate from the planetary mass-radius relationship. This observation requires that the 8–12 μm region of the spectrum be divided into two regions with roughly equal photon counts in each, and an SNR of ~5 on each. Then on the basis of this measurement, a decision can be made as to possible planetary characteristics, and a decision can be made on the priority for further observation and the necessary observation time.

Water, CO_2, and ozone have been grouped together since all are strong bands. For every star in the reference list, a 5 sigma indication of the presence of ozone at terrestrial strength can be obtained in 20 days of observation. The detection algorithm assumed is to observe the entire 8 to 12.5 μm region of the spectrum with R = 20, and two to three measurement points per resolution half width. Thus, in the core of the 9.7 μm ozone band, there will be three measurement points. Outside, the continuum is expected to be free from disturbance from 8 to 12.5 μm. Thus there will be six measurement points below the line center and six above it to define the continuum and wings of the band. It has been estimated that to see the band with a total band SNR = 5, it will be necessary to obtain the data with an SNR of 10 per R = 20 FWHM. Since the sensitivity changes with wavelength, this is the 10 μm SNR.

F.3. Survey of Nearby Stars

The attached list (Appendix F-2) has 167 stars. It is expected that 10% of these will fall into the galactic band where observations are not advisable, leaving 150 other stars. There is no abrupt edge defining the observable stars, and if necessary, additional stars can be added to the list at moderately greater distances.

From the number of stars, it is estimated that the nearest neighbor stars will be typically 8^o apart. It should be easy to move from one to another in ~1000 seconds and have the instrument settle in another ~1000 seconds, or 10^4 vibration periods. Thus if $Q \approx 1000$, there will be 10 decay periods before observations must start, and any amplitude can be expected to decay by more than a factor of 20,000.

Each day, the spacecraft will communicate with Earth for up to 1 hour. This leaves two 11-hour periods available for observations, or one 23-hour stretch on an already acquired target. For an 11-hour period, the SNR is reduced by a factor 0.677 over that obtainable in 24 hours. The 24-hour SNR for the entire 8 to 12.5 μm band and

24 hours of observation are shown in the attached tables (Appendix F-1). Appendix F-2 shows the SNR obtainable with 57 close-configuration stars using the 11.57-m baselines. Appendix F-3 shows how 111 different wide-configuration stars can be observed using the 28.43-m baselines.

Every star can be observed to SNR > 5 broadband in one 11-hour session with the interferometer, in which three independent sky maps are obtained, thus reducing the possibility that a single spurious event produces an apparent planet image. (In fact because modulation pattern varies with wavelength it is hard for a spurious event to mimic a point source.) There is an allowance for downloading data once per day, and for slewing and settling. Set up is done towards the end of settling time. Thus the total time is used with ~92% efficiency for observing.

The interferometer maps as it obtains spectra of every source in the field. Thus, "search" time can be reused for spectroscopy and spectroscopy time can also be used to search the field to fainter limits, seeing smaller and smaller objects. In the two lists, there are 61 stars potentially harboring terrestrial planets that could be discovered during the search mode, but the SNR is high enough to determine the radius and temperature of over 1/3 of the stars during this period. For the few "best" candidate stars—eight in all—even ozone, water vapor and CO_2 may show up in this first exercise! Yet even for the stars with the lowest SNR in this list, there is a reasonable prospect of seeing ozone at SNR 5 for band detection in a 20-day observation. One could observe the environs every one of these four times in the first year of life of the interferometer. Then for the next four years, one could characterize planets around more than 1/2 of the stars. If every other star has a planetary system, this device could make detailed studies of the complete sample, with maps and spectra of every object seen well.

APPENDIX F-1. COMPARISON OF DIFFERENT TRUSS INTERFEROMETER PERFORMANCES

Summary

Some of the numbers below are so short that they cannot be realistically achieved. Nonetheless, it can be seen that there is a ratio in the speed with which these devices get results. Instrument B is six times faster than instrument D. Instrument A is four times faster than instrument B. In addition, each device provides higher angular resolution than the less sensitive one. The major issues in deciding between different devices are:

1) Scientific goals
2) Cost risk.

Clearly it is necessary to understand how these issues play out in terms of practical matters.

Case A 40-m truss, four 3.5m apertures

Numbers of stars available within each distance category for this device

	3.5 pc	5 pc	10 pc	15 pc	19 pc
Lockheed	6	8	48	108	167+

Time to detect Earth SNR = 5 over entire band

Distance	3 pc	5 pc	10 pc	15 pc
Time	(0.25) hrs	(0.35) hrs	(2) hrs	(7) hrs
# stars	6	8	48	108

Time to determine size and temperature of Earth 2 bands SNR = 7

Distance	3 pc	5 pc	10 pc	15 pc	19 pc
Time	1 hr	1.4 hrs	8 hrs	1.17 hrs	
# stars	6	6	48	108	> 150

Time to detect ozone and water at 7.5 to 10 μm R = 20 SNR = 10

Distance	3 pc	5 pc	10 pc	15 pc
Time	10 hrs	14 hrs	3.3 days	11.7 days
# stars	3	6	48	108

Time to detect Mars size at Earth-like temperature

Distance	3 pc	5 pc	10 pc	15 pc
Time	7.3 hrs	10	2.4 days	8.5 days
# stars	3	6	21	48

Case B 30-m truss, 7.5 to 17.5 μm

Results

This device can detect planets out to an angular distance of ~0.05 arcseconds. It is limited to making observations for CO_2 to planets about 0.1 arcsec at greatest elongation.

Numbers of stars available within each distance category for this device

	3.5 pc	5 pc	10 pc	15 pc	22.5 pc	40 pc
Ball	4	6	13	14	81	85 to 27pc
Lockheed	3	6	21	70 predicted	-	-
TRW	3	6	29	59	111	156
AVERAGE	**3**	**6**	**21**	**48**	**96**	**150::**

Time to detect Earth SNR = 5 over entire band

Distance	3 pc	5 pc	10 pc	15 pc	22.5 pc	40 pc
Time	8(1.0) hrs	8(1.2) hrs	9 hours	1.5 days	7.6 days	76 days
# stars	3	6	21	48	96	150

Note that the device is likely to be time limited somewhere between 100 and 150 stars.

Time to determine size and temperature of Earth 2 bands SNR = 7

Distance	**3 pc**	**5 pc**	**10 pc**	**15 pc**	**22.5 pc**
Time	8(4) hours	8(5) hours	1.5days	6 days	30 days
# stars	3	6	21	48	96

Time to detect ozone and water at 7.5 to 8 µm R =20 SNR = 10

Distance	**3 pc**	**5 pc**	**10 pc**	**15 pc**
Time	1.4 days	1.8days	15.1days	63 days
# stars	3	6	21	48

Detection of CO2 and long wave water band limited to 10pc, 21 stars.

Time to detect Mars size at Earth-like temperature

Distance	**3 pc**	**5 pc**	**10 pc**	**15 pc**
Time	16(12) hrs	16(14) hrs	4 days	16.5 days
# stars	3	6	21	48

Case D 18-m truss, two 1.4-m apertures

Case D Results

For a solar system twin, it can detect an earth out to 10 pc. Planet needs a maximum elongation of 0.1 arcseconds.

Numbers of stars available within each distance category for this device

	3.5 pc	**5 pc**	**8 pc**	**10 pc**	**12 pc**
Ball	4	6	11	13	14
Lockheed	3	6	12	21	27
TRW	3	6	18	29	38
AVERAGE	**3**	**6**	**14**	**21**	**26**

Time to detect Earth SNR = 5 over entire band

Distance	**3 pc**	**5 pc**	**8 pc**	**10 pc**	**12 pc (Fstar)**
Time	8(6) hrs	16(11) hrs	1.5 days	4 days	8 days
# stars	3	6	14	21	26

Time to determine size and temperature of Earth 2 bands SNR = 7

Distance	**3 pc**	**5 pc**	**8 pc**	**10 pc**	**12 pc (Fstar)**
Time	1 day	2 days	6 days	16 days	32 days
# stars	3	6	14	21	26

Time to detect ozone and water at 7.5 to 8 µm R=20 SNR = 10

Distance	**3 pc**	**5 pc**	**8 pc**	**10 pc**
Time	9.5 days	15.4 days	52 days	106 days
# stars	3	6	14	21

Time to detect Mars size at Earth-like temperature

Distance	**3 pc**	**5 pc**	**8 pc**	**10 pc**	**12 pc (Fstar)**
Time	2.9 days	5.3 days	17 days	46 days	92 days
# stars	3	6	14	21	26

Note: All times are cumulative. That is, time spent in any task obtains data towards all other tasks requiring longer observing times. The sequence of increased information is then: detection, characterization of size and temperature, detection of smaller planets and detection of ozone and water vapor.

APPENDIX F-2. CLOSE CONFIGURATION STARS

HD	Yale BS	Gliese	BayerFlam	Dist.pc.	Mag	Spectrum	* dia.	T/Tsun	24hSNR
209100	8387	Gl 845	Eps Ind	3.626342	4.69	K5V	1.85	0.78	74.1
22049	1084	Gl 144	18Eps Eri	3.218021	3.73	K2V	2.32	0.87	69.3
10700	509	Gl 71	52Tau Cet	3.647372	3.49	G8V	2.09	0.93	63.2
26965	1325	Gl 166 A	40Omi2Er	5.044391	4.43	K1V	1.55	0.88	50.2
185144	7462	Gl 764	61Sig Dra	5.76668	4.68	K0V	1.31	0.9	45.3
20794	1008	Gl 139		6.059872	4.26	G8V	1.72	0.93	33.2
190248	7665	Gl 780	Del Pav	6.107616	3.56	G5IV-Vvar	1.82	0.96	30.3
115617	5019	Gl 506	61 Vir	8.525149	4.74	G5V	1.09	0.96	27.2
109358	4785	Gl 475	8Bet CVn	8.371003	4.27	G0V	1.15	1.02	26.4
39587	2047	Gl 222 A	54Chi1Ori	8.663259	4.4	G0V	1.11	1.02	25.4
1581	77	Gl 17	Zet Tuc	8.592542	4.22	F9V	1.16	1.04	25.1
203608	8181	Gl 827	Gam Pav	9.21659	4.22	F6V	1.01	1.1	24.1
114710	4983	Gl 502	43Bet Con	9.154994	4.26	G0V	1.11	1.02	23.2
170153	6927	Gl 713 A	44Chi Dra	8.057368	3.57	F7Vvar	1.5	1.07	22.5
30652	1543	Gl 178	1Pi 3Ori	8.025682	3.19	F6V	1.52	1.1	22.2
38393	1983	Gl 216 A	13Gam Le	8.969414	3.58	F7V	1.36	1.07	20.7
98230	4374	Gl 423 B	53Xi UMa	10.41667	4.8	G0 Ve	0.88	1.02	20.6
98231	4375	Gl 423 A	53Xi UMa	10.41667	4.33	G0 Ve	1.11	1.02	18.7
19373	937	Gl 124	Iot Per	10.53408	4.05	G0V	1.23	1.02	17.1
33262	1674	Gl 189	Zet Dor	11.65094	4.71	F7V	0.84	1.07	17.1
121370	5235	Gl 534	8Eta Boo	11.34173	2.68	G0IV	2.3	1.02	16.9
16895	799	Gl 107 A	13The Per	11.23217	4.13	F7V	1.05	1.07	16.7
161797	6623	Gl 695 A	86Mu Her	8.399832	3.42	G5IV	1.88	0.96	16.3
142860	5933	Gl 603	41Gam Se	11.121	3.85	F6V	1.12	1.1	16.3
141004	5868	Gl 598	27Lam Se	11.75364	4.43	G0Vvar	1.06	1.02	15.4
210027	8430	Gl 848	24Iot Peg	11.75641	3.76	F5V	1.05	1.12	15.4
110380	4826	Gl 482 B	29Gam Vi	11.83012	3.52	F0 V	1.11	1.21	14.4
110379	4825	Gl 482 A	29Gam Vi	11.83012	3.46	F0V...	1.12	1.21	14.4
34411	1729	Gl 197	15Lam Au	12.64542	4.71	G0V	0.95	1.02	14.3
2151	98	Gl 19	Bet Hyi	7.474959	2.8	G2IV	2.34	1	14
102870	4540	Gl 449	5Bet Vir	10.90037	3.61	F8V	1.43	1.06	13.8
9826	458	Gl 61	50Ups An	13.46801	4.09	F8V	0.98	1.06	12.5
17206	818	Gl 111	1Tau1Eri	13.97429	4.46	F5/F6V	0.84	1.12	12.4
222368	8969	Gl 904	17Iot Psc	13.7912	4.13	F7V	1.05	1.07	11.8
22484	1101	Gl 147	10 Tau	13.7193	4.28	F9V	1.11	1.04	11.3
105452	4623	Gl 455.3	1Alp Crv	14.76887	4.02	F0IV/V	0.89	1.21	10.9
197692	7936	Gl 805	16Psi Cap	14.67136	4.13	F5V	0.95	1.12	10.8
126660	5404	Gl 549 A	23The Bo	14.57089	4.06	F7V	1.01	1.07	10.7
61421	2943	Gl 280 A	10Alp CMi	3.497359	0.38	F5IV-V	5.84	1.12	10.5
128167	5447	Gl 557	28Sig Boo	15.46551	4.46	F3Vwvar	0.78	1.13	10.5
120136	5185	Gl 527 A	4Tau Boo	15.59576	4.5	F7V	0.82	1.07	10.2
40136	2085	Gl 225	16Eta Lep	15.04438	3.72	F1V	1.01	1.19	9.92
20010	963	Gl 127 A	Alp For	14.11233	3.95	F8V	1.27	1.06	9.6
182640	7377	Gl 760	30Del Aql	15.37279	3.36	F0IV	1.03	1.21	9.4
142373	5914	Gl 602	1Chi Her	15.85289	4.61	F9V	1.02	1.04	9.2
90589	4102	Gl 391		16.21534	4	F2IV	0.93	1.17	9
81997	3759	Gl 348 A	31Tau1Hy	17.09986	4.6	F6V	0.72	1.1	8.9
76943	3579	Gl 332 A		16.43115	4.11	F5V	0.96	1.12	8.9
23249	1136	Gl 150	23Del Eri	9.043227	3.53	K0IV	2.57	0.9	8.6
215648	8665	Gl 872 A	46Xi Peg	16.24959	4.19	F7V	1.03	1.07	8.6
139664	5825	Gl 594		17.5162	4.64	F5IV-V	0.71	1.12	8.5
156897	6445	Gl 670 A	40Xi Oph	17.39736	4.41	F2/F3V	0.77	1.17	8.5
-		Gl 351 B	-	18.55632	4.65	F0 IV	0.56	1.21	7.9
23754	1173	Gl 155	27Tau6Eri	17.92436	4.22	F3/F5V	0.84	1.13	7.8
109085	4775	Gl 471.2	8Eta Crv	18.2083	4.3	F2V	0.78	1.17	7.8
58946	2852	Gl 274 A	62Rho Ge	18.49797	4.18	F0V...	0.76	1.21	7.6
185395	7469	Gl 765 A	13The Cy	18.59427	4.48	F4V	0.78	1.13	7.5

APPENDIX F-3. WIDE CONFIGURATION STARS

HD	YaleBS	Gliese	Bayer Flam	Dist.pc	Mag	Type	* dia.	T/Tsun	24hSNR
156274	6416	Gl 666 A		8.786574	5.53	M0V	0.56	0.62	67.9
201092	8086	Gl 820 B	61 Cyg	3.503609	6.03	K7V	1.4	0.71	58.9
201091	8085	Gl 820 A	61 Cyg	3.482743	5.21	K5V	1.54	0.78	46.8
	-	Gl 702 B	-	5.085953	6	K5 Ve	1.08	0.78	40.7
156026		Gl 664		5.968011	6.33	K5V	0.94	0.78	40.4
131977	5568	Gl 570 A		5.905977	5.75	K4V	0.95	0.81	35.2
156384	6426	Gl 667 A		6.97107	6.29	K4V	0.81	0.81	34.6
216803	8721	Gl 879		7.637086	6.48	K4Vp	0.75	0.81	34.3
219134	8832	Gl 892		6.525711	5.56	K3Vvar	0.92	0.85	31.3
16160	753	Gl 105 A		7.208766	5.82	K3V	0.72	0.85	30.5
32147	1614	Gl 183		8.813679	6.22	K3V	0.65	0.85	28
192310	7722	Gl 785		8.823789	5.73	K3V	0.65	0.85	27.8
122064	5256			10.10407	6.49	K3V	0.58	0.85	27.5
223778	9038	Gl 909 A		10.78981	6.4	K3V	0.64	0.85	26
188088	7578	Gl 770		14.21666	6.17	K3/K4V	0.67	0.85	26
191408	7703	Gl 783 A		6.051803	5.32	K2V	1.27	0.87	25.7
4628	222	Gl 33		7.46046	5.74	K2V	0.82	0.87	25.4
10361	487	Gl 66 A		8.14664	5.8	K2 V	0.94	0.87	24.9
38392	1982	Gl 216 B		8.969414	6.13	K2 V	0.85	0.87	23.6
149661	6171	Gl 631	12 Oph	9.778039	5.75	K2V	0.81	0.87	23
166620	6806	Gl 706		11.09755	6.4	K2V	0.7	0.87	22
131511	5553	Gl 567		11.53536	6.02	K2V	0.88	0.87	21.7
155886	6402	Gl 663 A	36 Oph	5.985157	5.07	K1 Ve	1.29	0.88	19.6
10476	493	Gl 68	107 Psc	7.467702	5.22	K1V	1.03	0.88	19.2
17925	857	Gl 117		10.38098	6.03	K1V	0.88	0.88	19.1
37394	1925	Gl 211		12.2414	6.23	K1V	0.79	0.88	18.5
10360	486	Gl 66 B		8.14664	5.9	K0V	0.96	0.9	18.3
100623	4458	Gl 432 A		9.538344	5.98	K0V	0.82	0.9	18.3
10780	511	Gl 75		9.976057	5.63	K0V	0.81	0.9	17.2
	-	Gl 635 B	-	10.79564	5.4	K0 V	0.89	0.9	17.1
13445	637	Gl 86		10.91346	6.12	K0V	0.78	0.9	17.1
3651	166	Gl 27	54 Psc	11.10741	5.85	K0V	0.83	0.9	16.3
72673	3384	Gl 309		12.17285	6.39	K0V	0.66	0.9	16.1
69830	3259	Gl 302		12.58178	5.97	K0V	0.82	0.9	15.2
158633	6518	Gl 675		12.79754	6.43	K0V	0.65	0.9	15
104304	4587	Gl 454		12.90656	5.55	K0IV	0.83	0.9	14.9
166	8	Gl 5		13.70238	6.14	K0V	0.78	0.9	14.8
103095	4550	Gl 451 A		9.156671	6.45	G8Vp	0.55	0.93	14.6
101501	4496	Gl 434	61 UMa	9.541074	5.33	G8Vvar	0.88	0.93	14.4
82885	3815	Gl 356 A	11 LMi	11.17943	5.41	G8IV-V	0.85	0.93	14.2
75732	3522	Gl 324 A	55Rho1Cr	12.53133	5.95	G8V	0.68	0.93	13.9
14412	683	Gl 95		12.67748	6.34	G8V	0.61	0.93	13.9
196761	7898	Gl 796		14.64558	6.36	G8/K0V	0.61	0.93	13.9
182572	7373	Gl 759	31 Aql	15.14922	5.16	G8IVvar	0.88	0.93	13.9
182488	7368	Gl 758		15.49427	6.37	G8V	0.6	0.93	13.9
	-	Gl 25 B	-	15.53277	6.4	G8 V	0.61	0.93	13.5
158614	6516	Gl 678 A		16.44737	5.98	G8IV-V	0.68	0.93	13.3
	-	Gl 678 B	-	16.44737	6.2	G8 IV-V	0.66	0.93	12.7
122742	5273	Gl 538		16.60027	6.3	G8V	0.61	0.93	12.3
177565	7232	Gl 744		17.17033	6.15	G8V	0.62	0.93	12.2
111395	4864	Gl 486.1		17.17328	6.31	G7V	0.63	0.93	12.2
42807	2208	Gl 230		18.11594	6.45	G8V	0.55	0.93	12.2
140901	5864	Gl 599 A		15.2439	6.01	G6IV	0.68	0.95	11.9
6582	321	Gl 53 A	30Mu Ca	7.55287	5.17	G5Vp	0.97	0.96	11.6

20630	996	Gl 137	96Kap1Ce	9.159187	4.82	G5Vvar	0.92	0.96	11.4
43834	2261	Gl 231	Alp Men	10.14816	5.08	G5V	0.87	0.96	11.2
172051	6998	Gl 722		12.98364	5.86	G5V	0.7	0.96	11.2
140538	5853	Gl 596.1A	23Psi Ser	14.67136	5.86	G5V	0.7	0.96	11.1
4391	209	GJ 1021		14.94322	5.8	G5IV	0.71	0.96	11
160691	6585	Gl 691	Mu Ara	15.2765	5.14	G5V	0.85	0.96	10.9
217014	8729	Gl 882	51 Peg	15.36098	5.5	G5V	0.74	0.96	10.9
-		Gl 332 B	-	16.43115	6.18	G5 V	0.51	0.96	10.9
43162	2225	NN 3389		16.69449	6.38	G5V	0.57	0.96	10.9
25680	1262	Gl 160	39 Tau	16.7252	5.9	G5V	0.7	0.96	10.8
102438	4525	Gl 446		17.77462	6.48	G5V	0.55	0.96	10.7
117176	5072	Gl 512.1	70 Vir	18.10938	4.98	G5V	1.02	0.96	10.4
190771	7683	GJ 1249		18.87149	6.17	G5IV	0.51	0.96	10.2
102365	4523	Gl 442 A		9.239582	4.9	G3/G5V	0.99	0.97	10.1
147513	6094	Gl 620.1A		12.87167	5.39	G3/G5V	0.74	0.97	10
38858	2007	GJ 1085		15.5642	5.97	G4V	0.54	0.97	9.9
32923	1656	Gl 188 A	104 Tau	15.86798	5.6	G4V	0.84	0.97	9.8
-		Gl 188 B	-	15.86798	5.7	G4 V	0.61	0.97	9.8
-		Gl 291 B	-	16.67222	6.17	G4 V	0.49	0.97	9.8
17051	810	Gl 108	Iot Hor	17.24138	5.41	G3IV	0.72	0.97	9.7
39091	2022	Wo 9189	Pi Men	18.2083	5.65	G3IV	0.66	0.97	9.7
200525	8061	Gl 818.1A		18.73361	6.4	G3IV	0.51	0.97	9.6
224930	9088	Gl 914 A	85 Peg	12.40233	5.81	G3V	0.59	0.99	9.5
30495	1532	Gl 177	58 Eri	13.31558	5.49	G3V	0.69	0.99	9.5
53705	2667	Gl 264.1A		16.24959	5.55	G3V...	0.67	0.99	9.4
76151	3538	Gl 327		17.09402	6	G3V	0.53	0.99	9.4
165185	6748	Gl 702.1		17.36714	5.95	G3V	0.53	0.99	9.3
20766	1006	Gl 136	Zet1Ret	12.11974	5.54	G2V	0.64	1	9
193664	7783	Gl 788		17.56852	5.93	G3V	0.54	0.99	9
10307	483	Gl 67		12.64382	4.95	G2V	0.87	1	8.9
136352	5699	Gl 582	Nu 2Lup	14.55604	5.65	G2V	0.61	1	8.9
207129	8323	Gl 838		15.63722	5.58	G2V	0.63	1	8.7
65907	3138	Gl 294 A		16.19171	5.6	G2V...	0.61	1	8.7
20807	1010	Gl 138	Zet2Ret	12.07875	5.24	G1V	0.73	1.01	8.6
64096	3064	Gl 291 A	9 Pup	16.67222	5.72	G2V	0.59	1	8.6
143761	5968	Gl 606.2	15Rho CrE	17.42768	5.41	G2V	0.68	1	8.6
189567	7644	Gl 776		17.71479	6.08	G2V	0.49	1	8.6
130948	5534	Gl 564		17.94366	5.85	G2V	0.53	1	8.6
84737	3881	Gl 368		18.42978	5.09	G2V	0.81	1	8.6
137107	5727	Gl 584 A	2Eta CrB	18.62197	5.62	G2V	0.61	1	8.6
137108	5728	Gl 584 B	2Eta CrB	18.62197	5.96	G2 V	0.5	1	8.6
211415	8501	Gl 853 A		13.611	5.39	G1V	0.63	1.01	8.5
146233	6060	Gl 616	18 Sco	14.02525	5.49	G1V	0.6	1.01	8.5
72905	3391	Gl 311	3Pi 1UMa	14.27144	5.64	G1.5Vb	0.58	1.01	8.4
86728	3951	Gl 376	20 LMi	14.89425	5.35	G1V	0.63	1.01	8.4
190406	7672	Gl 779	15 Sge	17.66784	5.8	G1V	0.52	1.01	8.2
13974	660	Gl 92	8Del Tri	10.84599	4.87	G0V	0.9	1.02	8.1
95128	4277	Gl 407	47 UMa	14.07658	5.05	G0V	0.79	1.02	8.1
160269	6573	Gl 684 A	26 Dra	14.08848	5.34	G0V	0.68	1.02	8
157214	6458	Gl 672	72 Her	14.39263	5.39	G0V	0.67	1.02	8
84117	3862	Gl 364		14.88317	4.93	G0V	0.89	1.02	8
176051	7162	Gl 738 A		14.97903	5.34	G0V	0.68	1.02	7.9
63077	3018	Gl 288 A		15.19988	5.36	G0V	0.67	1.02	7.9
48682	2483	Gl 245	56Psi5Aur	16.51255	5.24	G0V	0.73	1.02	7.6
55575	2721	GJ 1095		16.86056	5.64	G0V	0.57	1.02	7.5
50692	2569	Gl 252	37 Gem	17.27414	5.74	G0V	0.54	1.02	7.4

APPENDIX F-4. OPTICS

The fundamental optics design that we have considered is scalable to accommodate a range of telescope baseline and aperture requirements. It also does not depend on the number of collectors, so that it may be directly adapted to/from a two collector test lab or precursor mission. A schematic of our optics design concept is shown in Figure F-1. For the specific configurations described in this report, the optics system requirements are listed in Table F-4.

Table F-4. Optics System Requirements

Baseline	9 m	21 m	40 m	Free flyer
Wavelength Band (TBR)	4 to 12 μm	7 to 17μm	7 to 17μm	3 to 23μm
Null depth	1.0E-04	3.7E-05	3.7E-05	3.7E-05
Telescope Diameter	0.6 m	1.7 m	3.5 m	6 m
f-ratio	*f*/1	*f*/1	*f*/1	*f*/1
Telescope Temperature	60 K	40 to 45 K	40 to 45 K	40 to 45 K
Optical Path Errors	7.2 nm	10.6 nm	10.6 nm	10.6 nm
Transmission Asymmetries	0.7%	0.4%	0.4%	0.4%
Pointing Jitter	82 mas	54 mas	26 mas	15 mas
Diff'l Polarization Rotation	0.4°	0.2°	0.2°	0.2°
Diff'l Polarization Delay	0.8°	0.5°	0.5°	0.5°

Collectors. Each telescope is a Cassegrain *f*/1 with flat tertiary on 2-axis flex pivots. The short focal ratio allows the telescope to be conveniently packaged in the launch vehicle shroud. The quality of the optics is diffraction-limited at 2 μm for phase detection and correction. Cold baffled tubes link the collectors to the beam combiner.

The technology for collector mirrors 1.7 m and smaller will either be cryo-null figured beryllium, as used in IRAS and SIRTF, or glass. The technology for the larger collector mirrors (3.5 m, 6 m) will be derived from NGST technology.

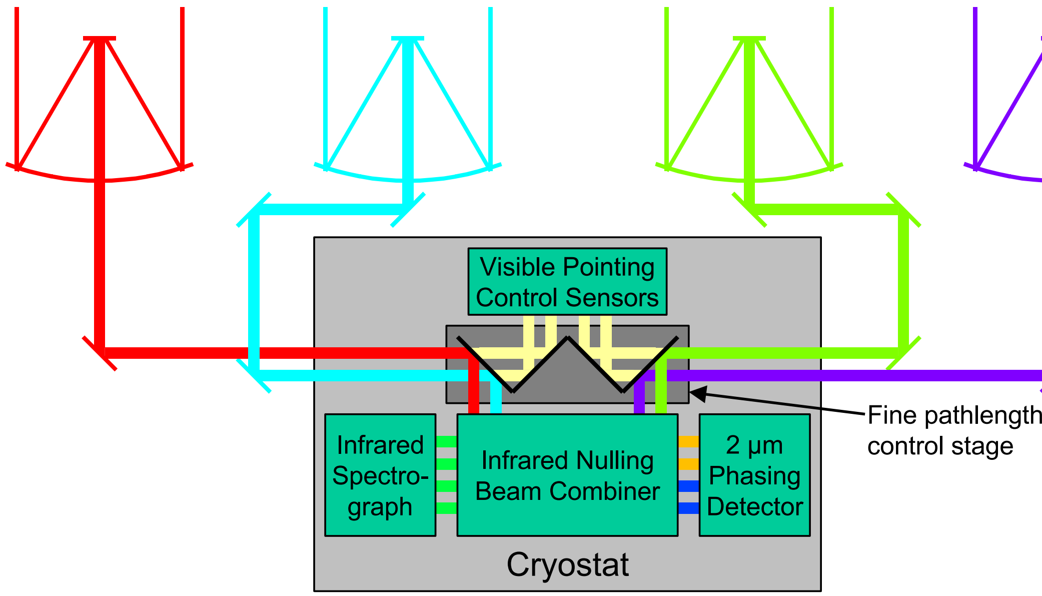

Figure F-1. TPF optics schematic.

Combiner. The nulling beam combiner (NBC) is an amplitude balanced imaging interferometer, based on a modified Mach-Zehnder (MMZ) concept published by Serabyn & Colavita (Applied Optics, Vol. 40, 1 April 2001, pp. 1668–1671), shown in Figure F-2. The Serabyn & Colavita concept provides a fully symmetric nulling interferometer by introducing the field flip using a pair of periscope mirrors prior to beam combination. We consider a variation of this design, using dielectric phase plates to introduce the π phase shift rather than the right-angle periscopes. This modification breaks the symmetry of the Serabyn-Colavita NBC, but it allows us to use the unbalanced ("bright") outputs to provide phase control information at a shorter wavelength (~2 µm), where the phase plate produces ~3π/4 phase shift. In this way, the phase is measured on the identical optical path that produces the science data.

A 2-µm detector with a 200-Hz readout produces a 20-Hz authoritative-control bandwidth to the path length correction. Fine path length adjustment is supplied by mounting the entrance dichroic mirrors and the pointing sensor mirrors on a stage that moves by PZTs along the axis of the incoming beams, as shown in Figure F-1.

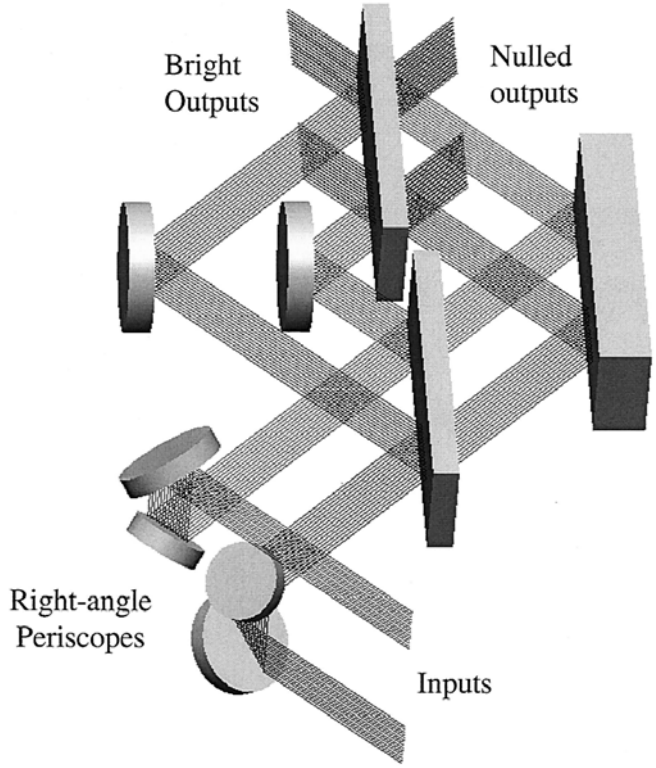

Figure F-2. Serabyn & Colavita modified Mach-Zehnder beam combiner.

The entrance mirrors to the NBC are gold film, so that IR light is reflected and visible light is transmitted. The visible light from each collector is directed onto a quad cell, which tracks pointing displacements and corrects for them by controlling the tertiary steering mirror on the collector.

The output of the NBC is fed into a prism spectrograph, with resolution $R \approx 20$. The required spectrograph temperature is 17 K. The detectors are SIRTF heritage Si:As BIBs, cooled to 8 K. A chopper placed in front of the detectors allows for suppression of low frequency background noise.

The NBC, visible light pointing sensor, phase detector, and spectrograph are all mounted on a single optical bench inside the cryostat. The optics are mounted and aligned on the optical bench warm. The assembled optical bench is then tested at flight temperature and the alignment is verified and corrected as needed. The verified optical bench is integrated into the cryostat and the alignment is re-verified with the cryostat in flight configuration and at flight temperature. From this point, the integrated cryostat is never warmed up again, so that the only environmental change the optics see is the launch environment. This method requires a window transparent in the range 0.5 to 20 μm, which could be retained or removed in flight, depending on how the cost/performance trade works out. The significant advantage of this approach is the ability to verify key optics and alignment requirements by test in the flight configuration with minimal reliance on analysis.

Drawings of our combiner system are shown in Figure F-3. Each pair of collector inputs uses the same MMZ NBC. The outputs of each pair of combined beams are fed backwards into the same MMZ again, this time without a π phase shift. Because the same MMZ optics are used for all four-beam combinations, the design can be readily adapted for a two-collector system. Conversely, a simplified two-collector combiner testbed of this type will serve to demonstrate all of the key technologies necessary for the four-collector combiner.

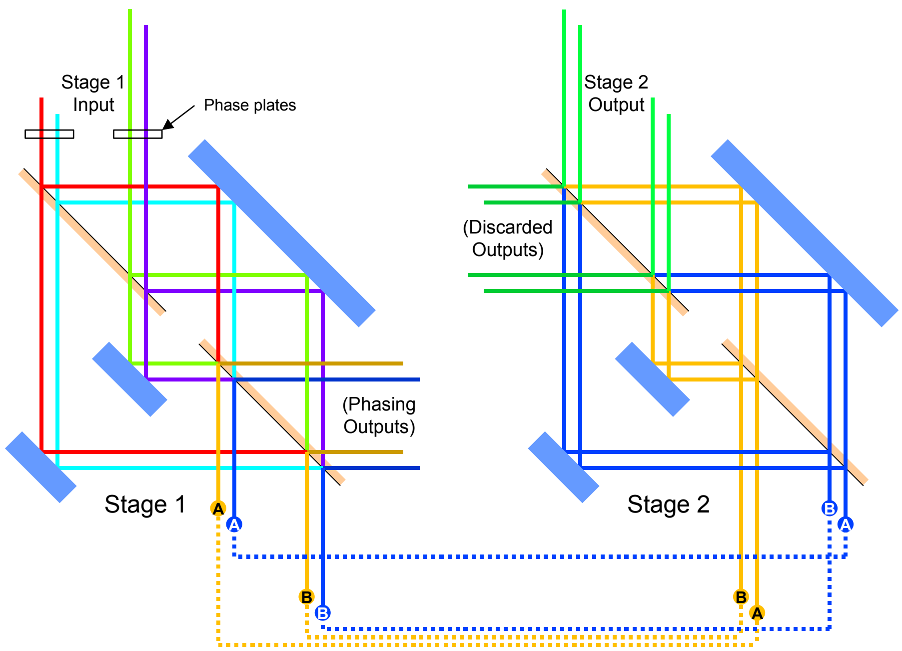

Figure F-3. TPF optics design.

Detectors. Three types of detectors are required for the TPF truss interferometers: 7 µm to 18 µm wavelength for data, 0.5 µm to 0.9 µm for star position, and 2 µm for phase detection.

Data Collection. The detectors required for collecting data will integrate for a period of ~8 seconds to 1 minute and then be read out. The characteristics of SIRTF detectors as used in IRAC appear appropriate. These are 256×256 Si:As detectors supplied by SBRC (now Raytheon). The DQE at 8 µm is 70%, read noise is 10.8 e^- (Fowler 32 sampling), and dark current is 3.8 e^-/s.

The TPF Book assumes DQE folded with optics into an overall efficiency term of 4%, read noise 1 e^-, dark current 5 e^-/s. This read noise is clearly optimistic, relative to SIRTF, and we ask whether this will cause any problems if we use detectors whose performance is identical to SIRTF.

The local zodiacal background puts 2900 photons/second into R = 0.2 and a 10 µm diffraction patch, regardless of telescope size and with allowance for likely inefficiency. Thus if R = 20, adequate for detection of ozone, there will be 290 photons per second detected. We can assume that this radiation is split between six detector pixels, and so is 48 counts-per-second-per-detector. Over 8 seconds (a likely shortest integration time), the signal count is 384, the dark count is 30, and the read noise is 10.8. Thus the overall noise will be ± 23 counts, whereas from signal alone it would be 19.6, an increase of 17%. This would result in an increase in integration time of 37%. This is just acceptable. If the integration times were extended to 60 seconds, the noise would be 57.4 whereas from signal alone 53.7 is expected, an increase of 7%, and an increase in observing time of 14.5% which is certainly acceptable. We conclude that SIRTF detectors are therefore adequate, but note however that there is a need to keep the number of illuminated pixels in the spectrograph focal plane to a minimum.

Star Position. These detectors are assumed to be CCDs. The temperature of the external shell of the dewar is 40 K to 60 K, and we would certainly expect CCDs to operate at these temperatures. However, we are expecting the beam combiner itself to be at about 17 K. At this temperature, there may need to be a selection of CCDs to find ones where the current is not frozen out. Alternative detectors do exist, but we are concerned to take advantage of the small size of pixels, and determine star positions to photon-limited precision. CCDs would seem to be best for this. Verification of appropriate CCD performance is needed.

Phase Detection. 2-µm detector arrays are being used at LN_2 temperatures in the BLINC mid-IR beam combiner and with these too, verification of appropriate performance at somewhat colder temperatures is required.

APPENDIX F-5.

Optics Schematic, 4 Telescopes

Basic optics configuration uses 4 telescopes and 2 stages of beam combination

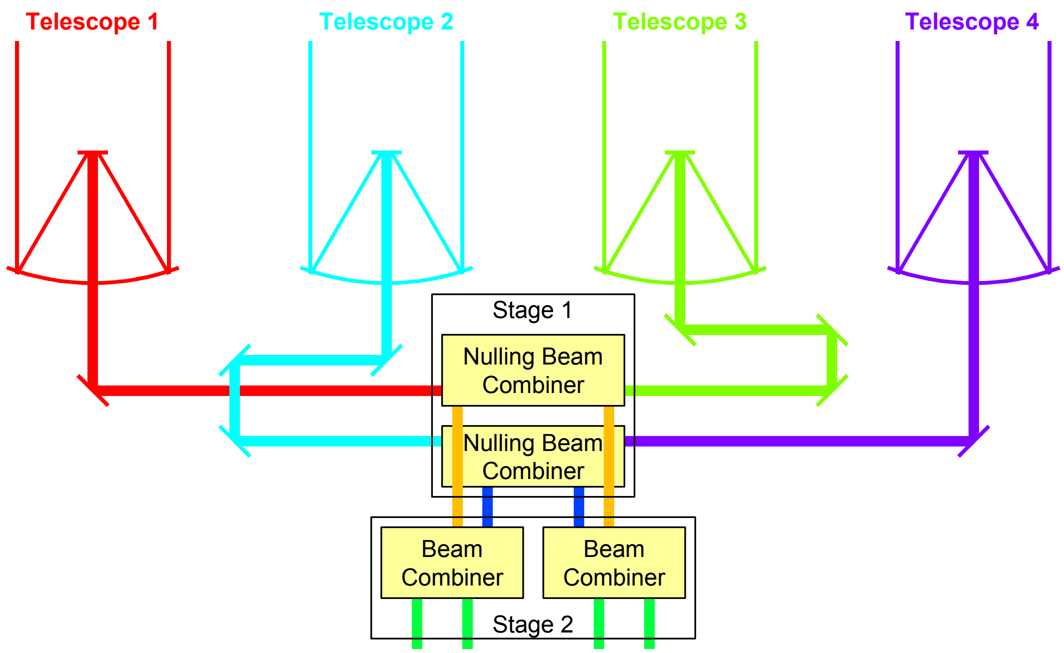

4 Beam Combiner

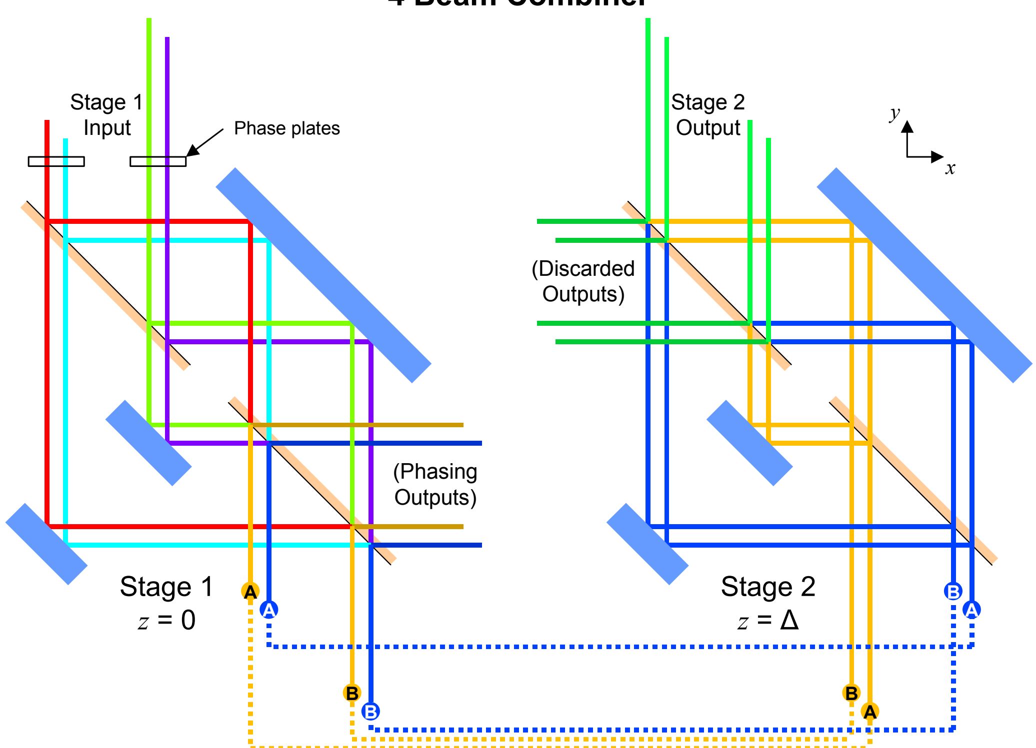

4 Beam Combiner

- The basic optics for the four beam combiner are the same as those for the two beam combiner, i.e., an MMZ with 3 mirrors and 2 beamsplitters.
  - *Each pair of beams is combined side by side in Stage 1.*
  - *The outputs of Stage 1 are sorted, and fed into Stage 2.*
  - *Stage 2 again uses the same MMZ optical elements, but now the beams traverse in a parallel plane, and in reverse order.*
  - *The four outputs of Stage 2 are fed into the spectrograph, just as in the two beam combiner design.*
- Crossover optics (between Stage 1 and Stage 2):
  - *To maintain symmetry, each of the four paths will need 4 reflections.*
- Phase control
  - *Path length control on Stage 2 is not as critical as Stage 1 because the nulling is complete in Stage 1.*
    - Stage 1 has the phase plates and the 2 μm phase detection/control system.
    - No phase plates or 2 μm phase detection in Stage 2.
    - Phase control in Stage 2 TBD.

Color Map

- The color scheme used to draw the light paths in the previous charts is derived from an RGB color map, where combined beams are represented by the corresponding mix of colors, given a choice of starting color for each of the four telescopes.

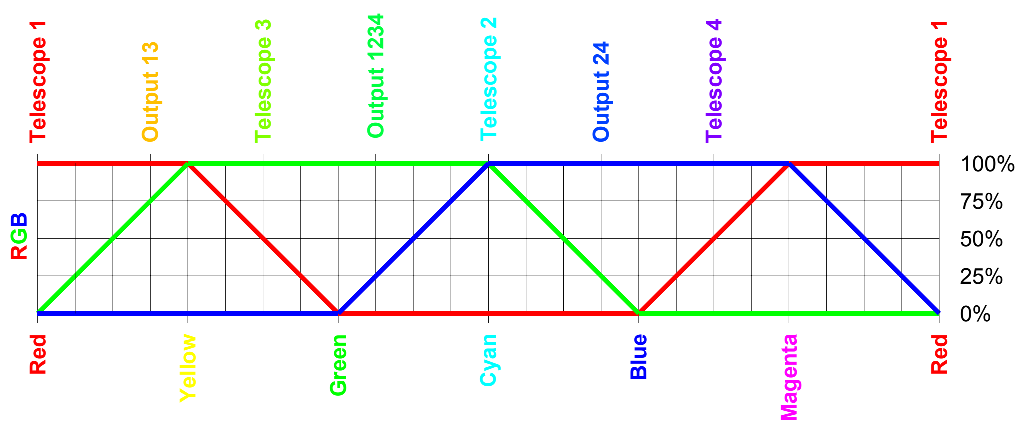

APPENDIX G
TPF Instrument Configuration for the Formation Flying Interferometer

1. Optical architecture.

The baseline optical architecture is assumed to be a dual chopping Bracewell configuration, with 4 collectors (1,2,3,4) equally spaced along a line, and a combiner spacecraft at an offset position (TPF book, p. 103). The collector beams are combined pair-wise. In the high resolution configuration, pairs 1-3 and 2-4 are formed using nulling beam combiners, and the two outputs are then cross-combined with a phase chopping offset that alternates between $+\pi/2$ and $-\pi/2$. In the low resolution configuration, pairs 1-2 and 3-4 are formed first before being cross-combined. For either configuration, the separation between the collectors can be adjusted, from a minimum of 15 m. Other nulling architectures (telescope layout, beam combination) are possible, and will be considered in more detail.

2. Optical layout drawing (if a deformable mirror is used, where is it?).

The optical layout is summarized in Figures 11.1 (optical paths to beam combiner), 11.2 (collector optics), and 11.3 (beam combiner layout) of the TPF book. A low-order deformable mirror may be needed in each beam line, to control large-scale wavefront aberrations (see (4) below).

3. Primary aperture shapes, dimensions, actual area, effective area, and baselines.

The primary apertures are nominally circular with a diameter of 3.5 m; they could be elliptical or some other shape, as long as they match in shape and size. The baseline telescope design is a Coudé folded Ritchey-Chrétien configuration with a small central obscuration of 1% plus a spider. The beams will be compressed to 150 mm for transfer to the beam combiner. Baselines for planet finding can be varied from 15 m to 150 m.

4. Primary aperture optical figure.

The primary mirrors will be near parabolic in shape. The fringe contrast necessary to suppress the signal from the star requires that the sum of all wavefront errors introduced by the optics prior to the beam combiner be less than ~100 nm rms. A wavefront error of ~100 nm provides a Strehl ratio of 99.6% at 10 μm, sufficient to meet the amplitude matching requirements for the null (TPF book, p. 103). The co-phasing requirements for nulling introduce more stringent tolerances, particularly in the low-order aberrations, since the coupling of the pupil to the spatial filter is wavelength dependent. As an example, initial estimates suggest tolerances of the order of 10 nm for focus error.

5. Operational wavelength range.

The wavelength range will be 7 μm to 20 μm for nulling and spectroscopy with 2 μm light used for pointing, OPD phasing and fringe tracking. The wavelength range will be 3 μm to 30 μm for imaging (TPF book, p. 2)

6. Amplitude matching requirement.

Intensity matching between each pair of telescopes is required to better than 0.2% at 7μm and 1.4% at 20 μm (TPF book, p. 93)

The transmission to reflection ratio of the beamsplitter must be matched to within ± 0.25% for the shorter wavelengths (TPF book, p. 106). Multi-pass beamcombiners that balance transmission and reflection are now being studied. The linear polarization and birefringence must also be controlled so as to avoid interference between different polarization components.

7. Corrected wavefront (after AO or spatial filtering).

The wavefronts will be spatially filtered prior to the detector by passing through a pinhole of diameter 0.6 of the Airy diameter of the final focusing element. This will yield an effective wavefront error better than 20 nm rms. Throughput will be cut by ~42%. (TPF book, p. 108).

8. Properties of null, including depth and leakage due to finite stellar diameter.

TPF's ultimate goal of nulling starlight to 10^{-5} -10^{-6} across the 7-20 μm region (in a series of spectral resolution $R = \lambda/\Delta\lambda \approx 20$ bands). The dual-Bracewell null will have θ^2 dependence. A null depth of ~2 x10^{-5} is adequate, because the local Zodi signal is high in a 1 AU orbit. The table below shows the individual requirements that contribute to this designed null depth.

9. Assumptions needed to achieve null depth, including optical path accuracy (piston) and pointing accuracy (tip/tilt).

Each of the following contributes 2×10^{-6} to the null, for each 2-telescope nulling interferometer; the resulting null performance is the sum of these contributions: 2×10^{-5}.

	λ = 7 μm	λ = 20 μm
Optical path errors	2.2 nm	6.4 nm
Intensity balance	0.14%	0.14%
Pointing jitter	0.37 milliarcsec	1.1 milliarcsec
Differential polarization rotation	0.08 deg	0.08 deg
Differential polarization delay	0.114 deg	0.114 deg

10. Properties of spatial filter, if any.

Simulations have shown that a null depth of 10^{-6} or better can be obtained with a spatial filter restricted to 0.6 of the Airy disk diameter (Ollivier and Mariotti, 1997). Spatial filters may be implemented using single mode fiber optics (currently not available at mid-IR wavelengths), feed horn waveguides, or pinholes (TPF book, p. 108).

11. Angular resolution at planet position, in the final image.

We adopt λ/(2B) as the angular resolution, equivalent to half the fringe spacing for a single Bracewell interferometer with baseline B. For any given target, the largest baseline is chosen that maintains an acceptable level of stellar leakage, relative to the contributions from local and exozodi.

	B = 15 m	B = 150 m
λ = 7 μm	0.048 arcsec	0.005 arcsec
λ = 20 μm	0.137 arcsec	0.014 arcsec

12. Inner and outer radius of effective field-of-view within which planets might be detected (instantaneous and after observations at multiple roll angles).

Planets can be detected at all position angles after the formation has been rotated through half a turn. We define the inner radius at which planets can be detected as the angular offset to the first maximum of the fringe response, given by λ/(2B), the same as the angular resolution defined above. The inner radii for different combinations of wavelength and baseline can be read from the table. The outer radius is defined by the size of the primary beam, given approximately by λ/D, where D is the collector primary diameter. For D = 3.5 m, the outer radius is 0.4 arcsec for λ = 7 μm, and 1.2 arcsec for λ = 20 μm.

13. Operating temperatures and thermal stability for key optical components.

The main optics will be passively cooled to below 40 K, to limit the impact of photons emitted by the instrument on the long wavelength sensitivity of the system (TPF book, p. 112). The mid-IR detectors will be cooled to approximately 5 K (TPF book, p. 132) to minimize dark current.

14. Effects of spacecraft parameters (vibration, pointing jitter, etc) on stability of null.

The null depth depends on co-phasing, amplitude balance and polarization matching of the 4 beams. The planetary signal is chopped at ~1 Hz, so only variations in the null depth at frequencies close to 1 Hz or its harmonics have an adverse effect. The primary sources of disturbance are expected to be the thruster firings used to position the spacecraft and rotate the formation, reaction wheels for attitude control (if used), and the actuated optics within the instrument. Laser metrology will monitor fast path fluctuations within and between the spacecraft, and co-phasing fringe trackers will measure the path differences from star to beam combiners. The relative attitudes of the spacecraft will be maintained at the arcminute level to maintain the correct polarization match.

15. Spectrometer design.

Spectrometer resolution (λ/Δλ) will be ~3 for planet detection, ~20 for planetary spectroscopy and ~3-300 for general continuum and spectral line imaging. Very high resolution ($R \approx 10^5$) using Fourier Transform Spectroscopy is an option for specific lines (TPF book, pp. 3, 62, 93).

16. Operations scenario (e.g. does the baseline change for each target?).

For each target system, the largest baseline is chosen that maintains an acceptable level of stellar leakage, relative to the contributions from local and exozodi. A baseline shorter than 30 m requires the low resolution configuration, since the minimum separation of the spacecraft is 15 m. Targets must be within ~45 degrees of the anti-sun direction to ensure full shade for the telescopes. The formation is rotated about the axis to the star, completing one rotation in approximately 8 hours (TPF book, p. 108).

17. Specify Q, defined as the operational ratio planet light/scattered starlight.

The ratio of planet flux to starlight leakage, is approx. 0.006 (see response to 19 for parameters used).

	Planet	Planet
3 pc	1.24×10^{-4}	2.12×10^{-2}
5 pc	3.51×10^{-4}	8.13×10^{-3}
10 pc	1.55×10^{-3}	2.75×10^{-3}
15 pc	2.44×10^{-3}	1.12×10^{-3}

18. Total optical efficiency for planetary light including reflection and transmission losses, effective vs. total collection area, filters etc. for both broadband and spectroscopic measurements.

The overall system efficiency includes reflections off many optical surfaces, transmission through filters and beamsplitters (0.12), detector quantum efficiency (0.5), and beam efficiency due to taking only the central part of the primary beam (0.6). This yields a net efficiency (Optics*Detector*Beam) of 0.04 (TPF book, p. 149). Gold mirror coatings have an efficiency of > 98.8% at wavelengths longer than 7 μm. Model predictions indicate that an ice layer build up of 0.60 μm thickness will degrade reflectance at 10 μm by no more than 1% (TPF book, p. 116).

19. Specify detected average count rates, in the effective planetary diffraction spot size (FWHM), from planet, diffracted star, scattered star, exozodi, local zodi, instrument thermal emission, detector dark count, and any other source. Assume the solar system at 10 pc.

	Photo-electrons per 10^4 s @ 10 μm	Photo-electrons per min @ 10 μm R = 20
Planet	72700	65
Local Zodi	8420000	7578
Exo-Zodi	4850000	4365
Nulled star	11300000	10170
Dark current	50000	45

The SNR after a 6-hour rotation is 11.6. Values are calculated for Double chopped Bracewell in a low-resolution configuration and 15-m separation of the collectors.

Note: Details on the time required for the separated spacecraft version of TPF to complete an observing program are given in the 1999 TPF Book.

APPENDIX H
Boeing-SVS Team
NRLA Design Reference Mission Analysis

H.1. The Non-Redundant Linear Array

1. Optical architecture (~2 or 4 null, chopping, hypertelescope, densified pupil, etc.)

NRLA exploits a hypertelescope with up to seven apertures distributed along a 100-m truss.

2. Optical layout drawing (if a deformable mirror is used, where is it?)

Each telescope employs a number of pupil relays to manage the afocal beam projected to the beam-combining optics. Along the way, apodization masks and coronographic elements manage the distribution of light in the focal plane. Phase delays are produced by conventional interferometric delay lines.

3. Primary aperture shapes, dimensions, actual area, effective area, and baselines.

Each telescope has an unobscured 3-m primary circular mirror with a collecting area of 7 m^2. Between four and seven of these telescopes would be distributed along a 100-m baseline.

4. Primary aperture optical figure

The telescopes are of a Mersenne design with the following features;
Primary: off-axis parabola
Parent diameter is 6.6 m f/1.25.
Telescope magnification is 15 with 200 mm beams through coarse trombones. The pupil relay system densifies the pupil into an array of up to seven 40 mm pupils on a close-packed circle configuration.
All telescopes' paths to densified pupil are identical in mirror number and orientation to preserve polarization and amplitudes. Coarse trombones and fine piston mirrors are used to control the piston.
The location of the pupil relay package is controlled by X and Y offsets of trombone mirrors.

5. Operational wavelength range

7 –17 µm

6. Amplitude matching requirement

NONE

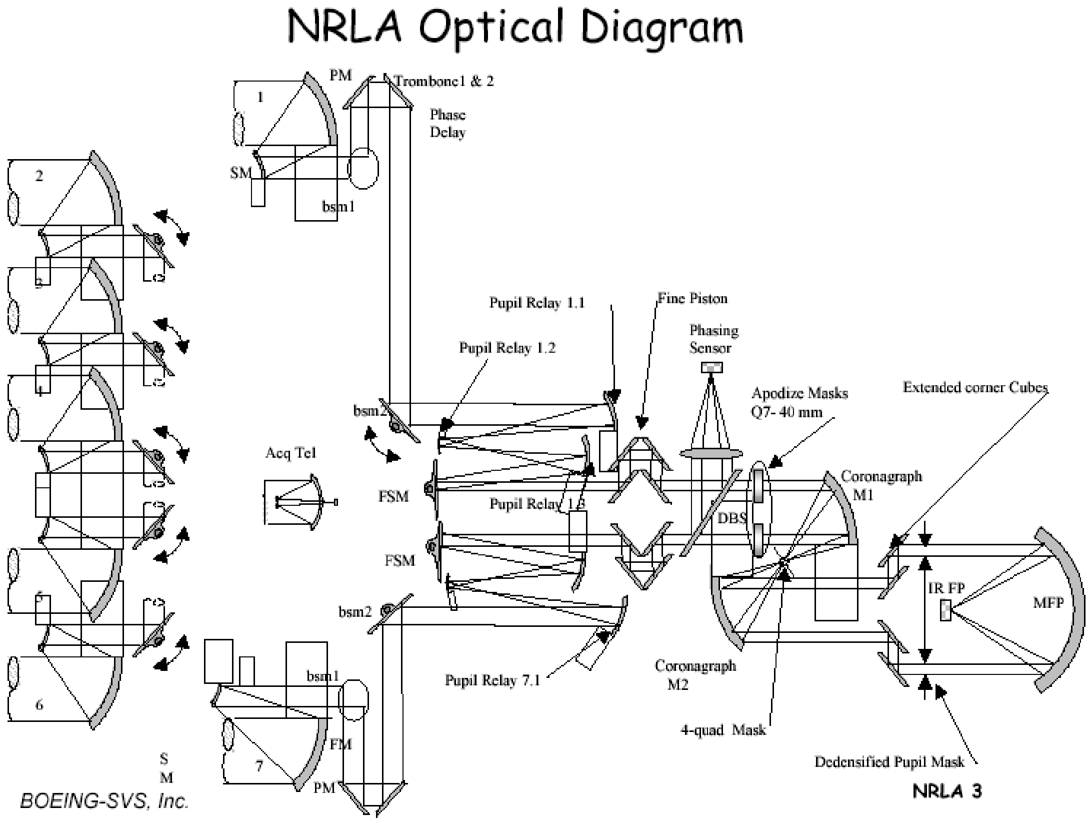

7. Corrected wavefront (after AO or spatial filtering)

Wavefront error $\lambda/120$
Cophasing (piston) error $\lambda/120$

8. Properties of null, including depth and leakage due to finite stellar diameter

The phase mask coronagraph reduces the net starlight throughput by approximately 2×10^3 (it varies somewhat with the size of the star compared to the phase mask diameter), and spreads this light out over a Gaussian-shaped background of size (FWHM) approximately λ/D [where D is the individual aperture size]. This spreads the residual starlight over many pixels in the final image, reducing the background in the vicinity of the planets. Near the center of the field-of-view the residual star background is about 2× the mean value.

9. Assumptions needed to achieve null depth, including optical path accuracy (piston) and pointing accuracy (tip/tilt)

Phase mask errors:
- Thickness error 0.1%
- Radial size error 0.1%

10. Properties of spatial filter, if any

NONE

11. Angular resolution at planet position, in the final image

20 mas

12. Inner and outer radius of effective field-of-view within which planets might be detected (instantaneous and after observations at multiple roll angles).

Planets can be detected to within about λ/B of the center of the image (~20 mas for the full NRLA at 10 μm), subject to SNR limits caused by the star residual background and other contributors. The outer extent of the field-of-view is set by the full field-of-view of the FPA and is nominally 2λ/*D* [1300 mas at 10 μm].

13. Operating temperatures and thermal stability for key optical components

Operating temperatures:

Optics/structure	100 K
FPA/cold shield	10 K

Tolerable coronagraph thermal gradients:

Radial	1 K
Longitudinal	0.5 K

14. Effects of spacecraft parameters (vibration, pointing jitter, etc) on stability of null

Tolerable array (observatory) mispointing error	35 nrad
Tolerable individual beamline angular jitter	25 nrad

15. Spectrometer design

Phase screens are employed to restrict the performance of the hypertelescope to specific bands. Filters deployed in a wheel are then used to detect individual spectral bands of interest. Fourier transform spectroscopy offers a more complex but efficient method of obtaining the desired spectra. A version of this design would use one phase mask covering the range 6.67 to 9.37 μm coupled into a Fourier transform spectrometer and designed to be used at cryo-temperatures.

16. Operations scenario (e.g., does the baseline change for each target?)

NRLA is an imaging system that rotates about the line-of-sight (LOS). A fixed LOS rotation rate (period = 5 hours) is used.

17. Specify *Q*, defined as the operational ratio planet light/scattered starlight.

Q varies somewhat with star angular size (leakage through the phase mask) but typically of order 1 at d = 10 pc for the ratio of planet signal to star residual within the planet diffraction spot.

18. Total optical efficiency for planetary light including reflection and transmission losses, effective vs. total collection area, filters etc. for both broadband and spectroscopic measurements.

[Transmission x QE] = 0.4

19. Specify detected average count rates, in the effective planetary diffraction spot size (FWHM), from planet, diffracted star, scattered star, exozodi, local zodi, instrument thermal emission, detector dark count, and any other source. Assume the solar system at 10 pc.

FPA noise:

Read	5 e^- rms per sample
Quantization	5 e^- rms per sample
Dark current	1 e^- sec^{-1} $pixel^{-1}$

Details of the error budget are summarized here:

Planet:	9 pe/sec
Star (diffracted residual):	1.5 pe/sec
Star (scattered):	0.2 pe/sec
Local zodi:	0.8 pe/sec
Exozodi:	1.9 pe/sec
Thermal:	1311 pe/sec
Dark current:	2 pe/sec

A set of images at consecutive rotational angles gives the complete spatial frequency coverage for image synthesis. The de-rotated images can be processed to derive the image of the stellar leakage (from an imperfect mask, pointing errors, aberrations, etc) for improved dynamic range. The non-redundant array provides robust data with a high degree of internal diagnostic information for calibration and compensation.

H.2. The Observing Program

Photometric Detection

After deployment and initialization at L2, the NRLA will begin its planet detection program. The NRLA design requires multiple snapshots of the target field to be taken as the observatory rotates about its line-of-sight (LOS), which is pointed at the target star. The NRLA is initially oriented to the target and the observatory is spun up about the LOS to a nominal rotation rate of 5 hours. The target star is then acquired in a wide field-of-view visible/near-IR camera and the attitude is stabilized. The individual telescopes are co-phased beginning with a single pair, then adding individual beamlines until all telescopes are co-phased under closed-loop control. At this point science observations on the target object begin.

Initial observations on a single target will use a broad continuum band (nominally, a 1-μm-wide band centered at 12 μm) in order to get a target system image. Two repeats (a total of three observations in this band) will be used to confirm the detection. This will determine if candidate planets are present. Since the NRLA is a linear array, but reconstructs two-dimensional images, a minimum of 1/2 rotation must be completed to obtain each image with full spatial sampling of the target field-of-view . The initial observation period will therefore be 1 1/2 rotations or approximately 8 hours total for most objects. The most distant systems may require longer observations for adequate detection SNR; this will be accomplished without changing NRLA spin rate or pointing, but by simply accumulating additional images and averaging. Only a single spectral bin is used for initial survey observations.

As the NRLA completes each target system observation, it is reoriented towards the next target object. Reaction wheels are used for system reorientation, with cold gas thrusters for wheel desaturation. Observation program planning will be conducted on the ground in order to optimize the sequencing of target objects. For the initial survey, angular repointings of approximately 10 degrees will be needed.

Table H-1. Summary of Photometric Detection Results

Distance (parsecs)	Detection time including 1 boresight rotation (hours)
3	2.5
5	2.5
10	2.5
15	2.5

Spectroscopic Characteristics

The baseline NRLA configuration uses filtered multispectral imaging for planet detection and characterization. A filter wheel containing the phase mask and a bandpass filter is used at the internal focus of the NRLA coronagraph to select appropriate infrared spectral bands (see Table H-2, below). This technique is conceptually the simplest and allows a phase mask filter to be optimized for each individual spectral band. Phase masks may be either reflective or transmissive, although use of a reflective version may require the filter assembly to be located in a separate assembly. A single, broadband phase mask can also be used, with some penalty in star leakage. The tradeoff here is that use of multiple, spectrally-optimized phase masks will require a high-precision filter assembly to maintain alignment of the phase mask to the coronagraph point-spread function. This is a design tradeoff requiring further study.

The NRLA can be designed to incorporate a dispersive spectrometer assembly, at some penalty in the optical system complexity downstream from the coronagraph (i.e., between the coronagraph and the focal plane). The baseline NRLA design can accomplish the TPF mission using sequential observations in filtered bands within the required mission lifetime. However, addition of a dispersive spectrometer would make the observations more efficient.

Table H-2. Summary of Spectroscopic Performance

	CO_2 or H_2O	**O_2 or O_3**
Time to characterize an Earth twin at 10 pc with an SNR ≥ 5	CO_2 in 65 hours	O_3 in 50 hours

APPENDIX-STAR DATA

NRLA "Full size" design, B = 100m, N = 7 apertures, *D* = 3m
Observations for detection at 12 μm, 1 micron bandpass

Hipparcos Number	Observation plus maneuver time (hr)	Cumulative targets	Cumulative time for all observable targets (hrs)	FOR check for observability. 1 indicates target is within the sky coverage of the instrument	Radial position-1 indicates the target angular position at the focal plane is large enough
		0	0		
71683	12.5	1	12.5	1	1
37279	12.5	2	25	1	1
71681	12.5	3	37.5	1	1
2021	12.5	3	37.5	0	1
46853	12.5	4	50	1	1
22449	12.5	5	62.5	1	1
95501	12.5	6	75	1	1
32362	12.5	7	87.5	1	1
8102	12.5	8	100	1	1
3821	12.5	8	100	0	1
35550	12.5	9	112.5	1	1
99240	12.5	9	112.5	0	1
89937	12.5	9	112.5	0	1
16537	12.5	10	125	1	1
27072	12.5	10	125	0	1
57757	12.5	11	137.5	1	1
28103	12.5	12	150	1	1
109176	12.5	13	162.5	1	1
78072	12.5	14	175	1	1
50954	12.5	14	175	0	1
59199	12.5	15	187.5	1	1
70497	12.5	15	187.5	0	1
14632	12.5	16	200	1	1
7513	12.5	17	212.5	1	1
12777	12.5	18	225	1	1
102485	12.5	19	237.5	1	1
36366	12.5	20	250	1	1
116771	12.5	21	262.5	1	1
92043	12.5	22	275	1	1
112447	12.5	23	287.5	1	1
105858	12.5	23	287.5	0	1
17651	12.5	24	300	1	1
67153	12.5	25	312.5	1	1
15510	12.5	25	312.5	0	1
1599	12.5	25	312.5	0	1
64394	12.5	26	325	1	1
61317	12.5	27	337.5	1	1
61174	12.5	28	350	1	1
16852	12.5	29	362.5	1	1
108870	12.5	30	375	1	1
19849	12.5	31	387.5	1	1

Hipparcos Number	Observation plus maneuver time (hr)	Cumulative targets	Cumulative time for all observable targets (hrs)	FOR check for observability. 1 indicates target is within the sky coverage of the instrument	Radial position-1 indicates the target angular position at the focal plane is large enough
84893	12.5	32	400	1	1
21770	12.5	32	400	0	1
77257	12.5	33	412.5	1	1
71284	12.5	34	425	1	1
34834	12.5	34	425	0	1
12843	12.5	35	437.5	1	1
96441	12.5	35	437.5	0	1
72659	12.5	36	450	1	1
67275	12.5	37	462.5	1	1
46509	12.5	38	475	1	1
104214	12.5	38	475	0	1
96100	12.5	38	475	0	1
77760	12.5	38	475	0	1
76829	12.5	39	487.5	1	1
24813	12.5	40	500	1	1
16245	12.5	40	500	0	1
64924	12.5	41	512.5	1	1
23693	12.5	41	512.5	0	1
39903	12.5	41	512.5	0	1
50564	12.5	42	525	1	1
4151	12.5	42	525	0	1
15457	12.5	43	537.5	1	1
51459	12.5	44	550	1	1
10644	12.5	45	562.5	1	1
86736	12.5	46	575	1	1
57443	12.5	47	587.5	1	1
82860	12.5	47	587.5	0	1
910	12.5	48	600	1	1
80686	12.5	48	600	0	1
73996	12.5	49	612.5	1	1
47592	12.5	50	625	1	1
109422	12.5	51	637.5	1	1
7918	12.5	52	650	1	1
5862	12.5	52	650	0	1
97295	12.5	52	650	0	1
25278	12.5	53	662.5	1	1
53721	12.5	54	675	1	1
29800	12.5	55	687.5	1	1
29271	12.5	55	687.5	0	1
25110	12.5	56	700	1	1
86796	12.5	57	712.5	1	1
7981	12.5	58	725	1	1
97675	12.5	59	737.5	1	1
104217	12.5	59	737.5	0	1
40843	12.5	60	750	1	1
99461	12.5	61	762.5	1	1
3909	12.5	62	775	1	1
64792	12.5	63	787.5	1	1

Hipparcos Number	Observation plus maneuver time (hr)	Cumulative targets	Cumulative time for all observable targets (hrs)	FOR check for observability. 1 indicates target is within the sky coverage of the instrument	Radial position-1 indicates the target angular position at the focal plane is large enough
29650	12.5	64	800	1	1
15371	12.5	64	800	0	1
51502	12.5	64	800	0	1
32480	12.5	65	812.5	1	1
56997	12.5	66	825	1	1
114622	12.5	66	825	0	1
47080	12.5	67	837.5	1	1
49081	12.5	68	850	1	1
36439	12.5	69	862.5	1	1
110109	12.5	70	875	1	1
37853	12.5	70	875	0	1
80337	12.5	71	887.5	1	1
84862	12.5	71	887.5	0	1
18859	12.5	72	900	1	1
78459	12.5	72	900	0	1
73184	12.5	73	912.5	1	1
12653	12.5	73	912.5	0	1
113357	12.5	74	925	1	1
32439	12.5	74	925	0	1
89042	12.5	75	937.5	1	1
79672	12.5	76	950	1	1
58576	12.5	77	962.5	1	1
22263	12.5	78	975	1	1
105090	12.5	79	987.5	1	1
15330	12.5	79	987.5	0	1
7978	12.5	79	987.5	0	1
19335	12.5	80	1000	1	1
8362	12.5	80	1000	0	1
35136	12.5	81	1012.5	1	1
34065	12.5	81	1012.5	0	1
107649	12.5	82	1025	1	1
3765	12.5	83	1037.5	1	1
99825	12.5	84	1050	1	1
114924	12.5	84	1050	0	1
38908	12.5	84	1050	0	1
7751	12.5	84	1050	0	1
42438	12.5	84	1050	0	1
49908	12.5	85	1062.5	1	1
75181	12.5	86	1075	1	1
114948	12.5	86	1075	0	1
26394	12.5	86	1075	0	1
98470	12.5	87	1087.5	1	1
81300	12.5	88	1100	1	1
103389	12.5	89	1112.5	1	1
33277	12.5	90	1125	1	1
3093	12.5	91	1137.5	1	1
3583	12.5	91	1137.5	0	1
84478	12.5	92	1150	1	1

Hipparcos Number	Observation plus maneuver time (hr)	Cumulative targets	Cumulative time for all observable targets (hrs)	FOR check for observability. 1 indicates target is within the sky coverage of the instrument	Radial position-1 indicates the target angular position at the focal plane is large enough
98819	12.5	93	1162.5	1	1
44075	12.5	94	1175	1	1
43587	12.5	95	1187.5	1	1
91438	12.5	96	1200	1	1
77052	12.5	97	1212.5	1	1
23311	12.5	98	1225	1	1
72567	12.5	99	1237.5	1	1
56452	12.5	100	1250	1	1
69965	12.5	101	1262.5	1	1
72848	12.5	102	1275	1	1
40693	12.5	103	1287.5	1	1
114046	12.5	104	1300	1	1
19076	12.5	105	1312.5	1	1
100017	12.5	105	1312.5	0	1
27072	12.5	105	1312.5	0	1
13402	12.5	106	1325	1	1
34017	12.5	107	1337.5	1	1
88694	12.5	108	1350	1	1
44897	12.5	109	1362.5	1	1
62207	12.5	110	1375	1	1
27435	12.5	111	1387.5	1	1
107350	12.5	112	1400	1	1
54035	12.5	113	1412.5	1	1
77358	12.5	114	1425	1	1
43726	12.5	115	1437.5	1	1
544	12.5	116	1450	1	1
10138	12.5	116	1450	0	1
113283	12.5	117	1462.5	1	1
77801	12.5	118	1475	1	1
26779	12.5	119	1487.5	1	1
117712	12.5	119	1487.5	0	1
68184	12.5	119	1487.5	0	1
32984	12.5	120	1500	1	1
88972	12.5	120	1500	0	1
95319	12.5	120	1500	0	1
64797	12.5	121	1512.5	1	1
86400	12.5	122	1525	1	1
10798	12.5	123	1537.5	1	1
41926	12.5	123	1537.5	0	1
101997	12.5	124	1550	1	1
69972	12.5	125	1562.5	1	1
85235	12.5	125	1562.5	0	1
42808	12.5	125	1562.5	0	1
45343	12.5	126	1575	1	1
120005	12.5	127	1587.5	1	1
85295	12.5	128	1600	1	1
58345	12.5	129	1612.5	1	1
78775	12.5	129	1612.5	0	1

Hipparcos Number	Observation plus maneuver time (hr)	Cumulative targets	Cumulative time for all observable targets (hrs)	FOR check for observability. 1 indicates target is within the sky coverage of the instrument	Radial position-1 indicates the target angular position at the focal plane is large enough
28954	12.5	130	1625	1	1
99701	12.5	131	1637.5	1	1
34069	12.5	131	1637.5	0	1
113576	12.5	132	1650	1	1
116745	12.5	132	1650	0	1
74702	12.5	133	1662.5	1	1
48331	12.5	133	1662.5	0	1
67155	12.5	134	1675	1	1
439	12.5	135	1687.5	1	1
82003	12.5	135	1687.5	0	1
20917	12.5	136	1700	1	1
83591	12.5	137	1712.5	1	1
54211	12.5	138	1725	1	1
16134	12.5	139	1737.5	1	1
91768	12.5	139	1737.5	0	1
54646	12.5	140	1750	1	1
23708	12.5	140	1750	0	0
102186	12.5	140	1750	1	0
66459	12.5	140	1750	1	0
46733	15	140	1750	0	1
114570	15	140	1750	0	1
86614	15	140	1750	0	1
88175	15	141	1765	1	1
86486	15	142	1780	1	1
86201	15	142	1780	0	1
51523	15	142	1780	0	1
89348	15	142	1780	0	1
3810	15	143	1795	1	1
23941	15	144	1810	1	1
5799	15	145	1825	1	1
72603	15	146	1840	1	1
58803	15	147	1855	1	1
111449	15	148	1870	1	1
950	15	149	1885	1	1
40035	15	150	1900	1	1
2711	15	150	1900	0	1
63121	15	151	1915	1	1
43797	15	151	1915	0	1
96258	15	151	1915	0	1
12444	15	152	1930	1	1
86620	15	152	1930	0	1
50384	15	153	1945	1	1
62512	15	153	1945	0	1
32366	15	153	1945	0	1
59750	15	154	1960	1	1
76602	15	155	1975	1	1
73165	17.5	156	1992.5	1	1
33202	17.5	157	2010	1	1

Hipparcos Number	Observation plus maneuver time (hr)	Cumulative targets	Cumulative time for all observable targets (hrs)	FOR check for observability. 1 indicates target is within the sky coverage of the instrument	Radial position-1 indicates the target angular position at the focal plane is large enough
11783	17.5	158	2027.5	1	1
80179	17.5	159	2045	1	1
82020	17.5	159	2045	0	1
6813	17.5	160	2062.5	1	1
23783	17.5	161	2080	1	1
21861	17.5	161	2080	0	1
108036	17.5	162	2097.5	1	1
51814	17.5	163	2115	1	1
44143	17.5	163	2115	0	1
19205	17.5	164	2132.5	1	1
3505	17.5	165	2150	1	1
49809	17.5	166	2167.5	1	1
6706	17.5	167	2185	1	1
23482	17.5	167	2185	0	1
97650	17.5	168	2202.5	1	1
69989	17.5	169	2220	1	1
80008	17.5	169	2220	0	1
107975	17.5	170	2237.5	1	1
13665	17.5	171	2255	1	1
106559	17.5	172	2272.5	1	1
33302	20	173	2292.5	1	1
79822	20	173	2292.5	0	1
11029	20	174	2312.5	1	1
32851	20	175	2332.5	1	1
102805	20	176	2352.5	1	1

Note this design can search 176 of the targets in the list
Total time to search the easiest 150 targets = 1900 hours
(observation + maneuver)

APPENDIX I
TRW Team
Design Reference Mission Analysis

1. Optical architecture (apodized aperture, coronagraph, other)

Infrared Coronagraph

2. Optical layout drawing (if a deformable mirror is used, where is it?)

See the following figures for the optical layout of the telescope and coronagraphic imager. (The 4th mirror is a deformable flat with a 202×200 array of actuators to correct wave-front-error from ~1 µm to ~1 nm.)

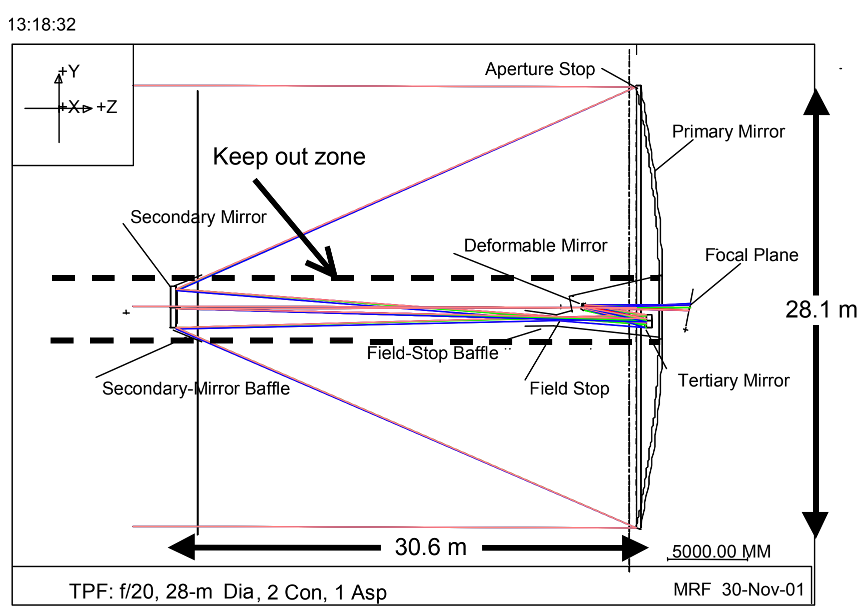

Figure I-1. Optical layout of the primary telescope.

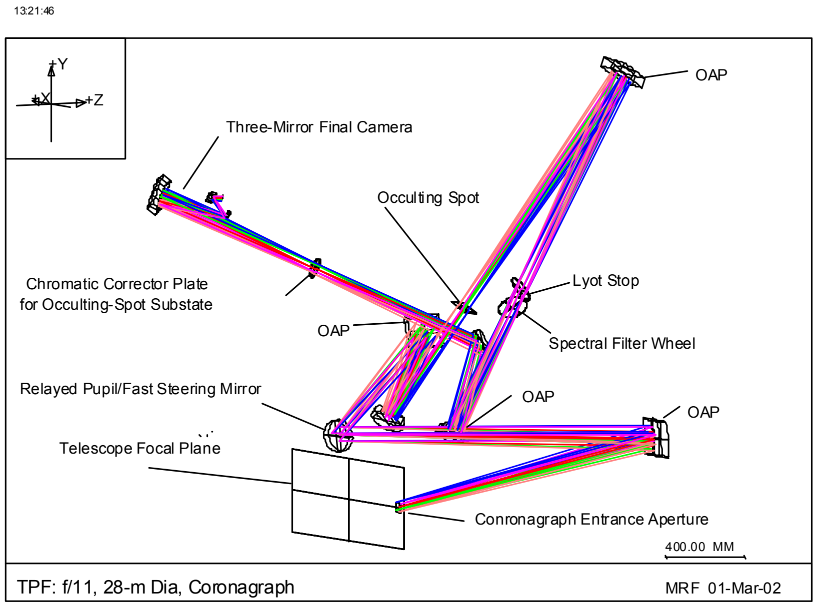

Figure I-2. Optical layout of the coronagraphic imager instrument.

3. Primary aperture shape dimensions actual area, and effective area.

28-m, 3-mirror anastigmat telescope with a segmented primary (36 hexagonal segments, 3.96 m flat-flat), 488.9 m^2 actual area. The results for the observing program were modeled using a 467 m^2 effective area which accounts for a simple Lyot mask that blocks the outer edges of the primary mirror and the support struts for the secondary mirror. This decision was based on modeling done by John Trauger at JPL that indicated that a simple Lyot mask would be adequate to control the diffracted star light. Detailed modeling by Bauer Associates indicates that a more aggressive Lyot mask may be necessary. For their work, an effective area of ~360 m^2 with an apodization function on the Lyot mask was used (see below).

4. Primary aperture optical figure

See error budget (Figure I-6) and optical prescription.

5. Operational wavelength range

The telescope is designed to be used across a broad wavelength range with good performance. The diffraction limit will drive the short wavelength limit of operation but 3 µm is achievable even at the loosest tolerance of diffraction limited at 7 µm. The long wavelength cutoff is driven by the thermal self-emission of the telescope. Since the telescope is < 35 K, the thermal emission does not become significant until ~20 µm and will not severely limit the sensitivity of the telescope until ~30 µm, outside the range of Si:As detectors.

The coronagraph, when working in imaging (detection) mode, will cover at least 7 to 17 µm with a goal of 3 to 28 µm. The coronagraph spectrometer has two modes: one covering the 6 to 12 µm band and the other the 12 to 24 µm band. The 6 to 12 µm band is the primary used for characterization and is used for the modeling. An optional general astrophysics imager would cover the 3–28 µm band.

6. Amplitude uniformity requirement

See error budget (Figure I-6).

7. Corrected optical figure (after AO, if an deformable mirror is used)

See error budget (Figure I-6).

8. Aperture mask shape including intensity and phase tolerances

Not applicable

9. Coronagraph mask shape including intensity and phase tolerances

The coronagraph spot shape is given by the following equation:

$$transmission(r) = \exp\left\{-8 * \ln(10) * \exp\left(\frac{-r^2}{2 * (d/2.35)^2}\right)\right\}$$

Where r is the distance from the center of the spot and d is a measure of the spot diameter. The mathematical form is an exponential of a standard Gaussian form in which d is the FWHM of the Gaussian curve. The 8*ln (10) factor sets the transmission at the center of the spot to 10^{-8}.

The physical occulting spot will be on a substrate approximately 35-mm square with the apodized spot in the center. The spot will have the transmission function of t(r) = exp. (-18.42*exp ($-r^2$/0.0172) where r is the distance from the center of the substrate in millimeters. This is quite small and the errors will be critical. The physical scale the errors will be important over are on the order of 1/5th of a pixel or 0.0136 mm at the occulting spot. We estimate that the intensity errors on this size scale need to be < 1% from the perfect shape as described by the mathematical equation.

10. Lyot mask shape including intensity and phase tolerances

The Lyot mask is modeled as a simple binary form that masks the outer edges, the central obscuration, and the secondary support struts. To date, no additional masking has been required given the small gaps between the mirror segments and the properties of the occulting spot. It is suggested that the mask be made of cut metal with no associated phase tolerances. The exact shape has not been shown to be critical, but alignment with the secondary support structure and central obscuration will need to be held tightly or the mask can be oversized at the expense of throughput.

Detailed modeling by Bauer Associates suggests that a more aggressive mask may improve the *Q* at the planet location at the expense of overall throughput of the system. They modeled a mask that has a diameter equivalent to 26 m at the telescope primary aperture with a gaussian cutoff at the edge extending an additional 2 m in from the edge. They found that the central obscuration only needs a simple binary mask, however the outer edge is better served with this apodized shape. They also masked out an area ~0.2 m at the segment edges which does not appear to be necessary. Figure I-3 is a comparison of the stellar flux after the Lyot mask: first without an outer stop (just the central obscuration and segment junctions) and the second with the Lyot mask as described. They are shown on the same color scale.

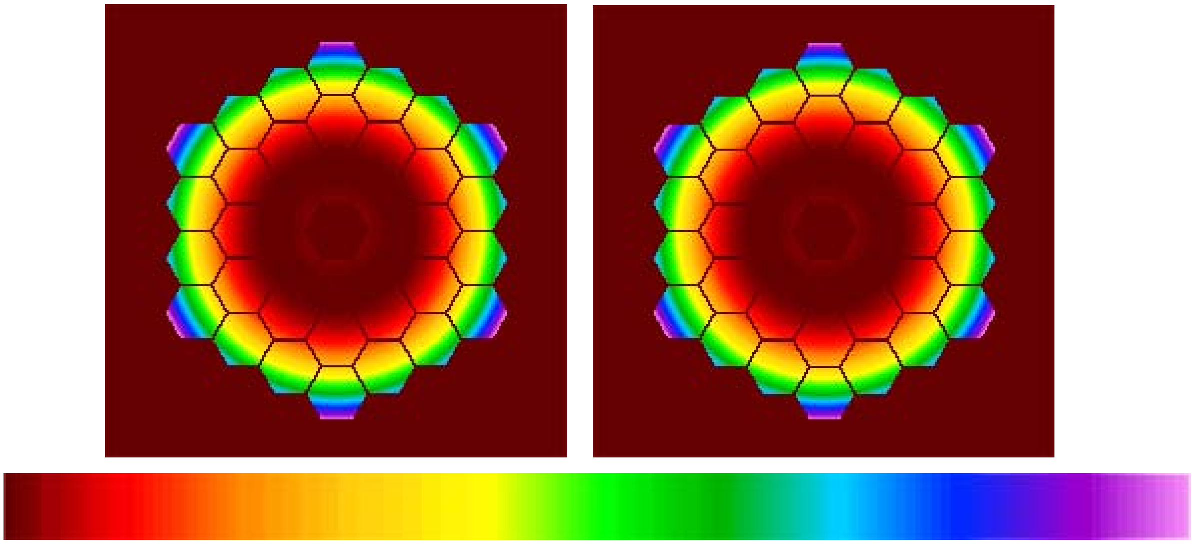

Figure I-3. Comparison of residual star light after the Lyot mask.

11. Angular resolution at planet position, in the final image (after Lyot, etc).

The sampling on the FPA is designed to be 25 mas per pixel over the entire field-of-view (5 pixels for $2.44\lambda/D$ at 7 µm. The current field-of-view is 12×12 arcseconds (512×512-pixel detector). The telescope resolution is 89.9 milli-arcseconds at 10 µm. If the more aggressive Lyot mask proposed by Bauer Associates is used, the radius of the first Airy ring increases to just under 100 mas at 10 µm.

12. Inner and outer radius of effective field-of-view within which planets might be detected (instantaneous and after observations at multiple roll angles)

Based on modeling by TRW, John Trauger at JPL, and Bauer Associates, this design can detect planets at separations of > 50 mas for a range of distances and stellar types. Closer than that, the planet signal is swamped by the stellar leakage. The outer radius corresponds to the extent of the focal plane array and is designed to be ~6 arcseconds.

13. Operating temperatures and thermal stability for key optical components

The telescope primary mirror is ~21 K average, 40 K maximum. When changing the observing attitude, the worst case hot-to-cold ΔT of the primary mirror elements is < 0.31 K, with an average of 0.23 K. The secondary mirror is predicted to be 25 K and the Science Instrument Module will be 30 K provided no more than 0.62 W of heat are generated in the compartment.

14. Effects of spacecraft parameters (vibration, pointing jitter, etc) on stability of PSF

See error budget (Figure I-6).

Modeling by Bauer Associates show that current requirements in the error budget have no appreciable effect on the PSF of the star as passed by the occulting spot and Lyot mask. This is shown in Figure I-4 below.

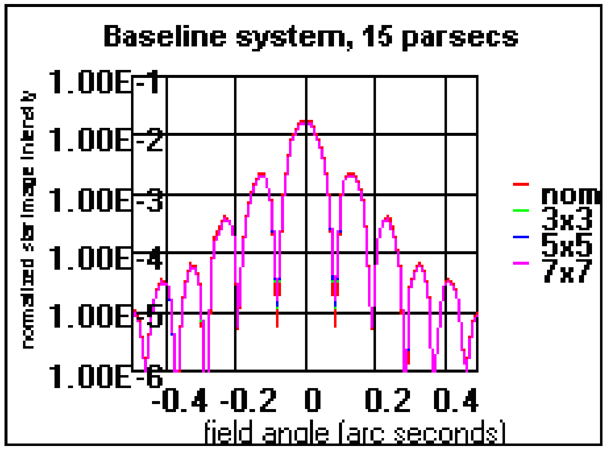

Figure I-4. Normalized intensity (1 = maximum intensity with no masking) for 4 "smearing" cases where the "smearing" is a function that combines the effects of jitter, low-frequency mirror PSD, and the zodiacal light background. Inputs for this model are 5 mas rms radius for jitter, lambda/10 (@0.633 µm) primary mirror PSD, and solar system zodiacal light levels for a system at 15 pc.

15. Spectrometer design

The spectrograph portion of the coronagraph instrument is shown in Figure I-5. It is a simple dispersive system that employs a multi-object slit mask at the image plane based on technology being developed for the NGST Multi-Object Spectrometer. Our baseline is a microshutter device, but we will incorporate the technology as validated by the NGST program. The dispersive element is tentatively identified as a grating, but it could also be a prism. The spectral resolution at the focal plane is designed to be 0.2 µm / pixel from 6 to 12 µm to cover the needed spectral band for minimal characterization. The advantage of using a grating is that it can be used in the 2nd order for the 6 to 12 µm band and in 1st order for 12 to 24 µm with a dispersion ½ that of the shorter band (0.4 µm / pixel). Promising targets can be initially characterized in the 6 to 12 µm band, then further characterized in the 12 to 24 µm band if desired. The spectrograph will use a second 512×512 Si:As BIB detector, identical to the one in the imager. The required spectral coverage and available slit masks will limit the field-of-view of the characterization instrument. We have designed the optical system for a 8×8 arcsecond field-of-view , but the slit mask may further limit the field-of-view to ~6×6 arcseconds.

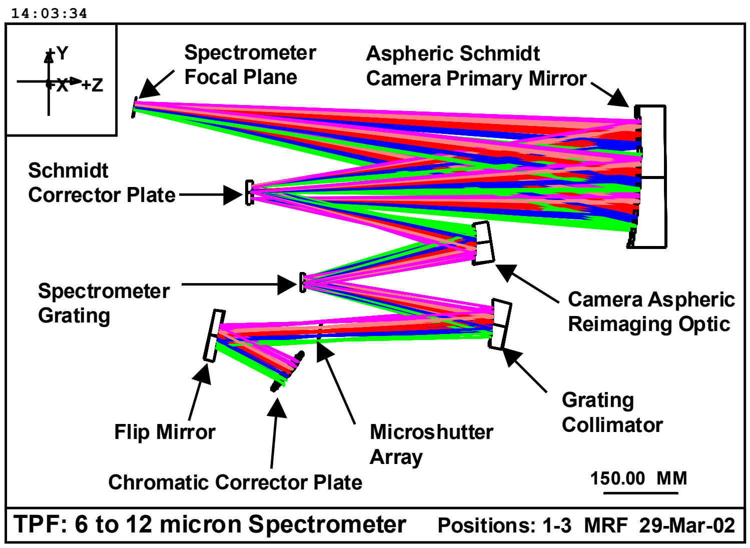

Figure I-5. Optical layout of the coronagraph spectrometer.

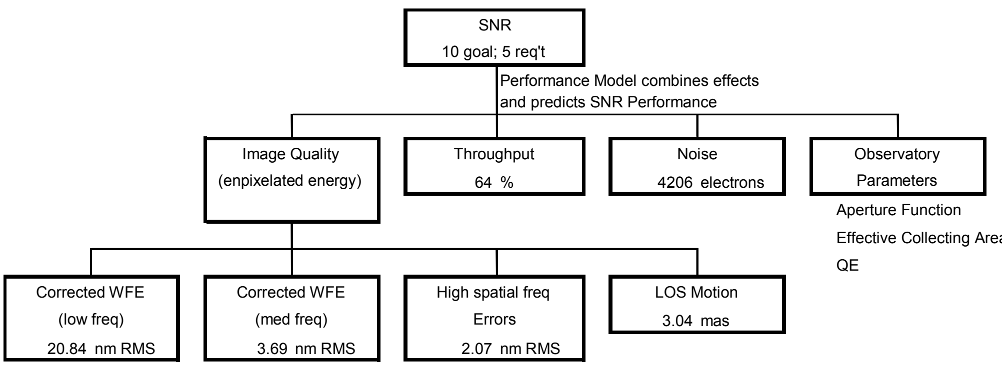

Figure I-6. Error Budgets.

16. Operations scenario (e.g. does the coronagraphic spot or apodized aperture mask change for each target?

The spot and filter may change depending on the spectral type of the star and expected habitable zone, allowing a much better job to be done in a much shorter time for those targets with a larger habitable zone or better contrast ratio. However, the number of spots and filters available for the detection mission is small, perhaps four of each.

The operation of the large aperture coronagraph for a given target is as follows:

1) Slew observatory to target
2) Acquire target with guide camera
3) Coarse align target to the coronagraph
4) Coronagraph guide system takes over (reflected starlight from occulting spot)
   - Fine Pointing Mirror corrects line-of-sight errors at a bandwidth of 10's of Hz.
5) If spectroscopic data, insert flip mirror to spectrometer optics
6) Select the filter to match stellar spectral type and orbit geometry (12 µm, R = 5 filter is default; may switch to 10 µm, R = 3 to 5, or 7 µm, R = 3)
7) Select occulting spot
   - Log-Gaussian spot as described in question 9 with 80-mas diameter is current default

- Larger spot diameters and/or Gaussian spots available for systems with larger habitable zones (angular size)
- Smaller spot diameters for systems with HZ separations of < 80 mas with corresponding Lyot masks optimized for the size and shape.
- For Gaussian spots, apodized Lyot mask will also be needed

8) Once target is acquired, all options selected, and major dynamic modes of the observatory have been allowed to settle, start integration
   - Maximum single integration time is ~1000 seconds due to cosmic ray flux (NGST result). Multiple reads expected for most observations. Data will be stored separately to allow cosmic ray removal algorithms to be applied.
   - Observatory will be rolled about the optical axis by ~10° at least once during the integration time to allow PSF subtraction. For very long observations (determined by the observing efficiency), the roll can be done multiple times. Roll may be inadvisable for some spectroscopy observations depending on the spectrometer design implemented.

Beyond this sequence, there are also calibration sequences that will update the primary mirror and deformable mirror figure using either the guide camera or a dedicated wavefront sensing camera, as well as provide photometric calibration for the instruments.

For the spectroscopy observations, the setup is the same as for imaging observations, except that a broadband 6 to 12 µm filter is used in the filter wheel and once the star image is lined up on the occulting spot, a mirror is inserted into the beam to direct the light to the spectrograph. A minimum of two apertures in the slit mask will be directed to open: one at the planet location and one on the opposite side of the star from it to permit starlight subtraction. Unless testing shows that the PSF is very asymmetrical, no roll will be used for these observations. Additional apertures in the slit mask can be opened for other objects in the field-of-view provided the spectra do not overlap.

17. Specify *Q*, defined as the operational ratio planet light/scattered starlight. What is the needed stability in the PSF/scattered light to see a planet for a given *Q*? Justify why you feel the instrument PSF is that stable (not necessary for configurations working at a *Q* of 1). The value of *Q* should be consistent with the properties of the optical system given above.

See Figure I-7 for mean value of *Q* versus radial distance from the star. The stability specified in the error budget is consistent with figure and provides adequate performance.

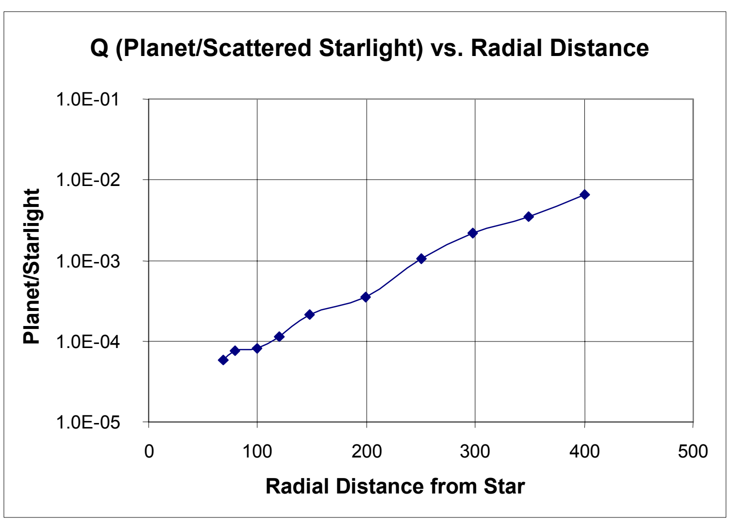

Figure I-7. Estimated *Q* for the modeled Coronagraph system.

18. Total optical efficiency for planetary light including reflection and transmission losses, effective vs. total collection area, Lyot mask loss, filters, etc. for both broadband and spectroscopic measurements

Broadband: The optical transmission is a function of wavelength. We have used all gold coatings on the optical elements and assumed an 80% filter transmission. This gives a total transmission of 0.67 at 12 µm. The Lyot mask losses in the TRW modeling efforts are ~5%. This yields a total system transmission of ~63%. This does not include the detector quantum efficiency which is approximately 0.407 at 12 µm.

Spectroscopic: The spectrometer uses the same optics as the imager, with the addition of six additional optical elements. The main loss in that optical train is due to the efficiency of the grating. A perfect grating has an efficiency of ~80%. The TRW model includes additional efficiency losses in the spectrometer, yielding a total transmission of 40%. This is for a 25 mas pixel at the slit mask and cannot be applied to the total incoming flux.

19. Specify detected average count rates in the effective planetary diffraction spot size (FWHM), from planet, diffracted star, scattered star, exozodi, local zodi, instrument thermal emission, and detector dark counts. Assume the solar system at 10 pc.

Table I-1 gives values for several filters that could be used during the detection mission. This has used the flux values provided by the SWG. The detector dark current is estimated to be 30 electrons per pixel, so the number of the pixels in the FWHM had to be calculated. All of these values have assumed a 67% optics transmission, the 95% Lyot mask efficiency, and a detector QE of 40.7%. These values have also been multiplied by the occulting spot transmission as a function of angular distance from the stellar position. No allowances have been made for LOS pointing errors or jitter in these values.

Table I-1. Counts per Second per FWHM of Airy Disk in a 20% Bandpass

Central λ	# Pixels per FWHM	Planet	Diffracted Star	Exozodi	Endozodi	Thermal Self-emission	Detector-dark Counts	Total
7	3.8	15.4	9.302E+05	281.08	281.08	3.083E-13	112.6	9.309E+05
10	7.7	115.6	1.279E+06	1699.19	1699.19	9.628E-06	229.9	1.283E+06
11	9.3	159.7	1.286E+06	2457.44	2457.44	3.671E-04	278.1	1.292E+06
12	11.0	176.9	1.523E+06	3299.49	3299.49	7.570E-03	331.0	1.530E+06
17	22.1	149.2	5.455E+06	8394.77	8394.77	1.266E+02	664.3	5.473E+06

I.2. Observing Program

The next part of the reference mission calls for evaluating the integration time for doing key parts of the TPF mission. These are enumerated below.

1.3. Detection Mission

We have used the Earth spectrum provided by the SWG and summed it over a 20%-wavelength band centered at 12 µm. The following table shows the required observing time for a single detection observation of the Earth in the Solar System oriented at 45 degrees to our line-of-sight. This is for the case of 1x the local zodiacal dust, at 12 µm, using the instrument configuration described above. The only variation is for the 15-pc case where a 60-mas occulting spot was used instead of an 80-mas spot.

Table I-2. Required Observing Time for a Single Detection Observation of the Earth

Case	Integration Time Required	# individual observations	Time to execute 10 degree roll	Total Observation time
3 pc	< 30 s	2	1 hour	3630 seconds
5 pc	200 s	2	1 hour	4000 s
10 pc	3325 s	4	1 hour	7000 s
15 pc	60800 s	64	3×1 hour = 5 hours	71600 s ≈ 20 hours

No time has been allocated for initial target acquisition in these values. This will add approximately 2 hours per observation to slew, acquire, and settle. It is likely that for the large angular separation systems, using a PSF obtained from a standard star or created from observations of many sources could be used to subtract the star light. This would eliminate the need for a roll and make the short observation targets much more efficient in terms of observation time.

Using the Earth at 10 pc again, we varied the zodiacal light intensity with the results documented in Table I-3. The effect of the presence of zodiacal dust in the external system is minimal using this system for any expected amount of zodiacal light contribution. The ratios of increased exposure time is similar for any distance of the Earth-Sol system.

Table I-3. Zodiacal Light Intensity Results

Zodi Factor	Integration Time Required	# Individual Observations
0.5	3320 s	4
2	3330 s	4
5	3360 s	4
10	3400 s	4
25	3520 s	4
50	3760 s	4

The performance of the Large Aperture InfraRed Coronagraph (LAIRC) against the canonical systems is quite good. As the separation becomes very small, the occulting spot must be smaller. This increases the flux coming in the system and makes the dynamic range of the detector an issue. We did not include this effect in the modeling, but based on current detector technology, the integration time for the individual exposures will need to be shorter when using the smaller occulting spots. This will affect the SNR of targets outside the stellar PSF because where there is little signal, the detector will be readnoise-limited. This will not affect the planet detection mission unless there are interesting planets in outer orbits.

Based on inputs from our science team and analysis of the probability of detecting a planet in a given observation given orbital dynamics and a range of inclination angles, each target should be observed three times during the detection mission. The timing of these observations should be phased to sample different phases of an orbital period of a potential terrestrial planet. This will have to be coordinated with the accessible part of the sky of the telescope at any given time.

I.4. Spectroscopic Characterization

Using the spectrograph described above, basic observations can be taken in the 6 to 12 μm spectral band at a spectral resolution of 0.4 μm after binning in the spectral direction, corresponding to R ≈ 19 at 7.5 μm. This will provide a minimum data set regarding the potential nature of the detected object by sampling a range of molecular lines. Specifically, lines of CO_2, O_3, CH_4, H_2O and N_2O are present in that wavelength band. We have taken as a minimum performance level of achieving a SNR = 7 on the lines of CO_2 and O_3 at 9.31 and 9.65 μm respectively. SNR of 7 is used to allow the subtraction of the averaged continuum to give an overall SNR = 5 in the line. We used the Earth's spectrum provided by the SWG as the input and calculated the SNR in the spectral bins used.

The table below gives the integration time required to achieve SNR = 7 and SNR = 10 for all wavelengths > 9 μm. Followup observations could probe for CH_4, N_2O, H_2O (all between 7 and 8 μm) or get higher resolution observations of the CO_2 and O_3 lines. Included in the table are observation times to achieve SNR = 7 at λ > 9μm in 0.2 μm bins and to achieve SNR = 7 at > 6.5 μm for detection of the other molecular species. The 15 pc case is excluded because of the excessively long integration times required.

Table I-4. Integration Time Required to Achieve SNR = 7 and SNR = 10 for all Wavelengths > 9 μm

Case	0.4 μm bins SNR = 7, > 9 μm	0.4 μm bins SNR = 10, > 9 μm	0.2 μm bins SNR = 7, > 9 μm	0.4 μm bins SNR = 7, > 6.5 μm
3 pc	500 seconds	900 s	1500 s	4.0 hours
5 pc	1.85 hours	4.0 hours	5.3 hours	22.4 hours
10 pc	25.3 hours	51.2 hours	81.5 hours	1143 hours
15 pc	625 hours (26 days)	1276 hours (53 days)	--	--

The plot below shows the detected spectra for the Earth at 10 pc. The error bars correspond to the maximum error in the observations for wavelengths > 7 μm. The actual error is ~1/2 that shown for the wavelengths > 10 μm due to the lower stellar flux as Poisson noise is the largest noise contributor.

I.5. Survey of Nearby Stars

To fully evaluate the system, a target list of 150 stars needs to be observed. The list provided by the SWG is extremely difficult for this architecture to use because of the very small inner radius of Habitable Zones that were used in the selection process. The inner working distance (IWD) of this architecture is about 50 mas and less than 90 stars on the provided list have inner HZ of at least that. Our Phase I study provided a list of 162 stars with a HZ corresponding to the Earth of > 75 mas, called the "Golden Oldies." Including the entire HZ, which extends ~30% inward of an Earth analogue orbit, the minimum HZ for that list would be 50 mas, our IWD. The table below lists the integration time required for a number of stars on Golden Oldies list, along with their characteristics.

It has not been possible (given the modeling tools and time available) to do a detailed calculation for 150 specific target stars. This is planned to be done once the technology drivers are more fully defined and better requirements on the telescope and spacecraft performance have been specified. However, using the range of integration times required as demonstrated above, a reasonable estimate can be calculated. Should the performance against an actual target list be needed, we would wish to use the Golden Oldies list since the list provided does not cover sufficient distance. The Golden Oldies is somewhat biased towards brighter stars because the required distance to get the larger minimum HZ separations is larger. That is reflected in the selection of sources in the table. It is also obvious from the table that reaching the 50-mas separation will require either a great deal of time or an even smaller occulting spot. With a smaller spot, the dynamic range issues for the focal plane start to become severe. A more aggressive Lyot mask could help the dynamic range problem but this has not been modeled.

Based on the above values and the values obtained for the Earth / Sol system at a variety of distances, a total integration time of 24 hours per source (on average) is not too far off, assuming optimization of occulting spot and Lyot mask for each inner HZ separation. Including 2 hours to slew and acquire the target and 3 hours per target for roll maneuvers, the total integration time to survey the complete list is 181 days. This is consistent with the need to complete the detection mission in ~1.5 years to allow 1 year for the characterization mission.

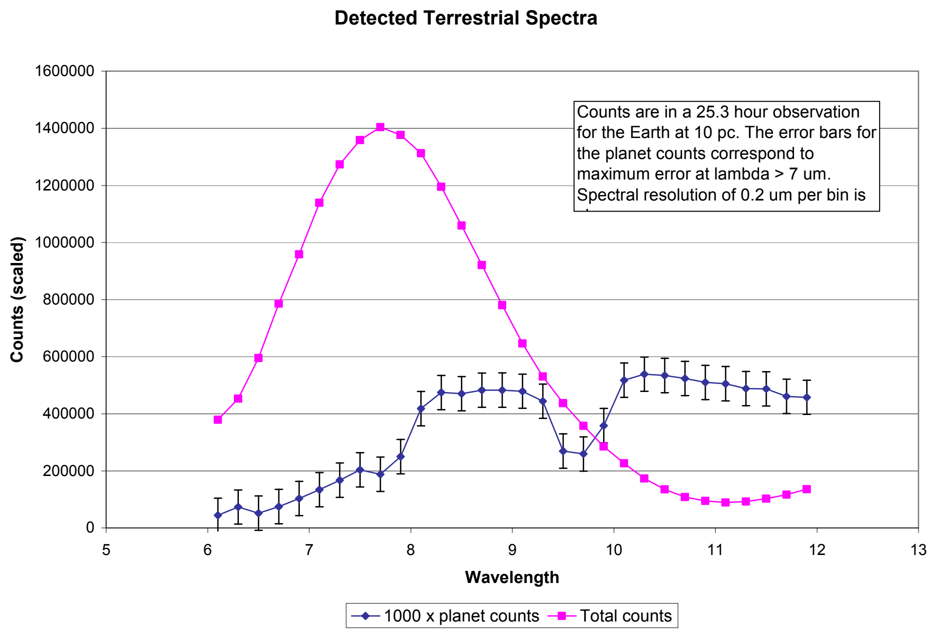

Figure I-8. Detected terrestrial spectra.

Table I-5. Integration Time Required for a Number of Stars on Golden Oldies List

Distance (pc)	Stellar Type	Angular Separation	Integration Time Case 1: 80 mas spot	Integration Time Case 2: 60 mas spot	Integration Time Case 3: 60 mas spot, separation reduced by 20 mas
12.1	G1	82 mas	53 hours	21.9 hours	175 hours
26.2	F0	88	950 s	950 s	950 s
5.9	K4	79	25.6 hours	11.1 hours	106 hours
10.1	G6	89	1900 s	950 s	2850 s
16.2	F2	139	2850 s	2850 s	2850 s
17.4	G0	76	6.1 hours	2.1 hours	35.6 hours
21.4	F5	101	2.4 hours	2.4 hours	3.96 hours
22.7	F7	80	10 hours	4.75 hours	38.8 hours